STAR FORMATION IN LOW MASS MAGNETIZED CORES: THE FORMATION OF DISKS AND OUTFLOWS

STAR FORMATION IN LOW MASS MAGNETIZED CORES: THE FORMATION OF DISKS AND OUTFLOWS

By
Dennis Duffin, B. Sc., M. Sc.

A Thesis
Submitted to the School of Graduate Studies
in Partial Fulfillment of the Requirements
for the Degree of

Doctor of Philosophy

McMaster University

DOCTOR OF PHILOSOPHY (2012) McMaster University
(Physics and Astronomy) Hamilton, Ontario

TITLE: Star Formation in Low Mass Magnetized Cores: The Formation of Disks and Outflows

AUTHOR: Dennis F. Duffin, B. Sc. (University of Toronto), M. Sc. (McMaster University)

SUPERVISOR: Professor Ralph E. Pudritz

NUMBER OF PAGES: xvi, 149

Abstract

Protostellar discs are generally thought to drive molecular outflows and jets observed in star forming regions, but there has been some debate as to how they form. The details of the driving and collimation of outflows help determine how much mass is cleared out and how much energy is fed back into the surroundings. Recently it has been argued that the magnetic brake is so strong that early protostellar disks cannot form.

We have performed 3D ideal magnetohydrodynamic (MHD) simulations of collapsing Bonnor–Ebert spheres, employing sink particles within an AMR grid and using a cooling function to model radiative cooling of the gas. This allows us to follow the formation and early evolution of the accretion disc $2-8\times10^4$ years further into the Class 0 phase of its evolution. We form a rotationally dominated disc with a radius of 100 AU embedded inside a transient, unstable, flattened, rotating structure extending out to 2000 AU. The inner disc becomes unstable to a warping instability due to the magnetic structure of the outflow, warping 30° with respect to the rotation–axis by the end of the simulation. The disc is unstable to a Parker instability and sheds magnetic loops, degrading the orientation of the mean threading field. This reduces and locally reverses the magnetic braking torque of the large scale field back upon the disc. The reduction of magnetic braking allows a nearly Keplerian disc to form and may be the key way in which low mass stellar systems produce rotationally dominated discs. We discuss the relevance of our disc misalignment concerning the formation of mis–aligned hot Jupiters.

Protostellar outflows are implicated in clearing mass from collapsing cores, and limiting the final mass of newly formed stars. The details of the driving and collimation of outflows help determine how much mass is cleared out and how much energy is fed back into the surroundings. The simulations generate outflows which are precessing, kinked, contain internal shocks and extend to a scale of 0.1 pc end–to–end. Our disc–wind theory describes magneto–centrifugal driving throughout the outflow bubble. The bulk prop-

erties of the outflow agree well with observations. The outflow has two components, a larger low speed wind ($v_r < 1.5$ km s^{-1}) dominated by a toroidal magnetic field B_ϕ, and an inner centrifugally driven jet dominated by $B_{\rm p}$ with speeds up to 20 km s^{-1}. The ratio of mass flux from the disk surface compared to accretion in the disk is measured to be $\dot{M}_{\rm out}/\dot{M}_{\rm in} \sim 0.1$ from the inner component, whereas in the outer component $\dot{M}_{\rm out}/\dot{M}_{\rm in} \sim 1.0$. The jet is misaligned and precesses as the disc warps by 30° with respect to the z–axis. We measure star formation efficiencies of $\varepsilon_{\rm core} = 0.63$ (and growing), higher than theoretical predictions of $\varepsilon_{\rm core} = 0.29-0.39$ and observations $\varepsilon_{\rm core} = 0.33$.

These new results reported in this thesis, show that disks can form in strongly magnetized media, in agreement with the observations - and that outflows are not as efficient in clearing away collapsing gas as has been assumed in various theoretical models. Both of these results have important implications for disk formation, and the origin of the IMF, as described in this work.

To Mom and Dad
To Grandma and Grandpa

Acknowledgements

My time at McMaster has been such an incredible journey. I have learned much about the Universe, while simultaneously experiencing the most profound moments of my life. What stands out most of all are the people that I have met and who have guided me along the way.

I owe much of what I have accomplished to Ralph Pudritz. He is an example of what it is to be a true scientist, someone who is interested in answering very basic questions about the Universe, communicating his boundless knowledge to others and binding this with his philosophy of life. I truly admire and respect him. During my time here I have attempted to learn this from him, and will continue to try in the future. I am thankful for his extreme patience with myself, and for sticking by me through some tough times. Without question he gave me the space that I needed when I needed it.

I give much thanks to my committee members as well. Often times the numerical world seems more real than the physical world. Christine Wilson's insight into what's actually going on has set a very important example for me to attempt to emulate as a theorist. At the same time, James Wadsley has inspired the opposite; what we're observing is nice, but what we can simulate is astonishing! I enjoyed very much attending Wadsley group meetings. I also thank Tom Abel, Robi Banerjee, Ralf Klessen, Nicolas Kevlehan and Shantanu Basu for insightful discussions and for setting strong examples. I had many great discussions and experiences in Heidelberg, particularly with Christoph Federrath, Daniel Seifried, Rowan Smith, Rahul Shetty, Dominik Schleicher and Simon Glover.

I have learned a lot from attending Pudritz group meetings of the past and present, and would like to thank those who have been a part of it. Discussions ranged from the origin of life itself to the scale of entire Galaxies, and why the answer to the former depends on the dynamics of the latter. Thank you to Eric Collins, Yasuhiro Hasegawa, Elizabeth Tasker, Kai Cai, Soko Matsumura, Mikhail Klassen, David Kirsh, Philippe Boisvert, Corey Howard, Alyssa Cobb,

Jeff Emberson and Patrick Emond.

I will remember many good times at McMaster with those now off doing other amazing things. Thank you to Sijing Shen, Nicolas Petitclerc, Nathan Leigh, Marie-Josée Colbert, Kristen Anne Woodley, Pamela Klassen, Charles-Phillipe Lajoie, Sarah Nickerson, Colin McNally and Evert Glebbeek. And those still here, Philip Ashby, Jerod Wagman, Patrick Rogers, Tara Parkin among a list of others too long to mention here.

My support over the many years at Mac has come from the most beautiful people I've met, those whom with I've shared my heart, my friends and my family. In the words of my friend David Hollowell, *"You never know what will happen in the future"*. True inspiration has come from my life in Kensington Market.

I dedicate this thesis to my family. To my Dad, Thomas Duffin, with whom I wish to share these final moments with but cannnot and to whom I will miss dearly in future successes and failures. Also to my Grandpa, who passed away knowing this moment would come. And finally to my Mom and my Grandma, the strongest people I know.

Table of Contents

List of Figures

List of Tables

Preface

This thesis includes one published, one submitted, and one pre-submission paper in Chapter 3, 4, and 5 respectively.

The paper *The early history of protostellar disks, outflows, and binary stars* in Chapter 3 was published in the Astrophysical Journal Letters in 2009, Volume 706, page L46. This paper was developed under the supervision of Professor Ralph E. Pudritz. I performed the simulations and wrote the entire paper. Professor Pudritz contributed many ideas on setting up and analyzing the problem, and also worked closely with me on the draft of the text and in analyzing the final results.

The paper *The long–term evolution of magnetized pre–stellar cores I: formation of warped discs* has been submitted to the Monthly Notices of the Royal Astronomical Society and is currently in the review stage. This paper was developed under the supervision of Professor Ralph E. Pudritz. I performed the simulations and wrote the entire paper. I am grateful to Christoph Federrath for the development of sink particles in FLASH, and to Ralf Klessen for my time at the Institute of Theoretical Astrophysics in Heidelberg in 2009 where many of the numerical aspects of this paper came together. I am grateful to Ralf Klessen, Robi Banerjee, and Daniel Seifried for fantastic feedback on the draft of the paper and in the analysis of the results. Professor Pudritz contributed many ideas on setting up and analyzing the problem, and also worked closely with me on the draft of the text and in analyzing the final results.

The paper *The long–term evolution of magnetized pre–stellar cores II: precessing outflows and the efficiency of star formation* will be submitted to the Monthly Notices of the Royal Astronomical Society. I performed the simulations and wrote the entire paper. This paper was developed under the supervision of Professor Ralph E. Pudritz. I am grateful to Ralf Klessen, Robi Banerjee, and Daniel Seifried for fantastic feedback on the draft of the paper and in the analysis of the results. Professor Pudritz contributed many ideas

on setting up and analyzing the problem, and also worked closely with me on the draft of the text and in analyzing the final results.

Chapter 1

Introduction

Stars are the primary source of visible light in the Universe, at the heart of what we see when we look up in the night sky. The cycle starting from the birth of massive stars, their death and subsequent recycling leads to the formation of metal–rich low–mass stars. The formation of stars has consequences for the origin of life in the Universe.

At the center of the formation and evolution of a protostar is the interplay of gravity and magnetic fields. Magnetic fields in collapsing clouds of gas remove angular momentum and control the fate of the disk and its star in the early stages of formation.

The process of making disks and stars feeds back onto the formation of other stars. Protostellar disks drive spectacular $0.1 - 1$ pc outflows and jets with velocities up to 400 km s^{-1} and molecular outflows with masses measured in solar masses. These outflows deposit energy and momentum into the giant molecular clouds that stars form in.

A collapsing molecular cloud forming a group of stars is halted when massive stars turn on and radiatively blow away all remaining low density gas.

The newly formed cluster expands dynamically. A Sun–like star drifts away from its siblings as the most massive star in its cluster goes supernova. The gas and dust in its protostellar disk are on their way to forming planets.

In this thesis, we are interested in the early stages of the star formation. In particular, we are interested in when a protostellar disk forms and what its properties are. We are interested in the size, strength, and magnetic structure of the protostellar outflow it generates and how the disk–outflow system limits the mass that a star can accrete. We discuss the consequences our results have on the formation of planets in Chapter 4 and on the ambient star forming cloud in Chapter 6.

1.1 Six major problems related to formation of stars in our Universe

There are a number of long–standing problems in the stellar life–cycle that remain unanswered. Six major problems are highlighted here which are requisite for understanding how a star is made.

What is the origin of initial mass function (IMF) of stars? The relative number of stars per unit mass (the IMF) is surprisingly independent of age, size, luminosity and metalicity of giant molecular clouds (Kroupa, 2001). The functional form is somewhat similar to a variable power–law (Kroupa, 2001) or log–normal function (Chabrier, 2005) with a power–law tail at the high mass end (Salpeter, 1955). What is the origin of this functional form of the IMF? Is it supersonic turbulence, gravity, or magnetic fields? A complex interplay between numerous physical processes? Furthermore, how indepen-

dent is the IMF and how does it vary with metallicity, number of stars, size or age?

What is the origin of the core mass function (CMF)? The CMF appears to have a log–normal structure similar to the IMF (Arzoumanian et al., 2011). Recent observations suggest that subsonic dense cores – such as the Barnard 5 core recently observed by Pineda et al. (2010) – are embedded in long massive filaments of gas (Men'shchikov et al., 2010; André et al., 2010; Pineda et al., 2011; Arzoumanian et al., 2011). Only in the most massive (unstable) filaments have cores and protostars been found (Arzoumanian et al., 2011). Supersonic turbulence produces a log–normal distribution of gas densities in molecular clouds (Padoan et al., 1997; Federrath et al., 2010b). The high density power–law tail is most likely created by gravitational collapse of the dense gas in a cloud (Ballesteros-Paredes et al., 2011). Does this translate into the formation of cores with a similar mass spectrum?

How does the CMF relate to the IMF? There are both observations and theory which suggest that the core mass function both looks like the IMF (André et al., 2010) and that there exists a one–to–one mapping from the CMF to the IMF via protostellar outflows (Matzner & McKee, 2000). However, it is far from certain that the CMF has the same form as the IMF across a wide range of physical conditions. It is also not clear at what rate protostellar outflows clear away material from cores, or how this depends on initial conditions. This is one of the major goals of this thesis.

How do we solve the angular momentum problem of star formation? Star forming cores have angular momenta on the order of $L_{\rm core} \approx 10^{54}$ g cm s^{-1}

(Goodman et al., 1993) while stars like our Sun have $L_* \approx 10^{49}$ g cm s^{-1}. Angular momentum is likely removed by magnetic braking (e.g. Mouschovias & Paleologou, 1980), viscous transport in a disk, star–disk interactions via a disk–wind (Matt & Pudritz, 2005), gravitationally driven spiral waves, or more simply binary formation (Larson, 2010). However, finding the correct balance of these process has proven theoretically difficult. What governs the transport of angular momentum such that we make protostellar disks and stars with low levels of angular momentum?

How do we solve the magnetic flux problem of star formation? The amount of mass per unit magnetic flux in cores is high such that the magnetic energy is near equipartition with gravity (Crutcher, 1999). However, in the Sun, the amount of mass per unit flux is around 10^8 times larger. Magnetic fields begin to decouple in small regions near the disk (Desch & Mouschovias, 2001) where Ohmic diffusion dominates. This does not reduce the flux sufficiently to solve the problem (Tassis & Mouschovias, 2007b) and some additional flux loss is required, perhaps through magnetic diffusion driven by reconnection or turbulence.

Why is the star formation rate per free–fall time in Molecular Clouds so small? Observations suggest that the galactic star formation rate is $3M_\odot$ yr^{-1}, more than 100 times smaller than we'd expect if the cloud simply evolved in a free–fall time (e.g. McKee, 1999). Turbulence decays in a crossing time, which is for molecular clouds, $t_{\rm crossing} \approx t_{\rm ff} \approx 10^6$ yr. It may be that clouds are transient and very inefficient. Another possibility is that they are long lived with a constant injection of energy and momentum from

protostellar outflows, prolonging the star formation process (e.g. Wang et al., 2010; Krumholz et al., 2012). Magnetic fields delay the global collapse of the cloud and help contain turbulent energy from outflows (Wang et al., 2010). By interacting with a larger scale turbulent environment, the GMC is able to further prolong the star–formation process (Krumholz et al., 2012). But, most important, as soon as massive stars form, they will begin to clear out all of the gas in the molecular cloud with a large flux of high-energy radiation (Murray, 2011). What isn't clear is which of these processes are key to solving the SFR of a molecular cloud and which are secondary.

Answering these questions will be key to understanding the formation of most stars in the Universe. At the centre of all of these questions are magnetic fields, protostellar disks and outflows. The frontier beyond this, where many other questions remain, is with the formation of the first stars, where it appears magnetic fields, disks and outflows play a stronger role than we previously thought.

1.2 Major problems treated in this thesis

We neglect the role of turbulence on large scales in the molecular cloud and also the importance of forming stars in clusters. The reason for our choice is that the well known fact that only very low levels of turbulent motion are present in low mass cores. We perform numerical experiments on isolated star forming clouds in order to understand how angular momentum and magnetic flux are transported and measure how much mass accretes onto a central star. The questions which this thesis specifically addresses help us understand the story of star formation.

What is the role of magnetic fields in star formation? In Chapter 3 we show that magnetic fields play a strong role in limiting the fragmentation of cores in the early phase of their existence. We find that this is softened by non–ideal magnetic processes, such as ambipolar diffusion (AD). More importantly, magnetic fields act to extract angular momentum from the core. They also launch protostellar outflows.

How do disks form? Magnetic braking is so efficient at extracting angular momentum that it can be catastrophic, as discussed in Chapter 2. However, we discuss a mechanism in Chapter 4 in which turbulence in a protostellar disk and outflow generate large regions of field reversals, scrambling the mean magnetic field, limiting the effects of magnetic braking.

Why do outflows precess? Magnetic fields threading protostellar disks are unstable to a warping instability as described by Lai (2003). The instability tends to excite misaligned rings of material towards a parallel alignment with the mean magnetic field. The arrangement of the field also torques the disk such that it precesses in a retrograde fashion. We demonstrate that this is possible during the early formation of protostellar disks in Chapter 4 and that a warped, precessing disk leads to a precessing outflow as described in Chapter 5.

What are the properties of early outflows? Simulations which generate the very beginnings of outflows suggest that there are two components, a fast ($v > 1$ km s^{-1}) and low density component as well as a slow ($v < 1$ km s^{-1}), higher density component. We follow such outflows into much more evolved states and analyze their physical properties in Chapter 5. We use a new

technique for characterizing the magnetic driving of outflows in simulations (Seifried et al., 2012b) to identify that outflows have two components with different physical properties. The low speed component has a high mass-flux and is sprung from the disk by toroidal pressure. This fits the definition of a 'magnetic tower' (Lynden-Bell, 2003). The inner component is driven magneto–centrifugally (Blandford & Payne, 1982; Pelletier & Pudritz, 1992).

How much mass gets accreted from a core into stars? In Chapter 5 we show that an envelope settles into a disk and pseudo-disk before launching an outflow, limiting the mass that may be expelled by outflows. Despite the fact the outflow has fairly large launching footpoint (2000 AU) and that mass flux rates off the vast majority of the disk match the average accretion rate through the disk ($\dot{M}_{\rm wind} = \dot{M}_{\rm accretion}$), mass accretion onto the star is highly efficient.

We begin by outlining the observational and theoretical problems of star formation in Chapter 2. We tie in many of the problems discussed above and review the current state of research. In Chapter 3 we describe our initial numerical simulations of isolated star formation with magnetic fields. We contrast hydrodynamic, magnetohydrodynamic and non-ideal magneto-hydrodynamic simulations during the onset of outflows, fully resolving the collapse.

We extend the collapse using sink particles (Federrath et al., 2010a) and find that disks form early despite efficient magnetic braking and warp due to the magentic field, as described in Chapter 4. The precessing outflow is described in depth in Chapter 5. Specifically, we describe the star formation efficiency and explain why it is so efficient.

In Chapter 6 we describe the direction of future research. This consists primarily of how non-ideal effects can be applied to the star formation process, and how to incorporate turbulent initial conditions. We use unpublished research to demonstrate some promising numerical experiments and speculate on possible results.

Chapter 2

Literature review

The process of forming a star is both simple and extraordinarily intricate. On the one hand, it is a gravitational phenomenon. Dense regions of gas collapse under the influence of gravity down to a point in which they cannot collapse any further. In this sense gravity will tend to create compact dense objects from diffuse matter if perturbations in that initial density field are strong enough. Throughout the story of making a star, physical processes such as magnetic fields, supersonic turbulent velocity fields, the redistribution of angular momentum, a slew of various cooling processes related to the quantum mechanical nature of the gas, radiative feedback, magnetic feedback in its various forms as well as dynamical interactions between stars also come into play.

The interplay of these physical processes with gravity govern the evolution of non-stellar structures such as protostellar disks and molecular clouds. The magnetic field is the only other mechanism, besides gravity, which continually connects the vast array of scales and densities at all stages of the star formation process. Molecular clouds have typical densities of about 10^{-22} g cm^{-3},

10^{15} times smaller than the density of the photosphere of our Sun (10^{-7} g cm^{-3}). The sizes of molecular clouds can range from 10-100 pc ($10^{19} - 10^{20}$ cm), while the radius of the Sun is nearly a million kilometers (10^{11} cm). Stars interact magnetically with their accreting protostellar disks by warping them (Lai et al., 2011) or by torquing them via a disk wind (Banerjee & Pudritz, 2006). The disk interacts with the protostellar envelope via magnetic braking (Mouschovias & Paleologou, 1986; Basu & Mouschovias, 1994) and by launching protostellar outflows (Blandford & Payne, 1982; Pudritz & Norman, 1986; Pelletier & Pudritz, 1992; Boily & Lynden-Bell, 1996; Lynden-Bell, 2003; Sherwin & Lynden-Bell, 2007; Seifried et al., 2012b). The dense envelope of a core further interacts magnetically with its greater molecular cloud regulating fragmentation and the dynamics of turbulence in the gas (Tilley & Pudritz, 2007; Price & Bate, 2008). The formation of molecular clouds themselves is in part influenced by the magnetic interaction of gas in the Galaxy – magnetized galactic spiral waves rapidly build up Jeans unstable spurs, accelerating star formation in galaxies (Kim et al., 2002; Shetty & Ostriker, 2006).

Magnetic energies in the universe are significant. The magnetic field in the first stars is amplified by dynamo processes to present day values. Schober et al. (2012) calculated the amplification of a 10^{-20} G seed field in the first stellar cores using dynamo theory amplified by gravitational collapse. They found on timescales shorter than the freefall time that magnetic energies rapidly saturated to build a 10^{-6} G field. Such field strengths are sufficient to launch magnetically driven protostellar outflows, and it is through these outflows that the intergalactic medium may become magnetized.

An approximate measure of the ratio of gravitational to magnetic energy is the mass–to–flux ratio. This ratio measures the strength of the mag-

netic field relative to gravity. If we observe a spherical cloud of gas along the z-direction with surface density profile $\Sigma_z(r)$ and a magnetic structure $B_z(r)$, we can calculate the mass–to–flux as

$$\mu \equiv \frac{\int_0^R 2\pi r \Sigma_z(r)\,\mathrm{d}r}{\int_0^R 2\pi r B_z(r)\,\mathrm{d}r} = \frac{\bar{\Sigma_z}}{\bar{B_z}} \propto \sqrt{\frac{E_{\rm grav}}{E_{\rm mag}}}, \tag{2.1}$$

where the gravitational energy of a sphere of mass M and radius R is $E_{\rm grav} \propto M^2/R$ and the magnetic energy is $E_{\rm mag} \propto 1/8\pi B_z^2 R^3$, thereby varying with the density structure of the sphere. If this ratio is less than a critical value, a perfectly coupled cloud of gas cannot undergo gravitational collapse. The critical value for gravitational collapse of a cloud with uniform mass–to-flux is about $0.17G^{-1/2}$ (Tomisaka et al., 1988), nearly the same as that for a highly flattened cloud $\mu_0 = (2\pi)^{-1}G^{-1/2}$ (Nakano & Nakamura, 1978). Note that for a uniform sphere where $E_{\rm mag} = E_{\rm grav}$, the mass–to–flux ratio is

$$\frac{E_{\rm grav}}{E_{\rm mag}} = 1 = \sqrt{\frac{3/5GM^2/R}{1/8\pi B^2 R^3}} \tag{2.2}$$

$$\sqrt{\frac{24}{5}\pi G}\frac{M}{\Phi} = 1 \tag{2.3}$$

$$\rightarrow \frac{M}{\Phi} = 0.26G^{-1/2}, \tag{2.4}$$

where Φ is magnetic flux. Clouds that have $\mu/\mu_0 < 1$ are called sub–critical ($\mu/\mu_0 < 1$) as magnetic tension balances gravity. Clouds that have $\mu/\mu_0 > 1$ are supercritical, and will collapse. Magnetic energy is greater than gravitational energy in sub–critical clouds while gravity is stronger in super–critical clouds.

Zeeman measurements of 27 nearby molecular clouds found mass–to–

flux ratios of $\mu/\mu_0 = 0.8 - 7.2$ or $E_{\rm mag}/E_{\rm grav} \approx 2.04 - 0.2$ (Crutcher, 1999; Troland & Crutcher, 2008). This indicates that while few clouds may in fact be sub–critical in mass, by far most are super–critical by a factor of a few. The strengths of the magnetic field are quite significant. Mass–to–flux ratios as high as 10 have been shown to have important consequences on disk properties (e.g. Mellon & Li, 2008).

Gravity still dominates the star formation process. Compiling the dust extinction maps of 23 nearby molecular clouds ($d < 200$ pc), Kainulainen et al. (2009) derived probability density functions of column density N (N–PDFs), where N is the number column density of the gas. They found that for molecular clouds not undergoing active star formation, the N–PDFs could be fit nicely by a log–normal distribution. However, for clouds undergoing active star formation, power–law tails were found at high densities. Example N–PDFs of two quiescent clouds and two clouds undergoing star formation are shown in Figure 2.1.

Using numerical simulations of colliding streams to model the formation of molecular clouds, Ballesteros-Paredes et al. (2011) showed that in simulations without self-gravity the clouds attained a log-normal structure to their N–PDFs. However, when self–gravity is included, the N–PDFs develop strong power–law tails in the high column density end.

Supersonic turbulence that characterizes the internal dynamics of clouds is likely responsible for setting this log–normal structure. Log–normal N–PDFs are known to be a consequence of general turbulent motions in the gas (e.g. Federrath et al., 2010b). Other possible sources of turbulence includes gravitational instability in a galactic disk (e.g. Shetty & Ostriker, 2006; Tasker & Tan, 2009), supernova explosions (Joung et al., 2009), expanding HII regions

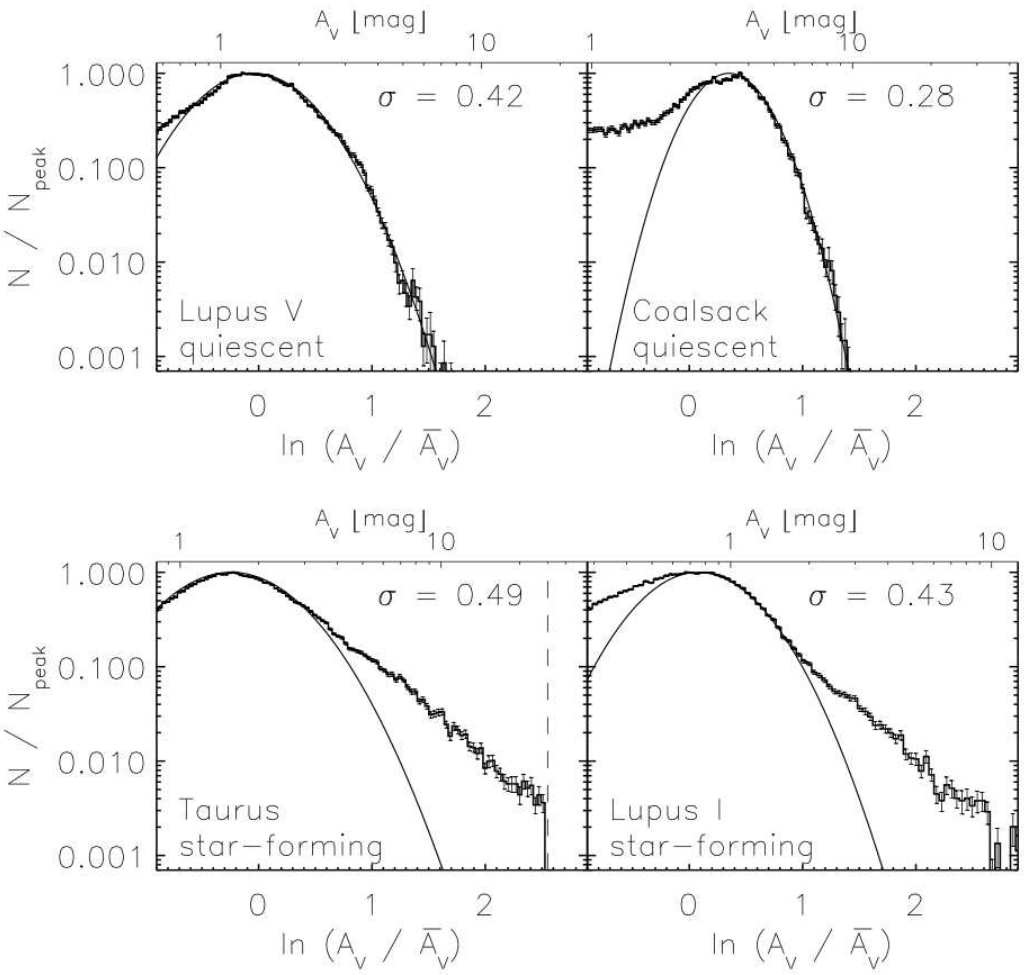

Figure 2.1 Column density PDFs of molecular clouds contrasting active and quiescent star forming clouds. The figure is presented in the recent letter by Kainulainen et al. (2009). The top two panels are non–active star forming clouds Lupus 5 and Coalsack and fit nicely to a log–normal distribution. The bottom two panels correspond to active star forming regions Taurus and Lupus 1. Their distributions are fit with a log–normal but have strong power–law tails in the higher densities. This is indication that the cloud is undergoing global gravitational collapse.

(Peters et al., 2011b), massive stellar winds and protostellar jets (Wang et al., 2010; Cunningham et al., 2011; Krumholz et al., 2012).

This suggests that although turbulence and other properties of the star–

forming environment may set the structure of the lower density gas, when the gas begins its global contraction into stars it is gravity which is dominating the dynamics of the higher density gas. As we discuss additional physical processes in the star–formation story, gravity ultimately governs the formation of stars.

In this chapter, we review the relation between gravity and the magnetic field in the context of forming low–mass stars like our Sun. In §2.1 we describe the current picture of star formation and describe the role of magnetic fields. The magnetic field plays a central role in holding together and forming a protostellar disk, and we conclude with a discussion on this in §2.2. Protostellar outflows are formed as a consequence of gravitational collapse, conservation of angular momentum and magnetic fields. We discuss the properties of outflows and how this may help answer one of the central questions in star formation in §2.4.

2.1 Low–mass star formation

Most stars in the Galaxy form in clusters (Kroupa, 2002), implying that the story of how a single low–mass star like our Sun are constructed is tied to how we make a group of stars of varying masses and luminosities. Clusters of stars form in turbulent molecular clouds (Larson, 1981) with supersonic velocity dispersions that increase with cloud size $R_{\rm pc}$ (in parsecs). Solomon et al. (1987) accurately measured a velocity dispersion–radius relation for 273 molecular clouds in the galactic disk and found a tight relation with cloud size, $\sigma_v = (1.0 \pm 0.1) R_{\rm pc}^{0.5\pm0.05}$ km s^{-1}.

The supersonic turbulent motion quickly generates filamentary structures of dense gas. Recent sub–mm observations of the Aquila Rift and the

Polaris Flare regions of the Gould Belt find that filamentary structures with embedded dense cores are very common (Men'shchikov et al., 2010, also see Figure 2.2). Filaments are two-dimensional concentrations of dense gas and form as a natural consequence of supersonic turbulence (Padoan et al., 2001; Mac Low & Klessen, 2004). Padoan et al. (2001) argued the origin of protostellar cores is from supersonic turbulence, which generates dense, subsonic filaments. Shocks in supersonic turbulent gas are where kinetic energy is lost, so these regions are expected to be sub–sonic and highly compressed by the accreting gas.

Filaments are unstable to fragmentation if their mass–per–unit (M/L) exceeds a critical value $(M/L)_{\rm crit}$. When this happens, the filament will fragment and create dense cores like 'beads on a wire'. A simple model of a dense filament is an isothermal, non–magnetic cylinder of gas in hydrostatic equilibrium with its surroundings (Ostriker, 1964). Such a filament has a cylindrical density profile

$$\rho(r) = \rho_c/(1 + (r/R_{\rm flat})^2)^{p/2}, \tag{2.5}$$

where $p = 4$ and $R_{\rm flat} = \lambda_{\rm J}$ for the special case for isothermal, non-magnetized filaments (Ostriker, 1964). The parameter ρ_c is the central density and $R_{\rm flat}$ is the flat part of the density distribution, equal to the Jeans length $\lambda_{\rm J} = \sqrt{\pi c_s^2/G\rho}$ for this special case. Another form of dense cylinder equilibrium solutions include the effects of helical magnetic fields, finding $p = 1.8 - 2$ (Fiege & Pudritz, 2000).

Real filaments are probably not in hydrostatic equilibrium, although we can use these types of models to see if they are unstable to fragmentation. Fitting the form of Equation (2.5) to real filaments in Aquila and Polaris,

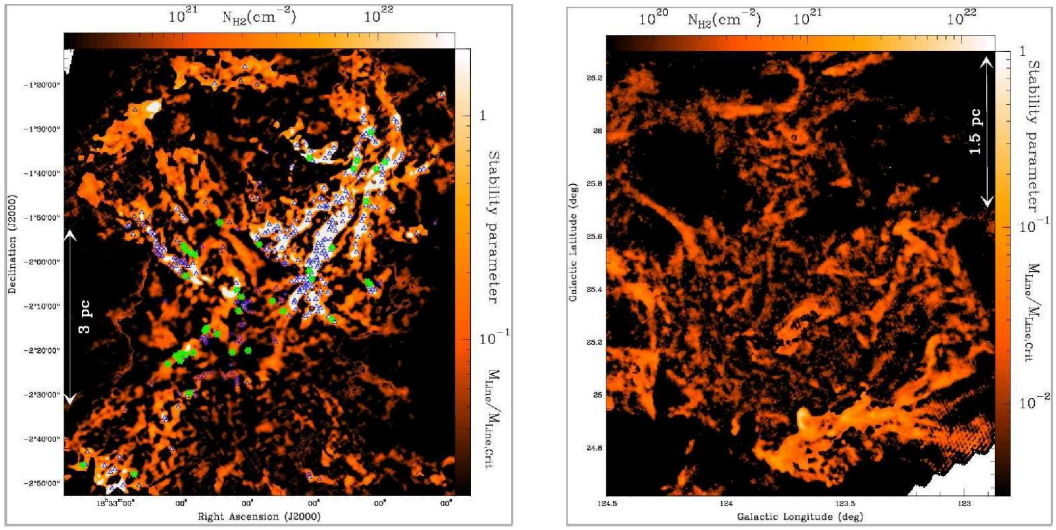

Figure 2.2 Mass per unit length of filaments in Aquila (left) and Polaris (right) in units of the critical mass per unit length of an Ostriker filament $(M/L)_{\rm crit} \approx 15 M_\odot$ pc^{-1} (Ostriker, 1964). Figure taken from André et al. (2010), where a curvelet analysis was used to enhance filament structure. In the left, protostars and cores are over–plotted from separate measurements (see André et al., 2010, for details). These correspond to regions of supercritical M/L. On the right, the Polaris region is sub–critical and has very little star formation.

Arzoumanian et al. (2011) find values of $p = 1.5 - 2.5$. These values are more similar to magnetically wrapped filaments (Fiege & Pudritz, 2000) than Ostriker filaments (Ostriker, 1964). The mass per unit length M/L for these filaments is found to be above critical in star forming regions (André et al., 2010). A comparison of star formation in two different filamentary clouds is shown in Figure 2.2, contrasting a star–forming region (Aquila) to a non star–forming region (Polaris). In Aquila, supercritical regions $(M/L > (M/L)_{\rm crit})$ correspond to young protostars and dense cores, while in Polaris, filament masses are sub–critical $(M/L < (M/L)_{\rm crit})$.

There is much evidence that before stars are made, there exists an intermediate stage where subsonic dense cores are formed. Filaments are created

in shocks generated by supersonic turbulence, and are regions where kinetic energy is dissipated (Padoan et al., 2001). Pineda et al. (2010) observed a supersonic to subsonic transition in the Barnard 5 region in Perseus that appears to be the transition from a low density turbulent environment to a dense, subsonic core. Using a wider field of view, the same authors showed that this core was embedded in a larger scale filament (Pineda et al., 2011). The filament was smaller than the filaments described by Arzoumanian et al. (2011), and fit better to a $p = 4$ model rather than a $p = 2$ model. This gives us an example of how cores are possibly constructed, and what their physical properties are. Using numerical simulations of a sphere with turbulent motions and self–gravity which formed filaments and cores, Smith et al. (2011) classified the structure of 350 cores they could identify. Nearly 75% of the cores were filamentary in nature. Filaments don't fragment directly into stars, but rather fragment into dense cores which build by filamentary accretion flow, and finally undergo global collapse.

Less commonly observed are isolated cores in hydrostatic equilibrium with their surroundings. Alves et al. (2001) measured the extinction of background stars for the dark cloud Barnard 68 to find a radial distribution of column density. This column density can be fit to a spherical core model in hydrostatic equilibrium with its surroundings (a critical Bonnor–Ebert sphere, Bonnor, 1956; Ebert, 1955), but supercritical with respect to collapse. Its mass is 2.1 $M_{\odot}$ and its temperature is 16 K. Further Bonnor-Ebert (BE) spheres with masses ranging from 0.5-6.4 $M_{\odot}$ have subsequently been observed (Teixeira et al., 2005). These cores are quiescent, having line–widths that are for the most part thermal, with minimal contributions from turbulent motions. The cloud Barnard 68 was found to have a ratio of turbulent to thermal energy

of $E_{\rm turbulent}/E_{\rm thermal} = 0.03$ (Hotzel et al., 2002).

Cores like BE–spheres are different than the cores that form in turbulent collapse in that they are near hydrostatic equilibrium. Ballesteros-Paredes et al. (2003) analyzed the cores that formed at stagnation points in a simulated box of turbulent gas. They found 67% of cores could be fit by a Bonnor–Ebert sphere profiles such that half were fits to sub-critical models. The cores themselves were all in fact in the critical state for collapse and shared only the density profile with a Bonnor–Ebert sphere (their fitted temperatures were also different than their simulated temperatures). Real BE–Spheres such as Barnard 68 have had time to adjust to their surroundings, and are not as dynamic as the cores we observe in filaments.

2.1.1 Isolated star formation

In studying the physical processes of how one assembles a star, it is much simpler to approach the problem from the perspective of spherical symmetry. In this sense, the existence of Bonnor–Ebert spheres in nature gives us an interesting laboratory to examine star formation in isolated clouds. Stars in clusters are the products of the fragmentation of filaments, with progenitor cores that are unlikely in hydrostatic equilibrium (Ballesteros-Paredes et al., 2003; Men'shchikov et al., 2010; André et al., 2010; Arzoumanian et al., 2011). An isolated laboratory however gives us direct insight into which physical processes are important by providing us with simple initial conditions that we can simulate with differing physics. Turbulence in cores can also be modelled separately to judge its relative significance in the recipe of making a star.

There is a long history of theoretical and numerical research into the

evolution of isolated spherical cores going back to the first one-dimensional calculations, including the effects of radiation transport (Larson, 1969; Penston, 1969). Larson (1969) discovered that a uniform sphere of gas quickly collapses into a compact first core when the gas becomes optically thick. The resultant density profile that resulted was $\rho \propto r^{-2}$. This type of analysis was later performed on a Bonnor–Ebert sphere model and produced qualitatively similar results (Foster & Chevalier, 1993).

A form of the collapse that is quasi-static and singular (perhaps corresponding to later stages of accretion) was solved for self-similar models by Shu (1977) who found that when the first core collapses, it attains a $\rho \propto r^{-3/2}$ profile, whereas the outer envelope retains the r^{-2} profile. The accretion rate for such a solution was $dM/dt = 0.96\ c_s^3/G$, much smaller than accretion rates found in numerical simulations of the collapse of Bonnor-Ebert spheres (Banerjee et al., 2006).

The recipe for making a star requires the addition of rotation, magnetic fields, turbulence and radiation. This makes the whole process a bit more problematic as the physical effects are highly coupled.

2.2 Angular momentum and magnetic flux

Observations of cores reveal rotational energies are usually much smaller than gravitational energies such that $\beta_{\rm rot} \equiv E_{\rm rot}/E_{\rm grav} \approx 2 \times 10^{-3} - 1.4$ with typical values of $\beta_{\rm rot} = 0.02$ (Goodman et al., 1993). These correspond to approximate angular momenta of around 10^{54} g cm s^{-1}. When compared to the angular momentum of our Sun $L_\odot \approx 10^{49}$ g cm s^{-1}, there is a mismatch, which is designated as the "Angular Momentum Problem" of star formation. There must be

a way to remove this excess angular momentum from the cloud or protostellar disk before material collapses onto the star. Various modes of redistributing angular momentum exist, such as vertical extraction by disc winds, viscous stresses in discs, spiral waves which distribute angular momentum outwards in the disc or fragmentation (Larson, 2010).

An important mode of transporting this angular momentum before collapse occurs is by magnetic braking (e.g. Mouschovias & Paleologou, 1980; Basu & Mouschovias, 1994). This can occur for any object rotating faster than its ambient medium with both threaded by the same magnetic field lines. Alfven waves, which are transverse MHD waves that propagate along field lines, are launched into the ambient medium and angular momentum is extracted from the embedded object. The magnetic braking torque on a typical disk is (e.g. Lai, 2003)

$$\tau_{\rm braking} = \frac{1}{2\pi} R B_z B_\phi^+ \hat{\boldsymbol{z}}, \tag{2.6}$$

where B_ϕ^+ is the magnetic field just above the disk midplane, R is the distance from the star. The timescale for this process to happen depends on the contrast in densities between the disk and envelope densities (Mouschovias & Paleologou, 1980)

$$t_{\rm braking} \approx \frac{8}{15} \frac{\rho_{\rm disk}}{\rho_{\rm env}} \frac{R}{v_{\rm A,env}}, \tag{2.7}$$

where $v_{\rm A,env} = B_{\rm env}/\sqrt{4\pi\rho_{\rm env}}$ is the Alfven speed of the envelope. Note that this analysis was originally intended for the magnetic braking of a core embedded in a molecular cloud.

2.2.1 Disk warping

Jets are observed to precess (Gueth et al., 1998; Arce & Goodman, 2001a). In the context of disk wind theory, this implies that their source disks should precess. A magnetic instability in disks can occur which is very similar to magnetic braking whereby the field threading the disk warps its midplane. Lai (2003) considered a thin disk threaded by a somewhat general magnetic field. By adding perturbations to rings of material in the disk, he showed that interactions of radial currents in the ring with background field produces net torque which increases the imposed mis–alignment. This instability leads to a disk warp and retrograde precession. The onset of disk warping has been recently achieved in Class 0 disks (Duffin et al., 2012b,a, see also Chapters 4 and 5). This helps explain why protostellar outflows precess and why a disk's angular momentum is mis–aligned with respect to the angular momentum of its star (for example, our Solar System is mis–aligned with the Sun by 7.15° (Beck & Giles, 2005).

2.2.2 Non-ideal magnetohydrodynamics

The star formation rate in the Galaxy is smaller than what we expect. Typical freefall times for molecular clouds are $t_{\rm ff} \approx 4 \times 10^6$ yr for densities $n = 10^2$ cm^{-3}. There is about $10^9 M_\odot$ of molecular gas inside the solar circle. If molecular clouds create stars in a freefall time, we'd naively expect $\dot{M}_* = 250 M_\odot$ yr^{-1}, which is 2 orders of magnitude greater than the observed rate $\dot{M}_* = 3 M_\odot$ yr^{-1} (Zuckerman & Evans, 1974; McKee, 1999). This led early studies to suggest that the supersonic turbulence observed in molecular clouds supported them against collapsing too quickly (Zuckerman & Evans,

1974). What may in fact be happening is a complex interaction between protostellar outflows, magnetic fields, radiation and even the interaction of larger scale turbulent motions (Wang et al., 2010; Bate, 2012; Krumholz et al., 2012). Over the last decade, simulations have shown that molecular clouds need not be equilibrium objects - and may only have to form a burst of stars before the gas is dispersed again through "feedback" effects. Only the densest self-gravitating part would form stars. Large scale simulations of molecular clouds and what may regulate star formation rates are further discussed in §2.3 (see also Mac Low & Klessen, 2004; McKee & Ostriker, 2007; Larson, 2010).

To understand the galactic star formation rate, along with the angular momentum and magnetic flux problems, molecular clouds were once thought to be sub–critical in their mass–to–flux ratios (Mestel & Spitzer, 1956). Only through the slow accretion of gas through field lines and the straightening of magnetic field lines by ambipolar diffusion could cores obtain super–critical mass–to–flux ratios. For sub–critical cores, the evolution of their mass–to–flux to super–critical via ambipolar diffusion takes roughly ≈ 10 Myr (Fiedler & Mouschovias, 1993; Duffin & Pudritz, 2008). During this time, clouds would collapse along field lines to form giant thin disks. Note that if all molecular clouds inside the solar circle evolved on an ambipolar diffusion timescale, star formation rates would be $10^9 M_\odot / 5 \times 10^8 yr = 2 M_\odot$ yr^{-1}, where we use 5×10^8 yr as a more accurate approximation of the AD timescale for $n = 10^3$ cm^{-3} (McKee, 1999). We'd also expect to observe many uncollapsed cores in the Galaxy.

Ambipolar diffusion is a phenomenon that occurs in magnetized gas in molecular clouds because the ionisation rate is typically very low ($n_{\rm ions} \approx 10^{-7} n_{\rm H}$). Although the process is not entirely diffusive (Brandenburg & Zweibel,

1994; Duffin & Pudritz, 2008), it is often modelled as such. The neutral molecules and atoms interact with the ions in the gas (electrons as well, but they are much less massive than the ions). The neutrals feel the magnetic force through these collisions with the ions. The field will diffuse over time with diffusivity

$$\eta_{\rm AD} = \frac{1.4B^2}{4\pi\gamma_{\rm AD}\rho_i\rho_n}, \tag{2.8}$$

where $\eta_{\rm AD}$ is the diffusivity of the magnetic field in the induction equation, ρ_i is the density of the ions, ρ_n is the density of the neutrals and $\gamma_{\rm AD}$ is the drag coefficient. Typically $\gamma_{\rm AD} \approx 3.28 \times 10^{13}$ g^{-1} cm^3 s^{-1} for molecular clouds where ions are HCO^+ or Na^+ and neutrals are H_2 (McDaniel & Mason, 1973). One usually models the ion density as a function of the neutral gas $\rho_i \propto \rho_n^{0.5}$ such that $\eta_{\rm AD} \propto B^2/\rho_n^{3/2}$. See Chapter 3 or Duffin & Pudritz (2008) for a complete discussion.

This picture of quasi–static collapse was overturned by two observational advances: that molecular clouds are supersonically turbulent (Larson, 1981) and that molecular clouds are on average super–critical in their mass–to–flux ratios (Crutcher, 1999; Troland & Crutcher, 2008, but note, not *all* clouds are!).

The turbulence in molecular clouds is Alfvenic in general ($v_A \approx v_{\rm rms}$), so magnetic fields will play a role. The effect of the magnetic field is to lower star formation rates per free fall time by slowing down the gas and narrow the log–normal distribution in the N–PDFs (Nakamura & Li, 2008; Padoan & Nordlund, 2011). Ambipolar diffusion may be accelerated due the turbulence in molecular clouds by a factor 2-4.5 (Li et al., 2012). The importance of ambipolar diffusion on cloud scales still exists, but its role is diminished as

molecular clouds typically evolve in a crossing time, except in the cases where mass–to–flux ratios are sub–critical (Kudoh et al., 2007; Nakamura & Li, 2008).

Where ambipolar diffusion and other non–ideal effects (such as Ohmic diffusion) are expected to be important are on the scales of protostellar disks. Non–ideal MHD disks have been shown in numerical simulations to fragment more easily (Duffin & Pudritz, 2009), form rotational structures more easily (Duffin & Pudritz, 2009; Mellon & Li, 2009; Dapp & Basu, 2010; Inutsuka et al., 2010) and launch different morphologies of outflows (Duffin & Pudritz, 2009) as compared to disks with purely ideal MHD.

Numerically, it is hard to model ambipolar diffusion because timesteps vary as the inverse of the cell-size squared $\Delta t_{\rm AD} \propto \Delta x^2$. As the simulation resolves smaller scales in a problem, the timestep decreases significantly. Much of the difficulty in modelling this can be solved either by implementing a purely implicit method (Tilley & Balsara, 2008), or through the use of super–time–stepping on an explicit diffusive method (Alexiades et al., 1996; O'Sullivan & Downes, 2007; Choi et al., 2008). In the super–time–stepping method the stability of the code is only ensured over a super–step of N smaller timesteps, which can give a factor 10 or more increase in the effective timestep (see discussion in §6.2).

The angular momentum problem is more than adequately solved by magnetic braking without the need of the old picture of quasi–static collapse. We discuss recent developments in disk formation theory that argue the problem is how to stop magnetic braking so that a disk can form.

2.2.3 Magnetic braking of disks

One of the surprises of recent MHD simulations is that magnetic braking can be so strong that disk formation is impeded. Recent simulations have shown that in 2D collapse of isothermal toroids (Li & Shu, 1996), magnetic braking does too good a job of extracting angular momentum and disks cannot form (Allen et al., 2003; Galli et al., 2006). Further numerical investigations found that only in either the hydrodynamic limit ($\mu/\mu_0 > 10$ Mellon & Li, 2008, 2009; Hennebelle & Fromang, 2008; Hennebelle & Ciardi, 2009) or in the limit of unrealistic magnetic diffusion (Li et al., 2011) could rotationally supported disks form. Neither of these limits are expected in general (unless turbulent magnetic diffusion of the field is much stronger than we expect).

The angular momentum problem has now been labelled the *magnetic braking catastrophe*. These results appear to contradict the observational facts - protostellar disks are commonly observed in the youngest class of protostellar systems we know of. Sub-mm observations of early Class 0 and Class 1 sources have been found to have disk–like contributions on scales greater than 100 AU (Jørgensen et al., 2009; Enoch et al., 2011). How can we reconcile theory which predicts that magnetic braking prevents disks from forming in these early stages of star formation with observations which show they are common?

One solution to this problem may be that turbulence acts to scramble the mean magnetic field thereby decreasing the effective magnetic braking torque and allowing disks to form (Seifried et al., 2012a; Duffin et al., 2012b). The exact way in which this works is described in Chapter 4. Another possibility is that the envelope is cleared out by protostellar outflows, so that the timescale of magnetic braking increases sufficiently as described by Equa-

tion (2.7). However, Class 0 objects have disks, and still have a significant component of their envelope (Jørgensen et al., 2009; Enoch et al., 2011).

A further way to form a disk is by decoupling the magnetic field completely on the scale of observed disks (50-100 AU) due to magnetic diffusion. Dapp & Basu (2009) show that disks can form on scales of $10R_{\odot}$ very early on. Using a more general approach in 3D, Inutsuka et al. (2010) find large 60 AU magnetically decoupled regions and associated disks. This may in part be the solution to the problem, however, detailed calculations show that for column densities in these early phases, dead zones are less than 10 AU or smaller because of ionization by X-rays and cosmic rays (Matsumura & Pudritz, 2003). Detailed 2D simulations also demonstrate that for high mass–to–flux values an 'unrealistic' amount of magnetic diffusion would be necessary to promote disk–formation (Li et al., 2011).

While much angular momentum is lost during the formation of the disk due to magnetic braking, simulations show that the star or sink particle still has too much angular momentum. In the formation of a Sun–like star from the collapse of an isolated BE–sphere, Duffin et al. (2012a) created sink particles with radius 3.2 AU, mass 0.3 $M_{\odot}$ and angular momentum $L = 10^{51}$ g cm^2 s^{-1}. Although this is more than 10^3 times smaller than the angular momentum originally in the core, it is still 100 times larger than the angular momentum currently in the Sun. On scales closer to the star, the coupled driving of a protostellar wind, driven by accretion power released by magnetospheric infall from the disk, regulates the stellar angular momentum (Matt & Pudritz, 2005). Such wind torques can spin down stars under 10% of their break-up speed provided mass loss from the disk surface follows the relation $\dot{M}_{\rm wind} \approx 0.1\dot{M}_{\rm accretion}$ (see section 2.4).

2.2.4 Magnetic fields and disk stability

Magnetic fields in the disk, in the core and in the molecular cloud act to reduce fragmentation (Price & Bate, 2007; Hennebelle & Teyssier, 2008; Duffin & Pudritz, 2009; Commerçon et al., 2010). Magnetic tension (with force density $\boldsymbol{f}_T = 1/4\pi(\boldsymbol{B}\cdot\boldsymbol{\nabla})\boldsymbol{B}$) arises when large gradients of magnetic force are generated. This is the case in the turbulent fragmentation of molecular clouds and in the fragmentation of cores and disks due to gravitational instabilities. The support can be so strong as to reduce the amount of fragmentation seen in simulations. This problem, in the theory literature, has now been called the *Fragmentation Crisis* (Hennebelle & Teyssier, 2008; Commerçon et al., 2010). It seems that in low–mass star formation with low levels of perturbations binaries only form when rotational energies are very high (e.g. Price & Bate, 2007) even when considering ambipolar diffusion (Duffin & Pudritz, 2009). It remains to be seen if a low level of turbulent velocity field could cause the necessarily level of fragmentation to explain the observed binary rate in stars (Duquennoy & Mayor, 1991; Kroupa, 2001).

One method of determining if a disk undergoes gravitational fragmentation, in the absence of a magnetic field, is by the Toomre parameter

$$Q = \frac{\kappa c_s}{\sqrt{\pi G \Sigma}}, \tag{2.9}$$

where Σ is the surface density, κ is the epicyclic frequency and c_s is the sound-speed. This parameter encapsulates the balance between self–gravity (Σ) in the disk in opposition to its internal pressure c_s and shear from differential rotation κ. For values of $Q < 1$, protostellar discs are unstable to forming spiral density waves or to fragmenting gravitationally. Additionally, the cooling

time in the face of turbulent heating in the disk must be less than a rotation period,

$$t_{\rm cool} < \frac{\xi}{\Omega(R)}, \tag{2.10}$$

where $t_{\rm cool}$ is the cooling time and Ω is the local rotation rate and ξ is a fudge factor (Gammie, 2001).

For magnetised disks, the important addition to the physics is the strength of the magnetic energy relative to the thermal energy, encapsulated by the plasma beta $\beta = c_s^2/v_{\rm A}^2$. One can write a modified version of the Toomre parameter as (Kim & Ostriker, 2001; Peters et al., 2011a)

$$Q_{\rm M} = \frac{\kappa(c_s^2 + v_{\rm A}^2)^{1/2}}{\pi\Sigma G} = \sqrt{1+\beta^{-1}}Q. \tag{2.11}$$

Typical values of β are $10^{-3} - 10$ in early protostellar disks, but are always highest in the disk plane (as $B_\phi \to 0$ in the disk midplane). Indeed there will be regions of considerable magnetic support in accretion disks for the lowest values of β.

2.3 Forming the seeds of star formation

The initial mass function (IMF) of stars is the statistical mass distribution of newly formed stars. The observed IMF is very similar within observational constraints over a wide variety of star forming environments, including old, present day, metal–rich, metal poor, small and large clusters of stars (Kroupa, 2002). This is a somewhat surprising result as we'd expect differences in fragmentation properties based on how efficiently the gas can cool, how turbulent the initial conditions are and how strong the magnetic field is. Stars seem to

be made in a very similar way despite a range of differing physical conditions. Understanding this fundamental observational result has become one of the most important problems in star formation (McKee & Ostriker, 2007; Larson, 2010).

Very early on it was observed that the number distribution for high mass stars decreased as a power–law function of mass (Salpeter, 1955). We write the relative concentration of stars $\xi_{\rm L}(\log m)$ as a function of mass $\log m$ in the following manner

$$\xi_{\rm L}(\log m) \propto m^{-\alpha}, \tag{2.12}$$

where $\xi_{\rm L}(\log m) d\log m$ is the number of stars in the mass interval $\log m$ to $\log m + d\log m$. Early measurements of stars from masses 0.4 - 10 $M_\odot$ found $\alpha = 1.35$ (Salpeter, 1955). This is the so–called 'Salpeter IMF', and it has been modified only very slightly since then to include a small uncertainty $\alpha = 1.3 \pm 0.3$ (Kroupa, 2001).

The value of α varies for lower masses and the distribution appears to turn over around $0.5 M_\odot$. The overal distribution has been modelled successfully several different ways. A model by Kroupa (2001) fits the IMF with a varying power–law fit such that

$$\alpha = \begin{cases} -0.7 \pm 0.7 & 0.01 \leq m/M_\odot < 0.08, \\ 0.3 \pm 0.5 & 0.08 \leq m/M_\odot < 0.5, \\ 1.3 \pm 0.3 & 0.5 \leq m/M_\odot < 1.0, \\ 1.3 \pm 0.7 & 1.0 \leq m/M_\odot \end{cases} \tag{2.13}$$

Using a log–normal function with a power–law tail to fit the mass func-

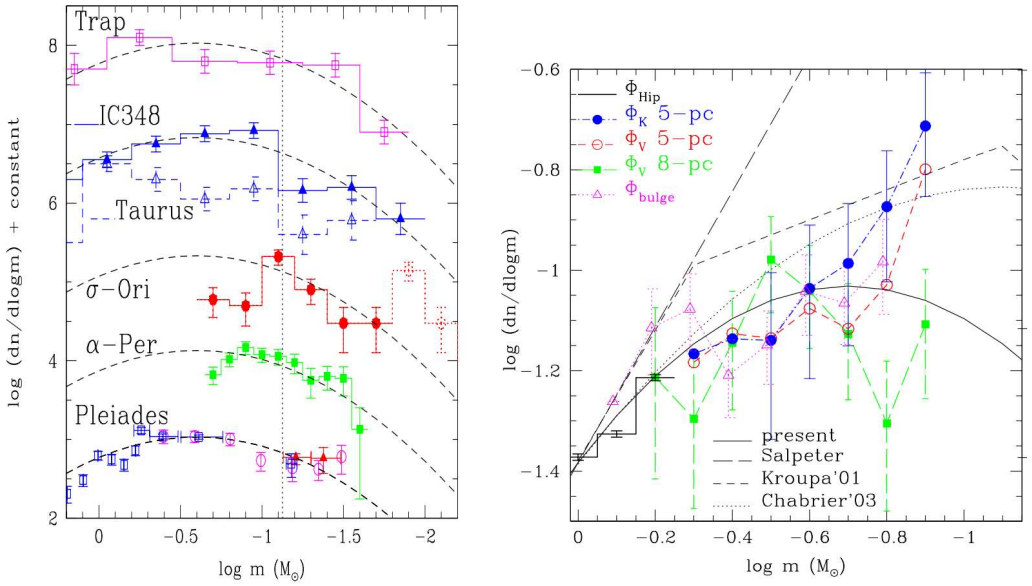

Figure 2.3 Initial mass function fits to observed mass distributions. On the left, several young low–mass systems fit with a scaled version of the IMF as presented in Equation (2.14). The dotted vertical line represents the Hydrogen burning limit, the dashed line the model. On the right, the model in Equation (2.14) is fit and compared to other IMF models, such as the one presented by Kroupa (2001) in Equation (2.13) and by Salpeter (1955). Both figures taken from Chabrier (2005)

tion, Chabrier (2005) found a form of the observed IMF as

$$\xi_{\rm L}(\log m) = \begin{cases} 0.093 \exp -\frac{(\log m - \log 0.2)^2}{2\times(0.55)^2}, & m \leq 1 M_\odot, \\ 0.041 m^{-1.35\pm0.3}, & m > 1 M_\odot, \end{cases} \tag{2.14}$$

This function has a typical turn–over at $m \approx 0.5 M_\odot$. This function is plotted against several young clusters in Figure 2.3 and compared to other model fits. The log–normal function provides an excellent fit to the data.

One way of attempting to explain the universal appearance of the IMF is first through the formation of dense cores. Indeed observations suggest that there exists a one–to–one relation between the core mass function (CMF) and

the IMF. Recent observations using Herschel have shown that the observed mass function of dense cores has the same form as the IMF although at higher masses by a factor 2.5-5 corresponding to a star formation efficiency $\varepsilon_{\rm core} \equiv M_{\rm star}/M_{\rm core} = 0.2 - 0.4$ (André et al., 2010). The difference is assumed to come from the clearing of mass away from the core by protostellar outflows (e.g. Matzner & McKee, 2000).

The exact physical nature of early outflows has been incomplete until the advent of numerical simulations into late stages of protostar formation (Seifried et al., 2012b; Duffin et al., 2012a). Numerical simulations find that protostellar winds are not as efficient at clearing mass as required to explain the observed differences between the CMF and the IMF. A number of different studies find star formation efficiencies of $\varepsilon_{\rm core} = M_{\rm star}/M_{\rm core} \approx 0.5 - 0.75$ (Machida & Matsumoto, 2012; Duffin et al., 2012a; Price et al., 2012) and in this thesis we find a value of 0.63.

Perhaps the similarity of the CMF to the IMF does not suggest a star formation efficiency for individual cores. Different cores should evolve into stars at different dynamical timescales corresponding to their free fall times. Even if the CMF resembled the IMF at one stage, it would evolve quickly into something else as stars are formed (Clark et al., 2007).

The proposed functional form of the CMF and IMF is useful from a theoretical stand–point because log–normal distributions in general can be explained by multiplicative processes (such as shocks). A supersonic turbulent gas, such as the typical molecular cloud, rapidly builds up a log–normal distribution in its column densities (Padoan et al., 1997; Kevlahan & Pudritz, 2009; Federrath et al., 2010b). The high mass end of the IMF may be explained by either gravity (Kainulainen et al., 2009; Ballesteros-Paredes et al., 2011) or

perhaps explosions of massive stars (Kevlahan & Pudritz, 2009).

Numerical simulations are now in a state where resolutions and computational resources allow them to generate enough statistics to test the IMF (Wang et al., 2010; Bate, 2012; Krumholz et al., 2012). Radiative heating of the gas is of particular importance, however. So too are magnetic fields and protostellar outflows. Newly forming stars inject kinetic energy and momentum back into their environment and this can help slow the star formation rate provided the outflows are strong enough (Krumholz et al., 2012). Wang et al. (2010) find that the coupled injection of outflow–like momentum from sink particles and magnetic fields helps contain the outflowing energy in the molecular cloud and slow the global star formation rate even further. This may be why the Galaxy has an observed star formation rate of $3M_{\odot}$ yr^{-1}, much lower than what would be expected for gravity alone (Zuckerman & Evans, 1974; McKee, 1999).

Protostellar outflows within larger simulations are crudely modelled as a boundary condition of sink particles in these simulations. As we will see in §2.4 the physical properties of early outflows are not entirely understood. Their exact structure, energy and momentum are important for properly modelling feedback into newly forming star clusters. The amount of mass cleared from a protostellar core may help us understand why the CMF looks like the IMF of stars.

2.3.1 Cooling and radiative feedback

As a protostellar core collapses and forms a protostar, radiation is emitted back into the gas both by the release of gravitational energy liberated by accretion

onto the star and by the star itself.

In the optically thin regine, the gas cools very efficiently to 10 K because of molecular lines and interactions between the gas and dust. As the gas becomes more dense, H_2 dissociates which costs energy and cools the gas further. Interactions between the gas and dust also play a role in cooling the gas as dust is an efficient emitter of thermal energy (e.g. numerical implementation by Banerjee et al., 2006). In the optically thick regime, radiation from these sources does not directly escape the cloud (except in the IR or at longer wavelengths), but rather is re-absorbed by the gas. Radiative energy slowly diffuses out of optically thick regions. Ultraviolet radiation from massive stars furthermore acts to ionize the gas, creating strong temperature gradients that push out much of the gas in molecular clouds.

There are different ways to model the effects of radiation transfer for low–mass stars. First, one can make assumptions about the optical depth and estimate cooling rates (Banerjee et al., 2006). This method does not allow gas to heat up from a central source, so it can be limiting in some sense, however it costs very little numerically. Offner et al. (2009) argue that radiation from low–mass protostars in a cluster environment is significant and can significantly heat protostellar cores and disks. Another way of modelling the diffusion of radiation is through flux–limited diffusion methods (Krumholz et al., 2007; Rogers & Wadsley, 2011). These methods track the diffusion of the radiation field through the gas, and can include sources such as protostars. High mass protostars dominate the distribution of luminosity and also emit UV flux which ionizes and pushes away material to form giant HII bubbles (Peters et al., 2011b).

Heating reduces fragmentation of cores by increasing the Jeans length

$\lambda_J \propto \sqrt{T}$. For disks, increasing the temperature increases the Toomre Q parameter as $Q \propto \sqrt{T}$, not accounting for magnetic support of the disk.

Heating of the gas has a profound effect on not only the fragmentation of disks (Offner et al., 2009; Commerçon et al., 2010) but also on how the turbulent cloud itself fragments and forms cores (Krumholz et al., 2007; Commerçon et al., 2011; Krumholz et al., 2012; Bate, 2012). The effects of radiation on fragmentation is comparable to the effects of the magnetic field in reducing the number of cores formed (Price & Bate, 2009; Commerçon et al., 2011). In high–mass molecular clouds in which clusters of O and B stars can form, high energy UV radiation may strip entire clusters of their gas mass, limiting the star formation efficiency more dramatically than supersonic turbulence (Murray, 2011).

2.4 Protostellar outflows

Protostellar outflows are commonly observed emanating from young, embedded Class 0/I sources (e.g. Arce et al., 2007; Cyganowski et al., 2011). These outflows are 0.1-1 pc long, rotating (Zapata et al., 2010), turbulent, containing internal shocks and kinks (Gueth et al., 1998), at times episodic (Arce & Goodman, 2001b) and in some cases precessing (Gueth et al., 1998; Arce & Goodman, 2001a). They carry mass from the envelope and momentum, which gets deposited in the surround gas.

Also observed around protostars are higher speed, Herbig–Haro objects (Bally et al., 2007). These outflows have high speeds on order of 100 km s^{-1}.

A common relation for these jets is (Ray et al., 2007)

$$\frac{\dot{M}_{\rm outflow}}{\dot{M}_{\rm disk}} \approx 0.05 - 0.1, \tag{2.15}$$

Both molecular outflows and jets show similar properties (rotation, collimation) suggesting that they are driven from a rotating disk of gas and collimated by a magnetic field. The molecular outflow from Class 0 protostar L 1157 and the evolved HH 47 jet launched from a circumbinary disk are compared in Figure 2.4. The top panel shows a precessing jet embedded in a low speed molecular flow. The bottom panel shows a high speed jet with seemingly no low speed gas associated with it. Both are highly collimated and have associated disks.

2.4.1 Magnetic towers

The magnetic tower model describes the evolution of a magnetic bubble driven by the continual winding of field lines in a rotating accretion disk (Boily & Lynden-Bell, 1996; Lynden-Bell, 2003; Sherwin & Lynden-Bell, 2007). It uses a hydrostatic approach and minimizes the total magnetic and thermal energy in the bubble, using a variational approach to solve for the bubble height and radius (Lynden-Bell, 2003; Sherwin & Lynden-Bell, 2007). The solution depends on the winding of the threading field by the disk and the ambient pressure of the envelope (ram pressure from accretion of gas is considered separately). Different pressure profiles generate different bubble configurations. For pressure that depends too steeply on height ($\log p / \log z) < -4$), the outflow bubble is quite wide (Boily & Lynden-Bell, 1996). For constant pressure, the outflow structure is more conical and centrally collimated.

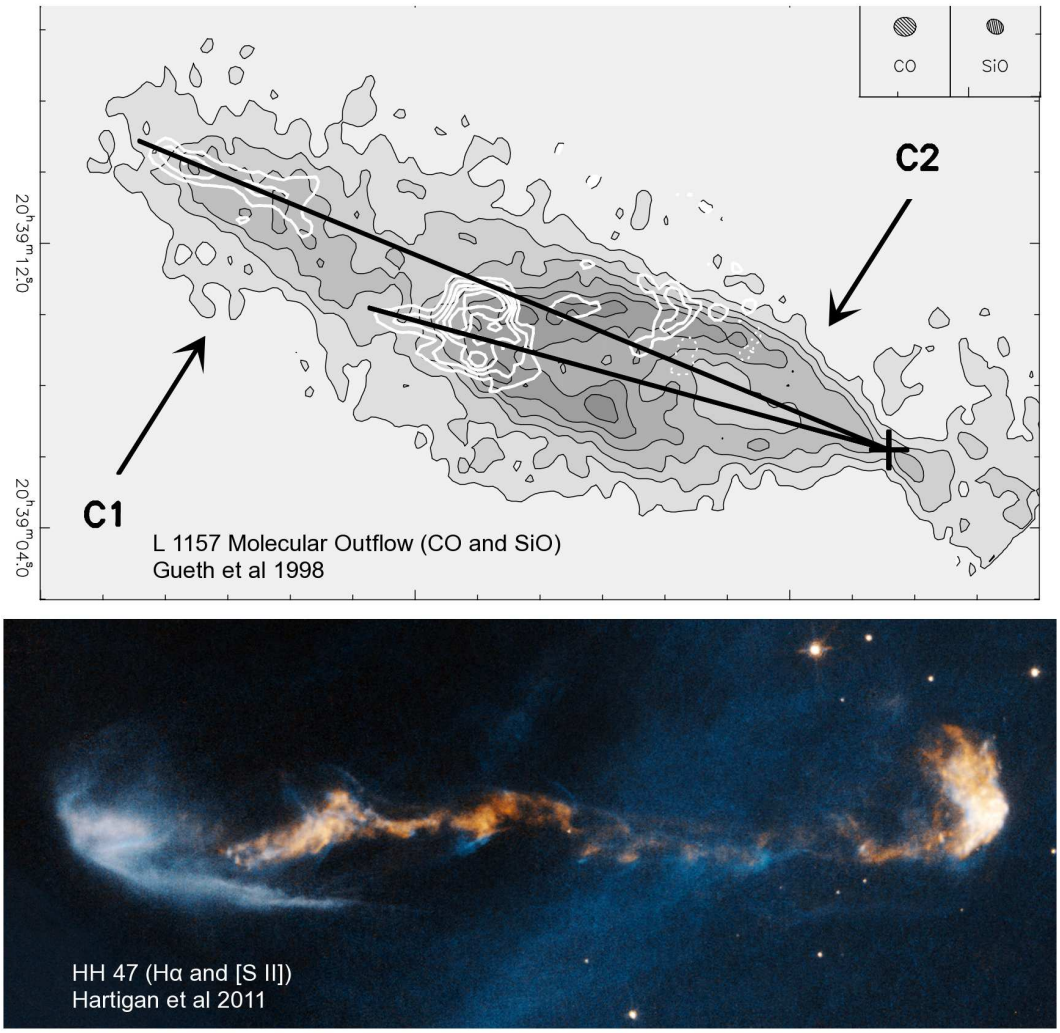

Figure 2.4 A precessing molecular outflow in L 1157 and HH 47. Above are the contours of SiO (white contours) and CO (grayscale) of the molecular outflow from the Class 0 source L 1157 (cross), taken from (Gueth et al., 1998). The SiO contours come from internal shocks in the outflow likely caused by precessing of an internal high speed component (inferred directions drawn by lines with a precession angle of $6-7°$). Each lobe is 0.23 pc. A jet is contained in the molecular outflow with speeds 50-100 km s^{-1}.
Below is an HST image of HH 57, mapping both Hα and [S II] transitions (credit NASA, ESA and P. Hartigan, see also Hartigan et al., 2011). HH 47 is 0.57 pc in length having velocities up to 300 km s^{-1}. At its source is a low mass binary system and circumbinary disk.

Field line structures are highly wound, with $B_\phi > B_z$ in the outer torus of the bubble (see middle panel, Figure 2.5). Simulations of collapsing protostars find that outflows often (but not always) have outflow cavities with these highly wrapped configurations (Lynden-Bell, 2003; Banerjee & Pudritz, 2007; Hennebelle & Fromang, 2008; Machida et al., 2009; Duffin & Pudritz, 2009; Seifried et al., 2012b).

Modelling the magnetic tower in protostellar systems analytically proves difficult largely because the disk gradually grows over time. This means that there is a changing ambient pressure profile in the envelope as well as an additional ram pressure due to accretion. Additionally, the magnetic tower model offers only a force–free ($\boldsymbol{J} \times \boldsymbol{B} = 0$) configuration for the field lines, and does not predict possible mass fluxes from the disk surface. This is an important observational test for any protostellar wind model.

Predicting cavity sizes due to the magnetic pressure in the flow is very useful for estimating the possible amount of gas cleared away from a collapsing envelope. If one was presented with a disk size and rotational profile, along with an envelope pressure scale, it would be possible to predict the outflow cavity size. Furthermore it would then be possible to estimate the amount of mass cleared away from the envelope.

2.4.2 Disk winds

Disk winds are dominated not by toroidal magnetic field pressure, but rather rely on "flinging" material through centrifugal forces. The primary aim of disk wind theory is to calculate magnetic field configurations that can accelerate gas by centrifugal driving along field lines that thread a Keplerian disk (Blandford

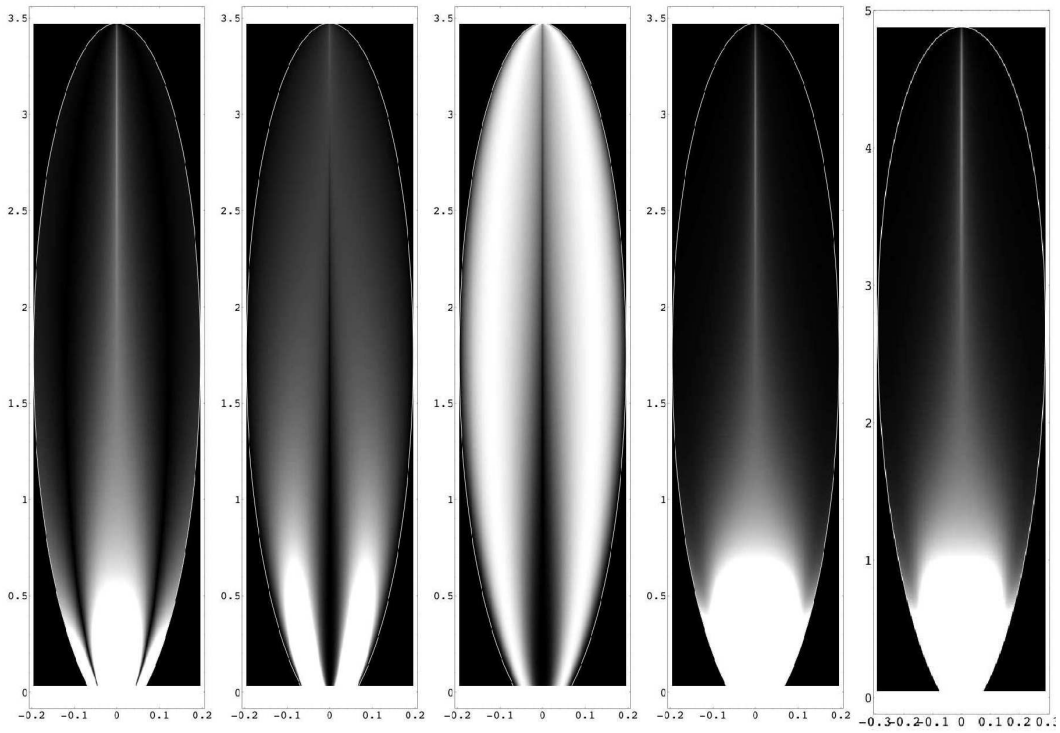

Figure 2.5 Predicted magnetic field structure of the "Magnetic Tower" model. For this model, the pressure scales with height from the disk as $p \propto z^{-3}$. From left to right: plots of $|Bz|$, $|B_\phi|$, $|B_\phi|/|B|$ and B^2 for toy model $\Omega(P)$ (disk rotation). Figure taken from Sherwin & Lynden-Bell (2007)

& Payne, 1982; Pudritz & Norman, 1986; Pelletier & Pudritz, 1992; Ferreira & Pelletier, 1995; Ferreira, 1997). It is then a straightforward task to find configurations in numerical simulations of protostellar outflows that are accelerated by the magnetic field against gravity and thermal pressure (Seifried et al., 2012b; Duffin et al., 2012a).

The self–similar model of Blandford & Payne (1982) showed that matter and angular momentum could be extracted by magneto–centrifugal driving of matter from a disk provided poloidal field lines spread out from the disk (field lines tilted more than 30° from the z–axis). The structure of the field lines are expected to be dominated by B_ϕ in the outer region, leading to high

degrees of collimation. Applied to protostellar disks, Pudritz & Norman (1986) showed in a semi-analytic way that magneto-centrifugally driven winds could explain both cold molecular flows and hot ionized jets from young protostellar objects. More importantly, the torques they exerted on the disk would extract a significant amount of angular momentum, and explain the rotation observed in protostellar outflows (Zapata et al., 2010). They predicted that the accretion rate in the disk would be related to the outflowing mass flux

$$\dot{M}_w \propto \left(\frac{r_{\rm A}}{r_{\rm d}}\right)^2 \dot{M}_a, \tag{2.16}$$

where $r_{\rm A}$ is the Alfven radius, and $r_{\rm d}$ is the radius of the disk. Pelletier & Pudritz (1992) generalised the model of Blandford & Payne (1982) in 2D and without the need for self–similarity. They derive that $\dot{M}_w = 0.1\dot{M}_a$.

This magneto-centrifugal model for disk–driven outflows has had success when applied to protostellar disks, predicting the rotational properties, mass loading, speeds and collimation (Pudritz et al., 2007). However, with the advent of simulations extending into the Class I regime (Machida et al., 2011; Duffin et al., 2012a), the model can be more directly studied. Several features are apparent in numerical simulations that challenge the standard model. Keplerian disks are not required to launch prototstellar outflows. Early outflows are launched from dynamically evolving disks that may be sub-Keplerian or even highly transient (Machida et al., 2011; Seifried et al., 2012b; Duffin et al., 2012a). Furthermore, gas may not be driven solely by magneto-centrifugal forces, but also by magnetic pressure.

A generalised numerical criterion for magnetic driving of the outflow has been developed that classifies the gas as locally being accelerated by the

magnetic field (Seifried et al., 2012b). Using assumptions from the jet theory, it can be used to compare against previous models such as Pelletier & Pudritz (1992). Duffin et al. (2012a) find a two–component flow in the Class 0 stage such that the outer regions of the protostellar outflow are highly wrapped and the inner region poloidal. The field is not co-rotational with the gas in the outer region, but co–rotational in the inner region. This suggests that in the outer regions the gas is being pushed out by the magnetic pressure rather than being flung out by the magnetic field. An outflow like this would correspond to a combination of the magnetic tower picture described above (Boily & Lynden-Bell, 1996; Lynden-Bell, 2003; Sherwin & Lynden-Bell, 2007) as well as magneto–centrifugal driven wind (Blandford & Payne, 1982; Pudritz & Norman, 1986; Pelletier & Pudritz, 1992).

Further development in disk wind theory is required to analytically model these coupled outflows. We need to know about mass flux rates in the outflow as well as their size and volume in order to understand how much mass is cleared from the envelope. Finding a simple relation between the CMF and the IMF would be a big step towards to understanding the IMF itself. The formation of log–normal density distributions in molecular clouds is understood as a result of supersonic turbulence (Padoan et al., 2001; Mac Low & Klessen, 2004; Kevlahan & Pudritz, 2009; Federrath et al., 2010b). The high–mass power–law tail is thought to be the result of global gravitational collapse of the cloud itself (Kainulainen et al., 2009; Ballesteros-Paredes et al., 2011). If these characteristics are then transfered to the cores themselves, we can begin to understand the universal nature of the CMF. It is not yet clear if protostellar outflows are the answer.

2.5 Outlook

The theory of star–formation is well on its way to understanding observational problems that have been around for over 60 years. How is angular momentum removed during protostellar collapse? How do we get low amounts of angular momentum in a protostar, but still form a protostellar disk? How is magnetic flux regulated in the collapse? Why do protostellar cores with high mass–to–flux produce stars with low mass–to–flux? Furthermore, why are stars made in a similar way in star clusters that are either old, young, metal–poor, metal–rich, big or small? Do protostellar outflows kick out gas from a collapsing core in a way that relates the CMF to the IMF in a one–to–one way?

In the following we perform numerical experiments on the isolated collapse of protostellar cores in order to answer this question. In Chapter 3, we study the early collapse of a protostellar core down to the numerical limit (pre–Class 0), comparing pure hydrodynamics with both ideal and non-ideal magneto-hydrodynamics (ambipolar diffusion). This study produces the beginnings of outflows and protostellar disks that suggest what may happen in the later stages (Class 0/I).

In Chapter 4, we extend the magnetohydrodynamic collapse by several 10^4 years by implementing sink particles. The collapse quickly forms a large, transient pseudo-disk and inner rotationally dominant sub–Keplerian disk. The disk forms as turbulent motions in the inner region – driven by magnetic buoyancy of magnetic field within the forming, flattened structure – scramble the mean threading field and reverse the magnetic braking torques on average. The magnetic structure of the inner disk drives it to warp 30° with respect to the z–axis.

We focus on the physical properties of the outflow of the collapse in Chapter 5. We find a precessing outflow which has components similar to outflows described by standard wind theory (Blandford & Payne, 1982; Pelletier & Pudritz, 1992), as well as a component driven by magnetic pressure, similar to the 'magnetic tower' (Lynden-Bell, 2003; Sherwin & Lynden-Bell, 2007). In particular, we find mass flux rates such that $\dot{M}_{\rm wind} = \dot{M}_{\rm accretion}$ in the outer region dominated by pressure. This contrasts to the inner jet region which we find has $\dot{M}_{\rm wind} = 0.1\dot{M}_{\rm accretion}$, similar to observations of protostellar jets (Ray et al., 2007; Pudritz et al., 2007).

Most importantly, in Chapter 5 we derive a high mass accretion efficiency ($\varepsilon_{\rm core} > 0.6$) which appears to be typical for isolated cores with other simulations finding efficiencies of 0.5-0.75 (Machida & Matsumoto, 2012; Price et al., 2012) in contrast to recent observations of cores in filaments (André et al., 2010) which find $M_{\rm star} = 0.33 M_{\rm core}$ and previous theoretical results which we show estimate $M_{\rm star} = 0.29 - 0.39 M_{\rm core}$. The problem we argue is that protostellar cores are dynamic over their free–fall time, accreting gas from their surroundings. Gas settles into a protostellar disk or pseudo-disk before launching of an outflow can begin, so much of the envelope has settled to the midplane by the time the core is being cleared of gas.

In Chapter 6 we discuss future prospects in numerical experiments of star formation. Namely, what is the role of turbulence in limiting the final mass onto the star? How do cores forming in turbulent environs differ from those in near isolation? Can we form a simple theoretical framework to understand the link between the CMF and the IMF? It is clear that the magnetic field is crucial at every level of star formation.

Chapter 3

The early history of protostellar disks, outflows, and binary stars

3.1 Introduction

Over the past decade numerical simulations have enabled the exploration of the central physical questions regarding the nature of star formation – from the collapse of an initial dense gaseous molecular cloud core to the formation of a star and its associated protostellar disk and outflow, and the emergence of a star's planetary system. The formation of disks and jets during star formation is central to many of these issues, but very little is known about the earliest phases of their evolution. How is the initial excessive angular momentum associated with the star's natal core removed – through magnetic braking (Basu & Mouschovias, 1994) and then outflows (Banerjee & Pudritz, 2006; Pudritz et al., 2007), or by spiral density waves in disks (e.g. Larson, 2010)? Do multiple stars form through gravitational fragmentation of cores or massive disks (Hosking & Whitworth, 2004; Price & Bate, 2007; Hennebelle

& Teyssier, 2008)? What is the significance of outflows and jets that are launched before most of the mass has collapsed into the disk (Lynden-Bell, 2003; Banerjee & Pudritz, 2006) in a wide variety of young stellar systems – from brown dwarfs (Whelan et al., 2005; Machida et al., 2009) to massive stars (Arce et al., 2007; Banerjee & Pudritz, 2007)?

Extraction of angular momentum by magnetic fields that thread the collapsing gas may be too efficient, according to recent 2D (Mellon & Li, 2008) and 3D axisymmetric (Hennebelle & Fromang, 2008) simulations, preventing the formation of rotationally dominated disks, even when the effects of imperfect coupling of the field with the gas are included (Mellon & Li, 2009). These results seemingly contradict the observations which clearly show that disks are present around most if not all young stars, even in environments in which the magnetic field is expected to be strong (Hartmann & Calvet, 1995). Hennebelle & Fromang (2008) performed 3D ideal MHD simulations of collapsing cores using a barotropic equation of state, concluding that no rotationally dominant structure formed from 10 to 100 AU for highly magnetized cores. Mellon & Li (2008) performed 2D ideal MHD simulations on collapsing singular isothermal toroids using a barotropic equation of state and an inner boundary at 6.7 AU (effectively a sink particle), finding that even moderately magnetized disks could not form. Such 2D models impose a high degree of mathematical symmetry and therefore miss the formation of bars and spiral waves in disks.

We improve on previous results through this 3D adaptive mesh refinement (AMR) investigation which includes a full treatment of the cooling (Banerjee et al., 2006) and the finite coupling of the magnetic field to the pre–stellar gas (ambipolar diffusion, Duffin & Pudritz, 2008). We find that ordered

disk–like structures can emerge on scales $\lesssim 10$ AU at early times ($\lesssim 10^5$ yrs) in magnetized systems. We have omitted a sink particle in this study as they are expected to affect the solution to within a few sink radii. Without sinks simulations are indeed limited to early disks, although they offer a full solution to the region within 10 AU where the heated core forms.

3.2 Methods

We model an isolated star forming core with a rotating Bonnor–Ebert (BE) Sphere (Bonnor, 1956; Ebert, 1955) commonly observed in nature (Alves et al., 2001; Lada et al., 2003; Teixeira et al., 2005). We construct an initial sphere that is large enough to be unstable to collapse and add a 10% over–density on top with a 10%, $m = 2$ perturbation to break axisymmetry. Such perturbations model the buffeting that observed star–forming cores undergo from supersonic turbulent gas motions that prevail in the surrounding low density molecular gas (our perturbation accounts for a 0.04% change in gravitational binding energy, so this is a rather quiescent core). The refinement criteria resolves the Jeans' length ($\lambda_{\rm J} = \sqrt{\pi c_s^2/G\rho}$) by at least 8 cells, limited by the ambipolar diffusion timestep.

Our BE spheres have a mass of $1M_\odot$ and initial central densities of $\rho_c = 6.07 \times 10^{-18}$ g cm^{-3}. The magnetic field is added to the core in the z direction – in agreement with recent observations (Kirk et al., 2009) – such that the ratio of the thermal to the magnetic energy in the gas, known as the the plasma beta ($\beta = 2c_s^2/v_{\rm A}^2$) is constant, where $c_s = 0.27$ km s^{-1} is the core's sound speed and the Alfven speed is $v_{\rm A} = B/\sqrt{4\pi\rho} \simeq 0.74 c_s/\Gamma$ (the latter relation for critical BE spheres). The mass-to-flux ratio Γ is a measure of

Model Set	low rotation	moderate rotation	high rotation
$\Omega t_{\rm ff} = \Omega\sqrt{3\pi/32G\rho_0}$	0.1	0.3	1.2
Angular rotation (Ω, s^{-1})	1.17×10^{-13}	3.52×10^{-13}	1.41×10^{-12}
Rotational beta ($\beta_{\rm rot}$)	0.0052	0.046	0.74

Table 3.1 Model parameters. Each model set has a mass of $M_{\rm core} = 1.1 M_{\odot}$, core temperature of $T_{\rm core} = 20$ K ($c_{s_{\rm core}} = 0.267$ km s^{-1}), external temperature of $T_{\rm ext} = 200$ K ($c_{s_{\rm ext}} = 0.845$ km s^{-1}), $\Gamma = 3.5$ and $\beta = 46.01$ and is run in 3 cases: hydrodynamic, ideal MHD and ambipolar diffusion.

the ratio of the gravitational to the magnetic energy in gravitating objects. If $\Gamma < 1$, the magnetic field is strong enough to prevent gravitational collapse and the core is called sub-critical, otherwise it is called supercritical. We set the mass-to-flux $\Gamma = 2\pi G^{1/2}\Sigma/B = 3.5$, where Σ is the column density, stemming from observations of magnetic fields in early cores which indicate $\Gamma \approx 1 - 4$ (Crutcher, 1999) and confirmed through simulations of cloud-scale turbulence (Tilley & Pudritz, 2007). The rotation values of our models were taken from previous simulations of early star–forming clusters (Tilley & Pudritz, 2007). We take the extremes and average values of rotation and interpret these as low, moderate and high rotating cores (Table 3.1). The moderate rotation model set has a ratio of rotational to gravitational binding energy of $\beta_{\rm rot} = 0.046$, in line with observations (Lada et al., 2003).

For each model set, we run a non–magnetic (hydrodynamic), a perfectly coupled (ideal magnetohydrodynamic) and more realistic, partially coupled (ambipolar diffusion) case for a total of 9 simulations (summarized in Table 3.1).

3.3 Do disks form?

By the time the maximum surface densities in the moderate rotation model set reach a value of $\Sigma_c = 4.2 \times 10^3$ g cm^{-2}, 0.1 $M_\odot$ is contained within 156 AU (about 10% of the core's mass is contained within 0.003% of its initial volume). The mass of the protostar (taken to be all material inside 1 AU or 10^{-3} $M_\odot$) is only 6 % of the total mass in the disk (taken to be everything inside 10 AU or 10^{-2} $M_\odot$). At this point, the non–magnetic, perfectly coupled and partially coupled clouds are 0.160, 0.194, and 0.175 million years old respectively due to different levels of rotational and magnetic support (corresponding to 5.9, 7.2 and 6.5 free-fall times, where $t_{\rm ff} = 0.027$ Myr is estimated using ρ_c of the initial BE sphere). An extended dense region has taken shape, the gas has been heated, and in the cases where magnetism is present, disk winds have started.

We present in Figure 3.1, snapshots of the structure of the region at the center of the collapse, taken at this time for our three different cases. The first panel (Fig 1a) representing the purely hydrodynamic case, is strikingly different in structure than the other 3 panels representing the magnetic cases. Despite having identical initial conditions, the non–magnetized, moderate rotation case has formed two bars, driving off–axis rotational modes which themselves create an off–axis bar. The wobbling in the collapse occurs through accretion along shocks and density perturbations in the gas. This stands in stark contrast to the obvious disk–like structures and outflows present in both ambipolar diffusion (Fig 1b) and ideal MHD cases (Figs. 1c & d)[1]. Strong oscillations of the disk radius were noted in the simulations of Price & Bate

[1]We provide movies of Figures 3.1a, b and c online illustrating the density and magnetic field line structure on all scales in the simulation.

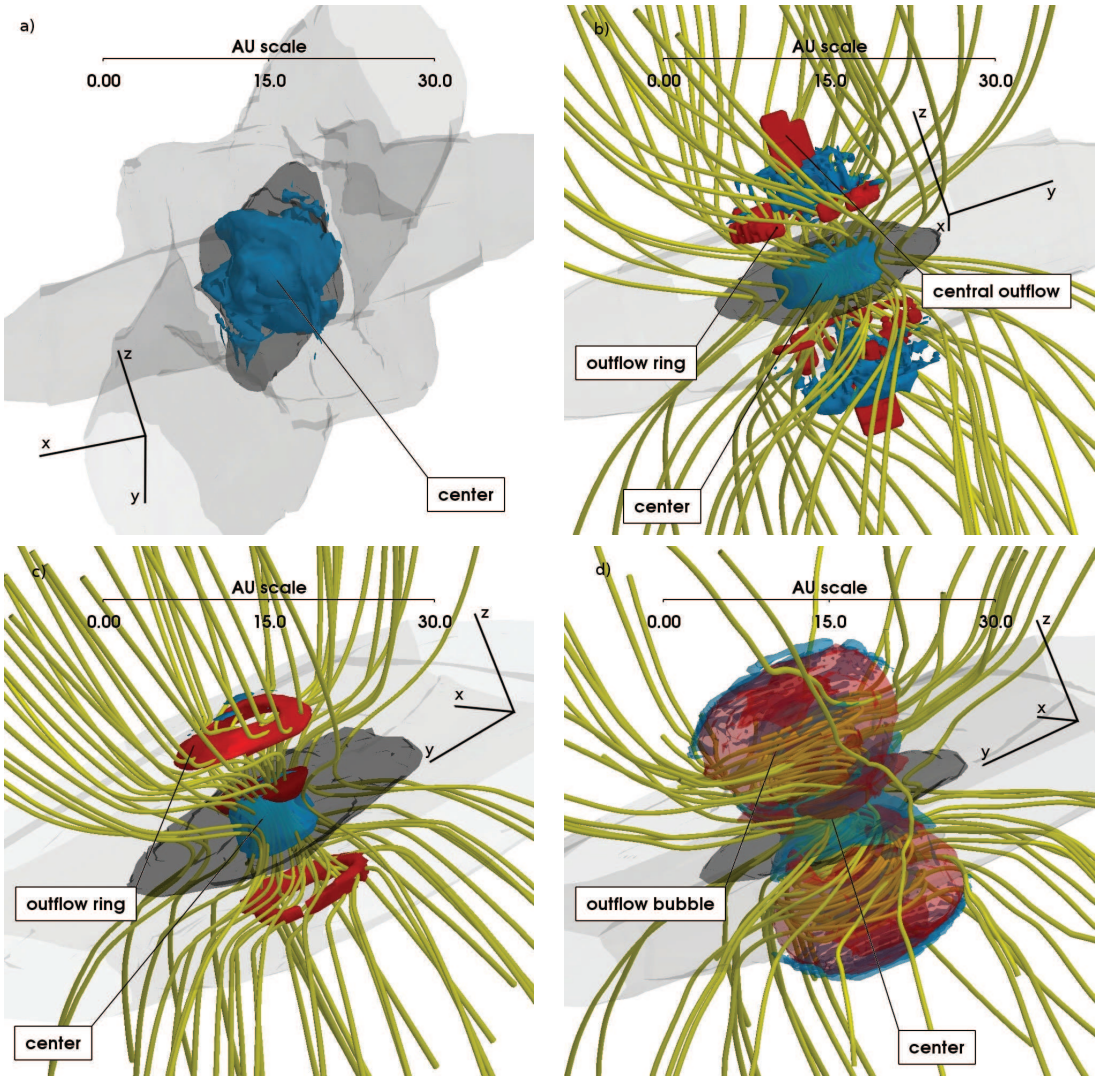

Figure 3.1 Inner disk of the moderate rotation model set at central surface densities of $\Sigma_0 = 4.2 \times 10^3$ g cm^{-2} for a) hydrodynamic, b) ambipolar diffusion, c) perfectly coupled cases and d) the evolved state of the perfectly coupled case at $\Sigma_c = 8.72 \times 10^7$ g cm^{-2}. Black and gray surfaces are $\rho = 10^{-12}$ g cm^{-3} ($n = 2.58 \times 10^{11}$ cm^{-3}) and $\rho = 10^{-13}$ g cm^{-3} ($n = 2.58 \times 10^{10}$ cm^{-3}) respectively. Temperature contours at $T = 85$ K are shown in blue. Outflow velocities contours, shown in red, are 0.3 km s^{-1} in c–d and $0.01 - 0.4$ km s^{-1} in b. Magnetic field lines are shown as yellow tubes.

(2007) which were also dominated by massive disks in their early phase. They also found that this behavior was suppressed by magnetic fields.

Most importantly, the magnetic disks, by preventing strong bars from

forming, are rotationally dominated whereas the uncoupled disk is not! This is illustrated in Figure 3.2a, where we see that the ambipolar diffusion case has a larger rotationally dominated disk ($v_\phi > v_{\rm infall}$) than the perfectly coupled case. We note also, by plotting v_ϕ/v_r of the most evolved perfectly coupled state of the collapse, that the rotational support is *growing* with time while hydrodynamic rotational support becomes increasingly unstable. In Figure 3.2a we also plot surface averaged plots of the ratio of the rotational velocity to the Keplerian velocity – the rotational velocity of a gas in a stable orbit around an enclosed mass. We find peak ratios of about 0.1–0.5 in all cases of the moderate rotation model (in fact some pre–binned values exceed 1 in the ambipolar case).

In the limit of low rotation, hydrodynamic spiral waves and bars in the purely hydrodynamic case are confined to a region of about 1 AU in radius. This has little effect on the braking of the cloud (Figure 3.2d) and rotationally dominated disks are allowed to form outside of 1 AU (Figure 3.2b). The hydrodynamic case is much more spherical in nature while the magnetized cases remain fairly flat, despite efficient magnetic braking. In the limit of low rotation, Fig. 3.2b shows that the rotation in the hydrodynamic case is nearly Keplerian and the magnetic case is much more sub–Keplerian, whereas in the case of moderate rotation shown in Fig 2a the opposite is true. Thus in the extreme low rotation limit where spiral modes and bars are strongly suppressed, early hydrodynamic disks do form.

Due to the bar, the distribution of specific angular momentum $j(R)$ (where R is the cylindrical radius; Figure 3.2d) of the hydrodynamic case is comparable to the cases where magnetic braking is present. In the low rotation model set, the bar is small and $j(R)$ does not compare as well to the magnetized

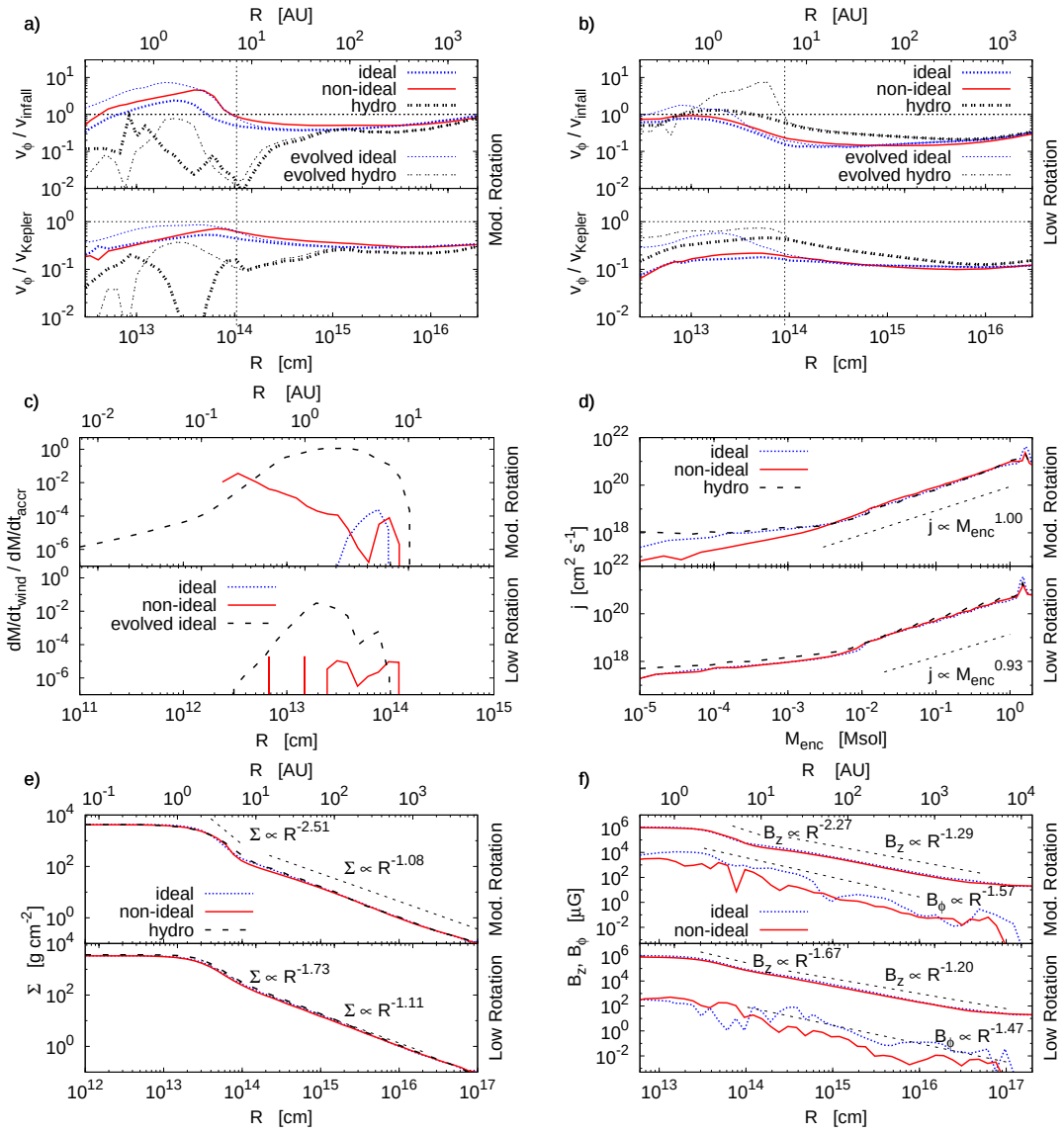

Figure 3.2 Azimuthally averaged plots (density weighted, see Banerjee & Pudritz, 2006) versus disk radius for ideal MHD, non–ideal MHD and hydro cases. In all figures the model sets are shown at a common central surface density of $\Sigma_c = 4.2 \times 10^3$ g cm^{-2} (moderate or mod. rotation) and $\Sigma_c = 3.4 \times 10^3$ g cm^{-2} (low rotation), when viewed face on. Figures a) and b) show the toroidal velocity in units of infall velocity and Keplerian velocity for the moderate and low rotation model sets respectively ('evolved' refers to hydro and ideal MHD end–states). The dotted horizontal lines represent a velocity ratio of 1. The dotted vertical lines represent a transition radius of 7 and 6 AU respectively. Figure c) shows the outflow efficiency of the magnetized cases as compared to the more evolved ideal MHD case. Figure d) shows specific angular momentum plotted against enclosed mass. The surface density distributions are shown in e), while the magnetic field distributions are shown in f).

cases. The hydrodynamic and perfectly coupled cases of the moderate rotation model set have similar maximal accretion rates of $\dot{M}_{\rm accr} \approx 4 \times 10^{-4}$ M$_\odot$ yr^{-1}, while the ambipolar case reaches maximal accretion rates of only $\dot{M}_{\rm accr} \approx 1 \times 10^{-4}$ M$_\odot$ yr^{-1} due to weaker magnetic braking and a stable disk. In the low rotation model set, mass accretion rates are $\dot{M}_{\rm accr} \approx 2 \times 10^{-4}$ M$_\odot$ yr^{-1} for the magnetized cases and $\dot{M}_{\rm accr} \approx 3 \times 10^{-4}$ M$_\odot$ yr^{-1} for the hydrodynamic case.

In the high rotation model set however, no cases form rotationally dominated disks as all three cases have formed some sort of bar on large scales (Figure 3.3). Clearly, it is through the suppression of instabilities in the collapse that magnetic fields promote early disk formation. Disk formation in systems without magnetic fields typically must wait until the mass of the central star dominates that of the surroundings sufficiently to suppress these instabilities.

3.4 Early outflows and magnetic fields

Figures 3.1b, c, and d are snapshots of the structure of outflows that are launched at these early times. A major result, shown by comparing 3.1b, c, is that outflows occur even when ambipolar diffusion is active. Outflows in a non–ideal MHD collapse have been demonstrated in 2D ambipolar diffusion without drift heating (Mellon & Li, 2009) and in 3D using an ohmic diffusion approximation (Machida et al., 2007b). This is the first such demonstration in a 3D ambipolar diffusion code. Our analytical understanding of the early outflow mechanism is the magnetic tower (Lynden-Bell, 2003). In this picture, the toroidal field in the disk is generated through the rotating flow and confined there by the accretion ram pressure. As the field winds up, it reaches a critical

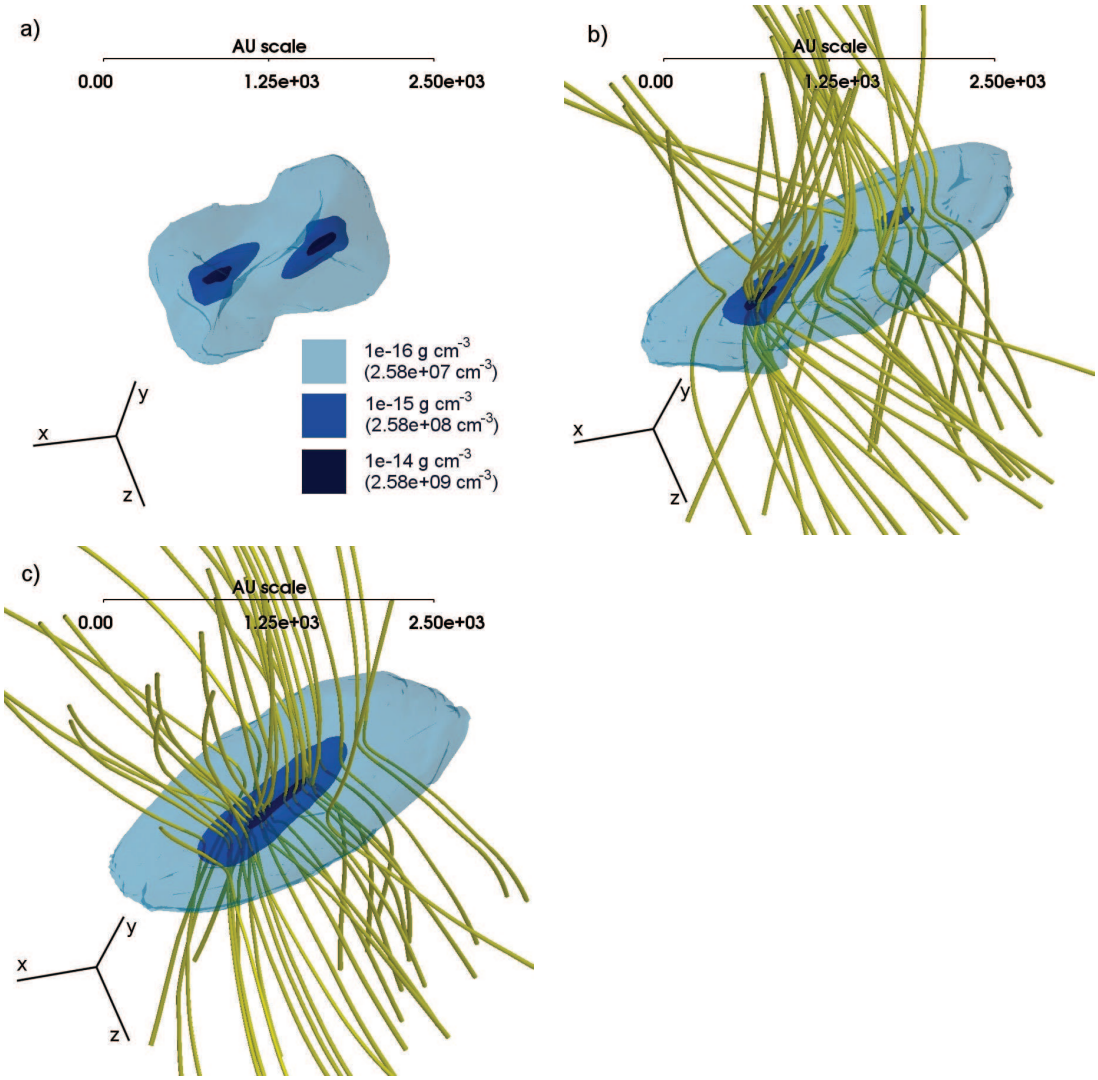

Figure 3.3 Large scale fragmentation of the high rotation model set for a) hydrodynamic , b) ambipolar diffusion and c) ideal MHD cases at similar scales and orientations. Density contours are given in the legend and magnetic field lines are drawn as yellow tubes.

strength in which the toroidal pressure is strong enough to overcome the ram pressure, moving wrapped field lines away from the disk and taking perfectly coupled gas with them – starting with the initial release in Figure 3.1c and the more developed magnetic bubble shown in Figure 3.1d). This acts to torque down the disk, removing angular momentum from the disk and increasing accretion rates[2].

In the ambipolar diffusion picture, these field lines can seep through the ram pressure as they are not so tightly coupled to the accreting gas. Effectively this leads to a smoothed out transition in the magnetic tower, with the side effect of substantial frictional drift heating.

We have also discovered the existence of a centralized, high–speed component to the ambipolar diffusion case's outflow ($v > 0.4$ km s^{-1} in an region roughly 1 AU in size). This component resembles a jet that is commonly observed in a more evolved perfectly coupled collapse (though less efficient)[3]. We note that the base of this component to the outflow lies on a cushion of heat generated by the friction between ions and neutrals as toroidal field lines seep through the accreting gas. This spike in drift heating is typical in ambipolar diffusion mediated C-shocks, regions where ion–neutral friction is strong (Wardle, 1991). This local heating effect produces strong gradients in temperature with $T > 110$ K in regions roughly 5 AU in size, both above and below the midplane. Within these regions are features roughly 1 AU in size with $T > 1000$ K (not unheard of in C–shocks). By comparison, the perfectly coupled outflow has a sharp temperature shock at about 50 K leading its outflow. In contrast, the low rotation model set shows very little drift heating and a

[2]A movie of the development of Figure 3.1d from Figure 3.1c is provided online.

[3]The velocity structure of the perfectly coupled outflow is seen in our online movie of the evolution of Figure 3.1d

similar weak outflow (Figure 3.2c). While the vertical field threading the disk B_z is identical for all low and moderate rotation, magnetized cases (Figure 3.2f), the toroidal field B_ϕ in the low rotation, magnetized cases is nearly 2 orders of magnitude smaller than in the moderate rotation, magnetized cases.

In Figure 3.2c we plot the ratio of mass loss rates $\dot{M}_{\rm wind}$ to mass accretion rates $\dot{M}_{\rm accr}$ for the moderate and low rotation model sets. For comparison we also plot this ratio for the evolved outflow of the perfectly coupled case at later times (labeled 'evolved ideal'). The evolved outflow is very efficient in the moderate rotation, ideal MHD case – the central outflow component exceeds speeds of 5 km s^{-1} and observed outflow rates of $\dot{M}_{\rm wind}/\dot{M}_{\rm accr} \sim 0.1$ (Hartmann & Calvet, 1995). Unfortunately, we cannot fully develop the ambipolar outflow due to timestep constraints. However, from this early footprint, we are led to believe that the outflow mechanism is working, and working nearly as well as the perfectly coupled case. In the low rotation, ideal MHD case, the outflow rates are significantly diminished by nearly 2 orders of magnitude in comparison to mass accretion rates, less than what is typically observed. This may have consequences on feedback effects in star forming clusters and the assembly of massive stars (Wang et al., 2010); protostellar energy injection is dependent on the rotational energy of the star forming core.

3.5 Fragmentation and binaries

In supercritical cores, 3D ideal MHD calculations have shown that strong perturbations (on the order of 50%) are needed in order for cores with $\Gamma \sim 2$ to fragment and form binaries, even with high rotation (Price & Bate, 2007; Hennebelle & Teyssier, 2008). We find that none of the low and moderate

rotation cases, magnetised or not, fragment. We therefore ran a high rotation model set with 4 times the angular rotation than our earlier model set (roughly 20 times the rotational energy, an extreme rotation (Tilley & Pudritz, 2007)), similar to the simulations of Price & Bate (2007) with a 10% perturbation amplitude. In Figure 3.3 we plot 3D density contours for all three cases of the high rotation model at the largest common central column density ($\Sigma_c = 68$ g cm^{-2}). The hydrodynamic case quickly fragments into a binary with a wide separation of roughly 1000 AU. The perfectly magnetized case forms a bar and does not fragment, stabilized through its magnetic pressure as well as through the effects of magnetic braking. Meanwhile, the ambipolar diffusion case produces an intermediate result. Early on a ring is formed which fragments into a bar–like massive object with a small companion at about 1000 AU.

For sufficiently high rotation ambipolar diffusion allows binaries to form without the need of strong (e.g. $\gtrsim 10\%$ in amplitude) perturbations. For typical rotation rates however, fragmentation can take place only if large perturbation amplitudes ($\approx 50\%$) are used in the initial conditions. Such a perturbation would amount to a 1% change in our BE sphere's gravitational binding energy. This relatively low level of 'turbulent' energy has been measured in B68 (Lada et al., 2003). This would suggest that a low level of turbulent energy (e.g. a few percent of the gravitational energy) is required in order to reproduce the overwhelming tendency for quiescent cores to form binaries in face of strong magnetic support.

3.6 Conclusions

In the early stages of a purely hydrodynamic collapse of a moderately rotating core, material joins the protostar by accreting through a chaotic series of bars and spiral waves. Our results show that in magnetized collapses however, the magnetic field suppresses these wave modes, and a small, regular disk appears at the earliest times. The weakening of magnetic control by ambipolar diffusion is insufficient to guarantee the formation of binary stars in typical cores with moderate rotation. Our results suggest that modest turbulent amplitudes ($>$ 10%) appear to be required. Regarding planet formation, the central density structure of early disks (Figure 3.2e) falls off as $\Sigma \propto r^{-(1.7-2.5)}$ much more quickly with disk radius than do protoplanetary disk models at later times, wherein $\Sigma \propto r^{-1.5}$ or r^{-1}. As the collapse winds up the field early outflows appear – even for partially coupled disks – and feed angular momentum and mechanical energy back into the star forming neighborhood. The density and magnetic structure of ideal and partially coupled disks is quite similar – the main difference is in the strength of the wound up magnetic field (at least an order of magnitude weaker in the ambipolar diffusions case).

Finally, we note that evidence for early localized intense drift heating near the disk at the accretion shock which heats materials up to 1,000K and beyond in a localized region, may be preserved in the observed composition of comets and meteorites. The rapid heating, and subsequent cooling of those crystalline Mg–rich silicate materials that passed through the accretion shock and through the region of high ambipolar heating is reminiscent of heating events that must have occurred for some of these materials seen in cometary grains (Wooden et al., 2007). These events have been attributed to shock

heating by spiral waves out to 10 AU in disks (Desch et al., 2005). As seen in Figure 1b, only a portion of the accreted disk material will pass through this localized heated region. Subsequent radial turbulent mixing of this flash heated material with the bulk of material that passed through a more gentle heating environment could in principle contribute to the wide mixture of thermal histories preserved in cometary grain materials.

3.7 Acknowledgements

We thank Robi Banerjee, Eve C. Ostriker and James Wadsley for fruitful discussions. DD was supported by McMaster University and REP by the Natural Sciences and Engineering Research Council of Canada. We are pleased to acknowledge the SHARCNET HPC Consortium for the use of its facilities at McMaster University. The software used in this work was in part developed by the DOE–supported ASC/Alliances Center for Astrophysical Thermonuclear Flashes at the University of Chicago. This research was supported in part by the National Science Foundation under Grant No. PHY05–51164.

Chapter 4

The long–term evolution of magnetized pre–stellar cores I: formation of warped discs.

4.1 Introduction

Our understanding of the formation and properties of protostellar discs around early, embedded protostellar objects is still quite limited although considerable effort has gone into simulating key physical attributes of early discs, such as their mass, degree of rotational support, size, and structure (Banerjee et al., 2004; Machida et al., 2006a; Banerjee et al., 2006; Banerjee & Pudritz, 2006; Mellon & Li, 2008; Hennebelle & Fromang, 2008; Duffin & Pudritz, 2009; Mellon & Li, 2009; Hennebelle & Ciardi, 2009; Bate, 2010; Seifried et al., 2011; Machida et al., 2011; Li et al., 2011; Zhao et al., 2011). The advent of the ALMA observatory will hugely accelerate our observational progress in this field, making the need for high resolution numerical simulations of disc

formation all the more urgent.

Low mass stars form in molecular cloud cores and much of the early portion of their lives is hidden behind envelopes of dense gas (Mac Low & Klessen, 2004; McKee & Ostriker, 2007). Sub-mm observations of six of the nine known Class 0 sources in Serpens were all found to have compact disc components on scales greater than 100 AU (Enoch et al., 2011). Furthermore, Jørgensen et al. (2009) observe both sub-Keplerian and Keplerian discs in a sample of 10 Class 0 and 9 Class I sources, concluding that protostellar discs must form in the pre–stellar regime.

Furthermore, theoretical work has long suggested that magnetized rotating discs would readily drive outflows through the release of gravitational energy during disc accretion (e.g. Blandford & Payne, 1982; Pudritz & Norman, 1986; Pelletier & Pudritz, 1992). Observations show that discs are coupled with 0.1-1 pc outflows (e.g. Arce et al., 2007; Cyganowski et al., 2011).

One of the surprising results of studies of gravitational collapse of magnetized parent "cores" is that under perfect magnetic coupling, it is nearly impossible to form a rotationally supported disc (Allen et al., 2003; Galli et al., 2006; Mellon & Li, 2008; Zhao et al., 2011). What forms rather is a pseudo–disc of gas, resulting from a net magnetic field along the short axis of the disc, but with mean motion inside the disc that is dominated by infall rather than rotation. However, considering the observations, there must be a way to form discs in magnetised systems early on in such a way so as to diminish magnetic braking resulting from ordered magnetic fields.

With a few exceptions, MHD simulations to this point have been unable to simulate the later evolution of Class 0/I protostellar systems starting from a natal core because of timestep constraints. As gas becomes denser, the Jeans

length decreases. We must resolve the Jeans length $\lambda_{\rm J} = (\pi c_s^2/G\rho)^{1/2}$ by at least 4 grid cells in order to ensure that our gas does not fragment artificially (Truelove et al., 1997). The timestep correspondingly decreases. Hydrodynamic simulations in SPH (Bate et al., 1995; Jappsen et al., 2005) and AMR (Krumholz et al., 2004; Federrath et al., 2010a) solved the problem of small timesteps by employing sink particles which accrete gas mass and momentum above a certain density threshold, provided it is energetically favourable for the gas to collapse. Magnetohydrodynamic (MHD) simulations of turbulent star formation employed the use of sink particles to study the effect of magnetic fields on massive star formation (Wang et al., 2010; Peters et al., 2011a; Seifried et al., 2012b, 2011), on the formation of stellar clusters (Price & Bate, 2008) and also on low mass star–forming regions using SPH (Price & Bate, 2008; Bürzle et al., 2011; Price et al., 2012). In the cases of isolated core formation, the magnetic field is an important ingredient in stabilizing the disc against fragmentation (Price & Bate, 2008; Commerçon et al., 2011; Peters et al., 2011a; Commerçon et al., 2011; Seifried et al., 2011).

Using 2D MHD simulations on a static grid, and employing a central boundary condition at 6.7 AU, Mellon & Li (2008) ran a number of simulations of collapsing singular isothermal toroids (Li & Shu, 1996) with varying initial mass–to–flux ratios from 4 to 400. The normalized mass–to–flux is defined as μ/μ_0, where μ is the mass–to–flux ratio and μ_0 is the critical mass–to–flux of $\mu_0 = (2\pi G^{1/2})^{-1}$. The authors find for $\mu/\mu_0 > 100$ (in the hydrodynamic limit) discs can form, although the magnetic field plays an important role in the dynamics. However for $10 < \mu/\mu_0 < 100$, discs did not form. Indeed, this result still stands een when ambipolar diffusion is included (Mellon & Li, 2009). It is only in the limit of unrealistic amounts of diffusion (considering

the Hall effect as well as Ohmic diffusion) that it is possible to recover discs in the strongly magnetised limit using these models (Li et al., 2011).

Three dimensional studies of collapsing cores without turbulence have found similar results; discs do not form for $\mu/\mu_0 < 5 - 10$ (Hennebelle & Fromang, 2008; Seifried et al., 2011). If the field is misaligned with the cores' rotation axis, discs can form for higher magnetic field strengths such that $\mu/\mu_0 < 3$ (Hennebelle & Ciardi, 2009). Although we note that these 3D simulations lack sink particles and have only evolved the collapse to very early pre–Class 0 phases, the disc is far from finished accreting, and not many rotation periods have passed by the end of the simulation. For instance, in similar simulations, using different initial conditions (a Bonnor–Ebert sphere) we found that we could produce a rotationally supported disc inside of 10 AU while using ideal MHD. We produced a slightly larger disc when modelling ambipolar diffusion and using the same initial condition (Duffin & Pudritz, 2009).

Using 1 AU sink particles and a prescription of Ohmic diffusion, Machida et al. (2011) show that disc formation is possible when using a 3D MHD simulation. The authors find that discs of 100 AU are possible in strongly magnetised models, primarily due to the formation of large inner regions where the magnetic field decouples from the gas due to ohmic diffusion (dead zones). Early discs form inside of this magnetic dead zone where magnetic braking cannot operate. We note that these dead zones are nearly 60 AU in radius (Inutsuka et al., 2010). Detailed calculations of Matsumura & Pudritz (2003) show that for typical high column densities in these early phases, dead zones are 10 AU or smaller. Non-ideal MHD simulations in 2D of the early collapse, spatially resolved down to stellar radii (without sink particles), also find that discs can

form in magnetically dead zones (Dapp & Basu, 2010). However, these discs are small (10 solar radii) and at very early stages.

Recently, Seifried et al. (2012a) demonstrated that Keplerian accretion discs can form if turbulence is introduced into simulations of magnetised collapse in a clustered environment. This occurs even for strong, initial mean magnetic fields. The turbulence scrambles the magnetic field and prevents a strong magnetic braking torque from building up. However, a general physical mechanism for this process is unclear.

In the present paper, we report simulations that uncover a very general mechanism by which the powerful effects of magnetic torques on early discs can be circumvented for highly magnetised cores ($\mu/\mu_0 = 3.4$). A Parker instability (Parker, 1966) arises in the inner region of the disc and magnetic loops and bubbles are shed. This is similar to the shedding of loops observed in local simulations of idealised Keplerian disks (Johansen & Levin, 2008). Most discussion of the Parker instability focuses on axisymmetric modes. However, a non-axisymmetric mode also occurs which can break symmetry above and below the xy-plane when coupled to a gravitational field that varies in height (Horiuchi et al., 1988). This has also been suggested as a way to warp galactic disks (Gomez de Castro & Pudritz, 1992).

The launching of loops and bubbles scrambles the mean magnetic field associated with the disc and outflow, leading to numerous regions of magnetic field reversal and hence localized changes in sign of the magnetic torque on the disc. The net effect is that angular momentum rather than being entirely transported by the outflow, is partially transported outward through the disc, allowing it to grow.

The resulting degradation of the mean field threading the disc by this

magnetic buoyancy has the same effect as turbulence - it reduces the effectiveness of the mean field's ability to brake the forming disc. The beauty of this mechanism is that it is self-sufficient - it is the flux trapped in the collapsing disc-like structure that generates the "turbulent" behaviour, generated by the Parker instability in the surrounding gas, which degrades the braking torque.

Our simulations are initialized with a perfectly aligned magnetic field with respect to the rotation axis. Interestingly, the disc becomes unstable to a warping instability and begins to precess. This warping instability has been predicted for protostellar discs threaded by magnetic fields such as those modelled in disc wind theories (e.g., see review by Pudritz et al., 2007). It results from magnetic torques on perturbed sections of the disc (Lai, 2003). Indeed, we show that the warping behaviour we observe is associated with the corresponding magnetic torques that we measure in the disc and the time–scales predicted by Lai (2003).The protostellar outflow itself warps our disc. Similar behaviour has been seen in simulations of accreting black holes (McKinney et al., 2012).

Another important result in our work is that the sense of disc precession is prograde with the mean rotation of the cloud – not retrograde as predicted by the MHD model of Lai (2003). This, we show, is possible in a disc where the vertical magnetic field has a number of reversals (and hence magnetic torque reversals) brought on by the intense buoyant rise of magnetic bubbles from the disc surface. We observe two clear signatures of large effective field reversals in the vertical direction, disc formation from prograde magnetic braking torques and prograde precession.

This chapter first discusses the physical properties of the disc in §4.3, its size, rotation, stability, accretion rates and magnetic structure. We com-

pare our disc precession and warping with estimates given by Lai (2003) in §4.4. We then go on to show that magnetic torques are responsible for the warping mechanism in §4.5. Furthermore, we demonstrate the existence of significant field reversals that effectively create a turbulent outflow with reversals in magnetic braking and precession torques. Finally, we discuss the relevance of significant disc warping with respect to the formation of mis–aligned Hot Jupiters.

4.2 Initial conditions and numerical methods

Different core mass–to–flux μ/μ_0 and rotation (defined by the ratio of rotational to gravitational energy, $\beta_{\rm rot}$) will produce cores with varying degrees of flattening and also change the structure of the outflow. For example, in a parameter study of high–mass cores, the variation of the magnetic field had strong consequences for disc and outflow properties (Seifried et al., 2012b, 2011). We add to the sphere uniform rotation (note that the specific angular momentum scales as $j = |\boldsymbol{r} \times \boldsymbol{v}| \propto r^2$) whose ratio of rotational and gravitational energy is high ($\beta_{\rm rot}$=0.3) and $\beta_{\rm plasma} = 2c_s^2/v_{\rm A}^2 = 19 - 21$ in the midplane, where $c_s = 0.27$ km s^{-1} is the core's sound speed. In this model, one can simplify the mass–to–flux ratio μ/μ_0 by $\mu/\mu_0 \simeq 0.74 c_s/v_{\rm A}$. We use $\mu/\mu_0 = 3.5$, a slightly super–critical core. In comparison to similar studies of collapsing high–mass cores (Seifried et al., 2011), our parameters of $\beta_{\rm rot}$ and μ represent a quickly rotating, highly magnetised core with respect to the parameter range they chose to explore.

We model our low–mass stellar core as described in previous papers (Banerjee et al., 2004; Duffin & Pudritz, 2009), by embedding an over–critical

Bonnor–Ebert sphere (Bonnor, 1956; Ebert, 1955) in a low density environment. We add to this density distribution a 10% overdensity and a 10%, $m = 2$ perturbation, such that $\rho(r) = \rho_{\rm BE}(1.1 + 0.1\cos(2\theta))$. This ensures collapse and breaks symmetry (Boss & Bodenheimer, 1979). The background is an isothermal, low density environment in pressure equilibrium with the sphere (the density is set by choosing a background that is 10 times warmer than the sphere). The box is roughly 0.81 pc in length, more than 10 times the size of the BE sphere. An important point here is that the total mass of the box is about $318 M_\odot$, while the mass of the actual Bonnor–Ebert sphere is about $1.1 M_\odot$ (with a diameter of 10^4 AU).

Modelling a core with an initial mass–to–flux ratio that is nearly critical is important for several reasons. Firstly, Zeeman measurements of nearby molecular clouds have uncovered values of $\mu/\mu_0 \approx 1 - 10$ (Crutcher, 1999; Troland & Crutcher, 2008; Crutcher et al., 2010). Secondly, there are recent numerical results suggesting that these types of magnetic field strengths will completely suppress formation of rotationally dominated discs (Mellon & Li, 2008; Hennebelle & Fromang, 2008; Duffin & Pudritz, 2009). Thirdly, simulations using the initial conditions presented here, but without sink particles, were shown to generate early molecular outflows (Duffin & Pudritz, 2009). Sink particles will allow us to examine the evolution of the disc to much later stages of the collapse (Federrath et al., 2010a).

We simulate the collapse with a customized version of FLASH 2.5 (Fryxell et al., 2000), a 3D adaptive mesh refinement code (AMR; Berger & Collela, 1989). We use the newly developed approximate Riemann solver for the 3D magnetohydrodynamics (Bouchut et al., 2007, 2010) which we have found to be more stable in our simulations, notably for higher magnetic field

strengths. We restrict ourselves to ideal MHD effects, and leave the non–ideal MHD effect of ambipolar diffusion – implemented in a previous paper (Duffin & Pudritz, 2008) – for future studies. We constrain $\nabla \cdot \mathbf{B} = \mathbf{0}$ with a parabolic diffusion method (Marder, 1987) before sink particle creation and with an elliptic projection method (Brackbill & Barnes, 1980) after sink particle creation for optimal stability. Sink particles are implemented as described by Federrath et al. (2010a), with particle merging turned on.

We use a sink radius of 3.2 AU for our main runs. We have also performed simulations with sink radii at 12.7 AU for longer times to test the effect of resolution on the result. We run the simulations with ideal MHD (for $\mu/\mu_0 = 3.5$) and pure hydrodynamics (for $\mu = \infty$). A list of models run are presented in Table 4.1. The accretion radius of a sink corresponds to 2.5 cells at the highest refinement level, and the critical gas density (beyond which gas can be accreted into particles) corresponds to the Jeans' density at the core temperature (20 K) of these cells. This gives $\rho_{\rm acc} = 3.69 \times 10^{-12}$ g cm^{-3} and $\rho_{\rm acc} = 5.91 \times 10^{-11}$ g cm^{-3} for 12.7 and 3.2 AU sinks respectively. The mesh is refined adaptively via a Jeans length argument, such that each Jeans length is refined by at least 8 cells and de–refined for more than 32 cells. An additional requirement is that the sink particle always has to be on the highest refinement level ($\Delta x_{\rm min} = 1.3$ AU).

For a complete list of models run, see Table 4.1. In our principal runs, we use the cooling function developed in previous publications (Banerjee et al., 2006), which incorporates numerous factors such as radiative cooling by molecular line emission, gas–dust interaction and radiative diffusion in the optically thick regime. Although H_2 formation and dissociation effects are included, these are likely unimportant due to the use of a sink particle.

Table 4.1 The different simulations run in this study. The principle results are obtained from the model 'MHD+cooling'. For each model the initial magnetic field is either $\mu/\mu_0 = 3.5$ or $\mu = \infty$, temperature of 20K and $\beta_{\rm rot}$=0.3.

model name	μ/μ_0	Sink Particle Size	Cooling
MHD+cooling	3.5	3.2 AU	Cooling Table
Hydro+Cooling	∞	3.2 AU	Cooling Table
Hydro+Polytrope	∞	3.2 AU	Barotropic
MHD-cool-12.7AU	3.5	12.7 AU	Cooling Table
MHD-poly-12.7AU	3.5	12.7 AU	Barotropic

We compare these results with identical collapse simulations but using a popular prescription of polytropic indices tied to the gas density. We use the identical polytropic prescription to a recent publication of core formation with magnetic fields (Machida et al., 2007b). The gas is isothermal initially at 20 K and the pressure is a function of density such that

$$P = \begin{cases} \rho c_s^2, & n < n_a, \\ \rho_a \left(\frac{n}{n_a}\right)^{7/5} c_s^2, & n_a < n < n_b, \\ \rho_a \left(\frac{n_b}{n_a}\right)^{7/5} \left(\frac{n}{n_b}\right)^{1.1} c_s^2, & n_b < n < n_c, \\ \rho_a \left(\frac{n_b}{n_a}\right)^{7/5} \left(\frac{n_c}{n_b}\right)^{1.1} \left(\frac{n}{n_c}\right)^{5/3} c_s^2, & n > n_c, \end{cases} \tag{4.1}$$

where $\rho = \mu_{\rm mol} m_{\rm H} n$, $\mu_{\rm mol} = 2.33$ is the mean molecular weight, $n_a = 10^{10}$ cm^{-3}, $n_b = 10^{16}$ cm^{-3}, $n_c = 10^{21}$ cm^{-3}. In our simulations, densities do not reach past the third polytropic prescription.

We find that runs with the polytropic prescription have larger timesteps by a roughly a factor 5 than the runs with the cooling function we use for our primary results. Qualitatively the results are very similar. In the hydrodynamic simulations fragmentation occurs in the case where the cooling function is used, but not when the polytropic prescription is used. We present results with the *cooling function* as they better approximate the true physical

conditions of the problem.

During the main stages of the outflow, low density highly magnetised bubbles are produced. These bubbles have very high Alfven velocities $v_{\rm A} = B/\sqrt{4\pi\rho}$ and correspondingly small timesteps. To correct for this problem without greatly affecting the solution, we employ a variable density floor such that $\rho_{\rm min} = 10^{-18}$ g cm^{-3} for $r < 1000$ AU, and $\rho_{\rm min} = 10^{-20}$ g cm^{-3} elsewhere. The density floor is the lowest possibly density in the simulation. This is only adds negligible mass to the simulation, while maintaining sufficiently large timesteps. Indeed, the difference in mass between start and end of the principle simulation is $-8 \times 10^{-7} M_{\odot}$, where the loss is most likely due to round off error transferring mass from the grid onto the sink particle.

4.3 Disc Properties

The evolution of our principle simulation (run 'MHD+cooling') is illustrated in Figure 4.1 which presents column density slices along the z and y axes over time. The initial BE sphere collapses into a flattened structure that grows to a radius of about 2000 AU before dissipating and fragmenting. The entire flattened structure launches a low speed outflow from its surface and the envelope is cleared away. Accretion occurs through the flattened structure. The inner 100 AU of this structure is dominated by rotational motion and is nearly Keplerian despite a strong magnetic field. The outflow is clumpy and the appearance of low density bubbles or eruptions is apparent. This inner region launches a high speed jet and warps over time with respect to the z axis.

We measure properties of the collapsed core by azimuthally averaging

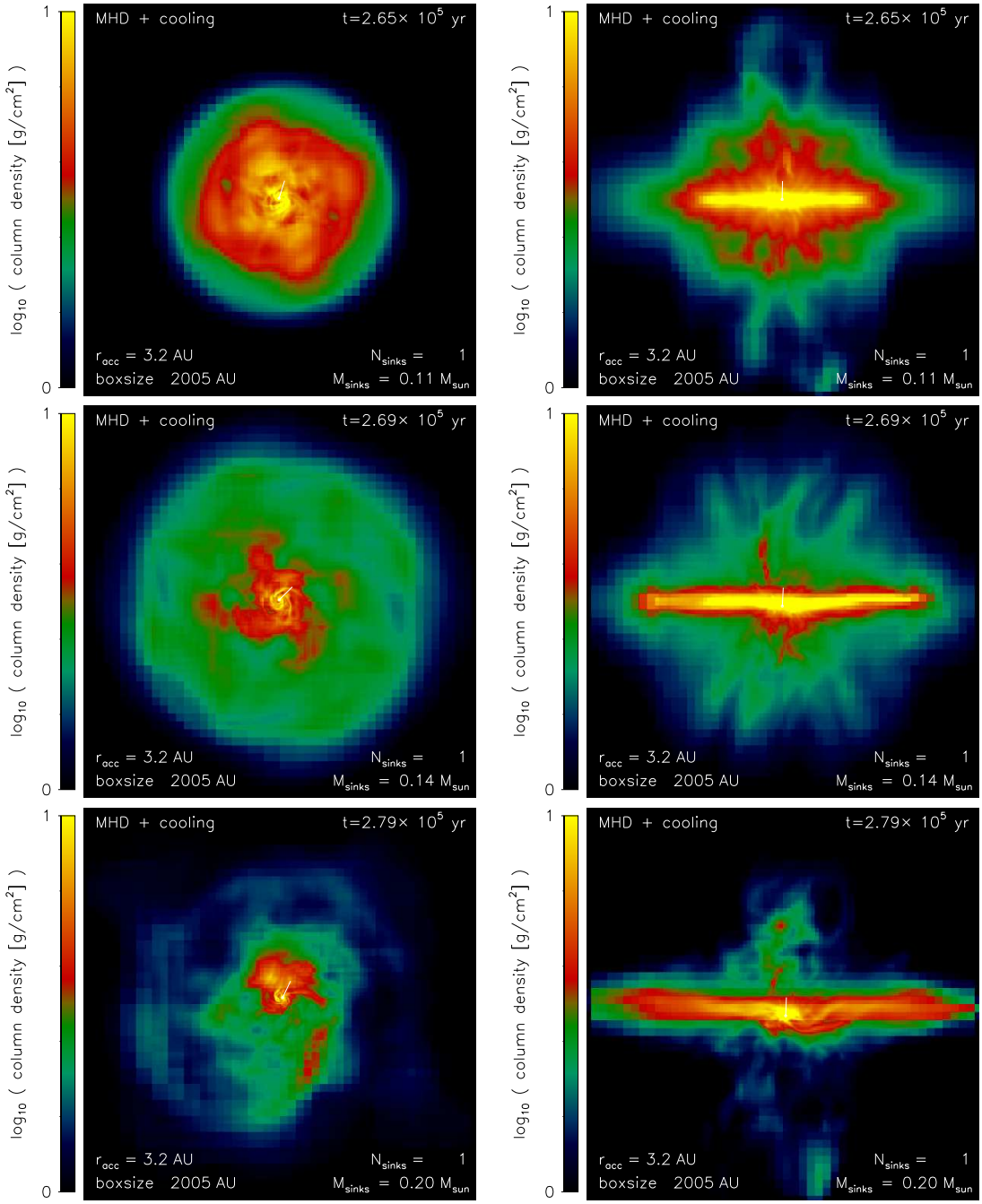

Figure 4.1 The left panels show a time lapse of the column density along the z–axis for the principle magnetic collapse 'MHD+cooling'. The right panels are similar but for column density along the y–axis. The three times correspond to times in Fig. 4.2-4.3. These are from top to bottom, $t = t_0 + 3.4 \times 10^3, t_0 + 10.3 \times 10^3, t_0 + 17.2 \times 10^3$ yr respectively, where $t_0 = 2.6 \times 10^5$ yr is the time where the sink particle was formed.

quantities (over the height of the core) in radial bins, only considering material which is inflowing (and only gas which is outflowing for properties concerning outflowing gas). We wish to compare the early disc structure reported in our work without sink particles (Duffin & Pudritz, 2009) to that of more evolved disc structures. For this reason we plot several evenly spaced radial profiles over time in Figure 4.3, starting from just after the sink particle has formed. We define this time $t_0 = 2.6 \times 10^5$ yr and show the evolution for the model at an additional 17.2×10^3 yr (until we run out of computing time). We compile our radial fits to these plots in Table 4.2.

4.3.1 Rotational Properties

In our simulation the disc is sub–Keplerian within a factor of a few out to 100 AU (Figure 4.2b). The inner 100 AU is an early disc because it is dominated by rotational motion. The radial velocity component of the outflow is fairly flat $v_r \propto r^{-0.17}$. Although the disk is sub-Keplerian, we expect that magnetic support aids rotational support against gravity. It is important to note that a structure whose velocity is largely dominated by radial infall motions is an example of something that has been considered 'not a disc' in the past (for example, in the work of Mellon & Li, 2008). In this sense, we find something surprisingly different than this previous result. Previous 3D simulations studying protostellar collapse using sink particles have also found 100 AU discs Machida et al. (2011).

Catastrophic infall motions were found by Hennebelle & Fromang (2008) and Hennebelle & Teyssier (2008), however these simulations lack sink particles and are therefore limited to very early times. Our results suggest that

Table 4.2 Various power–law fits from near the end of our simulation (see Figures 4.2 and 4.3). Fitting performed by least squares on the last data point in time between 6 and 1500 AU.

Variable	Fit
B_ϕ	$\propto r^{-1.67}$
B_r	$\propto r^{-1.92}$
B_z	$\propto r^{-1.30}$
$\lvert j \rvert$	$\propto r^{0.44}$
Σ_z	$\propto r^{-0.47}$
T	$\propto r^{-0.71}$
$\dot{M}_{\rm in}$	$\propto r^{0.09}$
$\dot{M}_{\rm out}$	$\propto r^{0.37}$
v_ϕ (disc)	$\propto r^{-0.56}$
v_r (disc)	$\propto r^{-0.43}$
v_r (outflow)	$\propto r^{-0.17}$
$t_{\rm warp}$	$\propto r^{1.94}$
$t_{\rm precession}$	$\propto r^{2.23}$

at early times, the disc undergoes a rapid transition after sink particle formation from a disc–envelope configuration to a disc–outflow configuration. The properties of our disc change greatly after this early time.

4.3.2 Disc–envelope to disc–outflow transition

In general, we find that power law profiles in Figure 4.3 remain constant over time, but extend to greater radial distances as the disc and the flattened envelope grow. There are a few exceptions to this. Firstly, the column density of the early disc is quite large (e.g. $\Sigma_z > 100$ g cm^{-2}) and rapidly decreases by a factor 10 in 3.4×10^3 yr. This is material with less angular momentum settling from above the midplane to the disc and being accreted by the sink particle. The mass accretion rates also change from very high (10^{-4} $M_\odot$ yr^{-1}) to lower (10^{-5} $M_\odot$ yr^{-1}) over the same time period. Once the disc has formed, the outflow is launched to sufficient size that any further accretion must occur

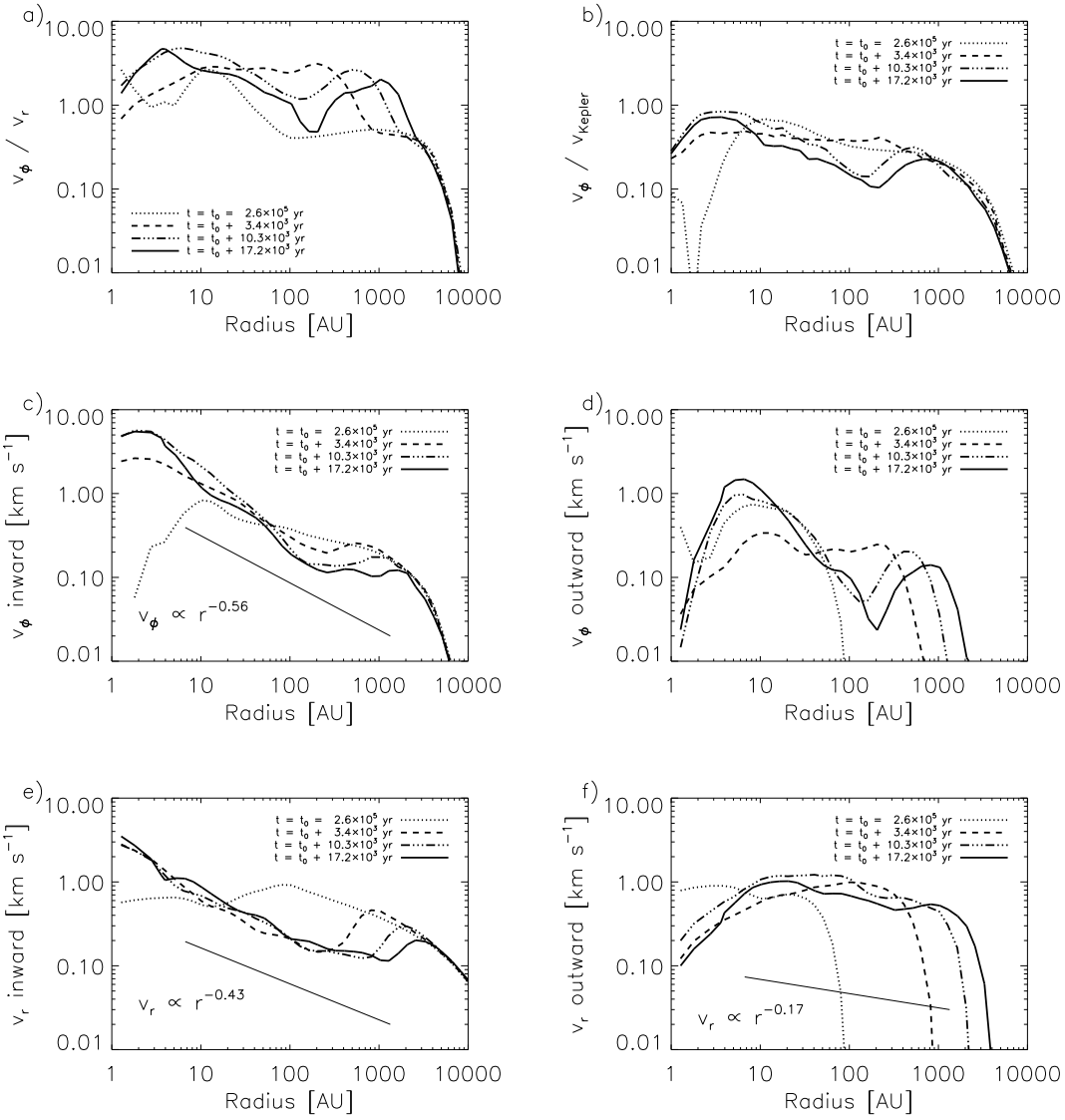

Figure 4.2 Disc profiles of rotational velocity over time for the principle simulation 'MHD+cooling'. Plotted are the surface averaged values of a) v_ϕ/v_r and b) $v_\phi/v_{\rm Kepler}$, where $v_{\rm Kepler} = GM_{\rm enclosed}/r$ is the Keplerian velocity. Outflowing gas is excluded. The density weighted surface average of toroidal velocity is plotted versus radius for c) inflowing and d) outflowing gas. Similarly, the averaged values of radial velocity are plotted for e) inflow and f) outflowing gas.

through the disc.

It is very important to note that the surface density of the disc outside

of 1 AU is below 96 g cm^{-2}, the value considered to be the optical depth of cosmic rays through the gas (Umebayashi & Nakano, 1981; Matsumura et al., 2009). This implies that our disc will not have a dead zone outside 1 AU (e.g. see detailed calculations of Matsumura & Pudritz, 2003). Recent papers have suggested the key to disk formation will be the creation of large magnetically decoupled regions in the disk (Dapp & Basu, 2010; Machida et al., 2011)

The fact that mass accretion through the disc (shown in Figure 4.3) is essentially independent of radius matches well with theoretical ideas of more evolved discs. However, there is still a slight dependence ($\dot{M}_{\rm in} \propto r^{0.09}$). The surface density we measure goes roughly as $\Sigma_z \propto r^{-1/2}$. We note that this is a surprisingly flat radial dependence in view of estimates of the Minimum Mass Solar Nebula (MMSN). Considering the current positions of the planets and estimating a column density by evenly spreading planetary material out in their respective orbits one can derive $\Sigma \propto r^{-3/2}$ (e.g. Hayashi, 1981). More recent fits considering migration of the giant planets find even steeper profiles of $\Sigma \propto r^{-2.168}$ (Crida, 2009). However, these fits were intended for data within 30 AU while our data extends out to 2000 AU.

4.3.3 Specific angular momentum

Our initial conditions had solid body rotation $j \propto r^2$, which evolves during collapse to $j \propto r^{0.44}$ (Fig. 4.3c). This is similar to the profile of Keplerian motion about a point mass $j \propto r^{0.5}$. Measuring N_2H^+ emission from 9 nearby low–mass class 0/I cores, Chen et al. (2007) found a tight relation between specific angular momentum and core size $j \propto r^{1.7\pm0.1}$, where r is the size of the core. The change in specific angular momentum profile we observe is a sign of

gravitational collapse and the formation of a disk.

4.3.4 Mass–to–flux ratio

Another interesting trend seen in our data from Table 4.2 is that the apparent mass–to–flux ratio in the disc grows with radius, $\mu \propto \Sigma/B_z \propto r^{0.83}$. Note that we are not actually following flux tubes, but simply 'observing' our simulation along the z–axis. Initially, the outer regions of the BE sphere had $\Sigma \propto r^{-1}$, $B_z \propto r^{-1}$, so μ was uniform. If this remains as such over time, then B_ϕ and B_r components must dominate the field configuration more and more as we approach the centre of our simulation. Our field is highly pinched and twisted, but more so as we approach the centre. Indeed, power law fits in Table 4.2 are consistent with this. The toroidal component grows faster than B_z, while B_r grows the fastest, consistent with the field also becoming mostly poloidal in the centre.

We find a steady profile of $\Sigma(r)/|\boldsymbol{B}(r)| \propto r^{0.6}$ over time (there is a quick transition in the initial 3.2×10^3 yr as $\Sigma(r)$ decreases, as seen in Fig. 4.3, suggesting that no major changes in flux relative to mass occur.

4.3.5 Fragmentation

The magnetised collapse forms a large 2000 AU disc structure with spiral waves which fragment by the end of our simulation. One can see that a fragment is present in the 2D column density image in Figure 4.1 (bottom left) 300-400 AU from the sink particle. After nearly 2×10^4 yr, the gas at 200 AU has completed roughly 1 rotation, while the disc at 10 AU has completed 60 rotations. Thus, the larger flattened structure past 300 AU is a highly transient feature and

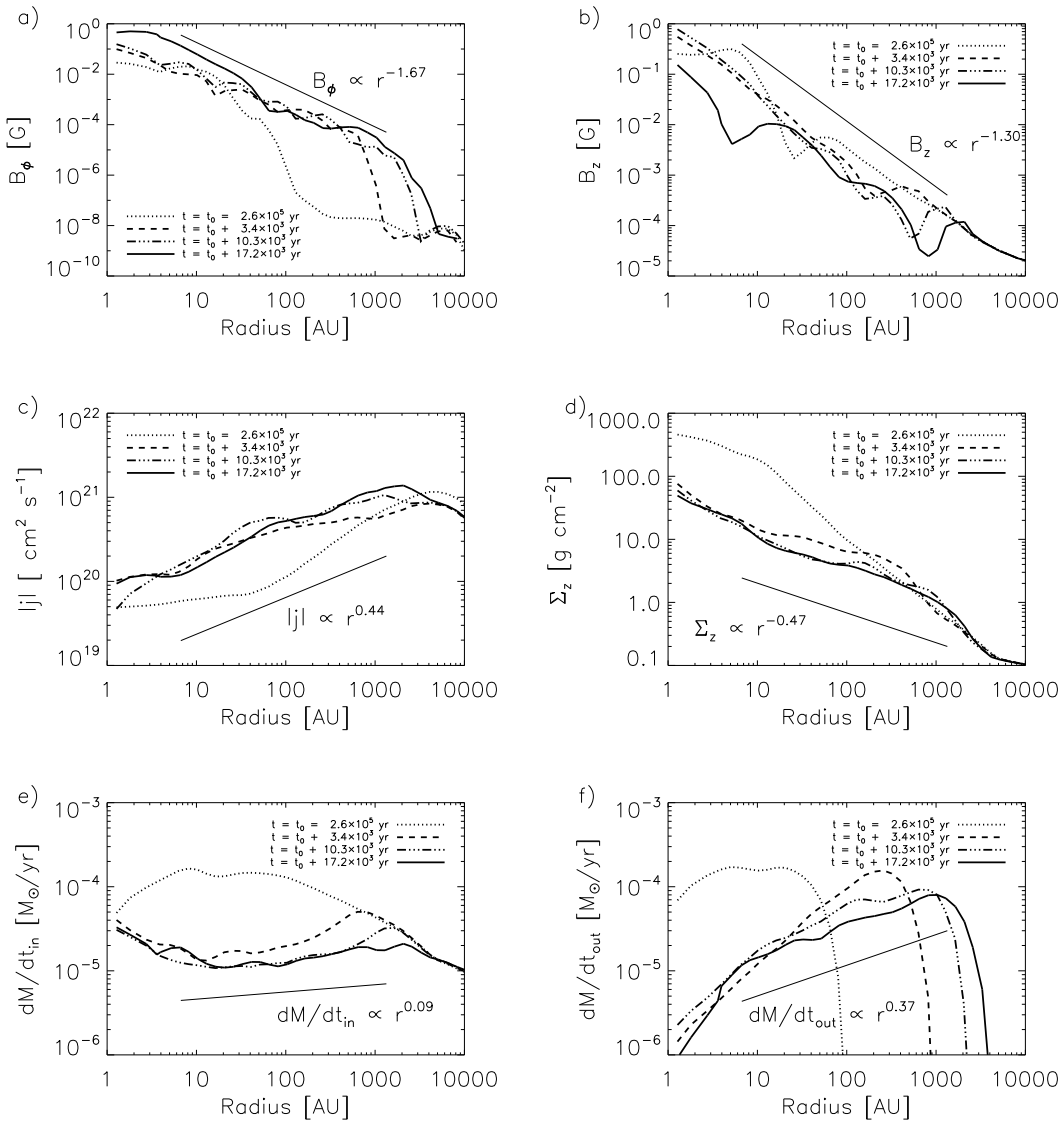

Figure 4.3 Surface averaged, density weighted disc profiles evolving over time for a–e) infalling gas or f) outflowing gas for the principle simulation 'MHD+cooling'. We plot the quantities a) B_ϕ, b) B_z, c) $|j|$, d) Σ_z, e) $\dot{M}_{\rm in}$, and f) $\dot{M}_{\rm out}$ versus cylindrical radius r for various times. Fitting performed by least squares on the last data point in time between 6 and 1500 AU.

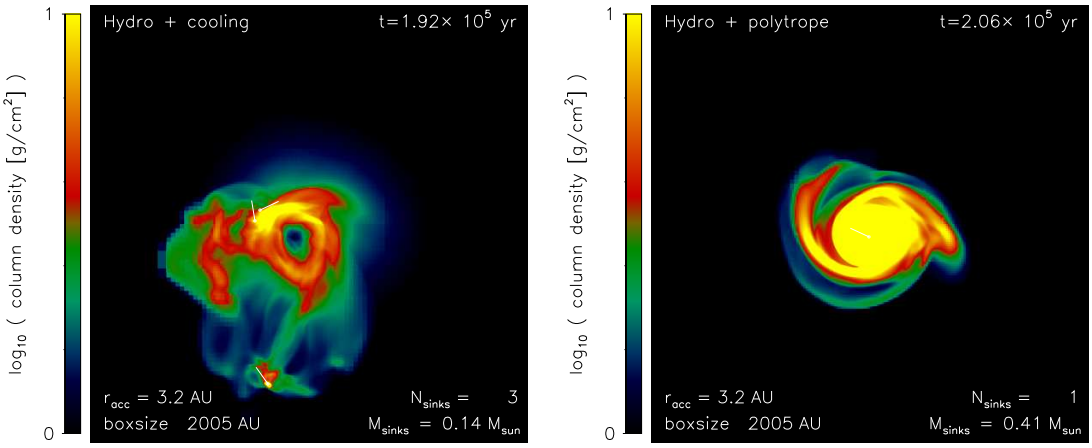

Figure 4.4 Column density of the disc at later times in the evolution of the hydrodynamic runs. The projected angular momentum vector of the sink particle is shown to guide the eye. The column densities along the z–axis for the hydrodynamic collapse are for models when using the cooling table (left) and when using a polytropic prescription (right).

fragments before one period has passed. This does not appear to limit the growth of the outflow from the structure's surface as the outflow extends out to 2000 AU (Fig. 4.2d).

4.3.6 Hydrodynamical collapse

In Figure 4.4 we show the column density in the xy-plane for two hydrodynamic simulations for comparison (with cooling and with a polytropic prescription both with 3.2 AU sink particles). In the cooling collapse (left), we form three sink particles. One particle begins migrating outwards, two others form in a pair orbiting the centre. The collapse with the polytropic prescription (right) forms a compact disc (radius of a bout 350 AU) with spiral waves, where much of the mass has already been accreted onto the sink particle (nearly 4 times as much mass as the simulation using the cooling function, likely as the polytropic run did not undergo fragmentation). There is a significant difference between

simulations as a consequence of changing the cooling function. The effect of different cooling prescriptions on fragmentation have been observed in previous studies (Commerçon et al., 2010).

Furthermore the difference between hydrodynamical and MHD runs is striking. The discs in the MHD runs have lower column densities in comparison to the hydrodynamic cases and are also much larger (Figure 4.1). This is due to the suppression of large spiral waves seen in the hydrodynamic collapse which torque down the disc at a faster rate than magnetic braking (Banerjee & Pudritz, 2006; Duffin & Pudritz, 2009). Fragmentation in the MHD case is postponed by the magnetic field (e.g. section 3.5 of Seifried et al., 2011). This magnetic tension also decreases the accretion rates through the disc and helps prop up the large flattened structure observed in our MHD simulation.

4.3.7 Comparison to observations

Large flattened structures with sub–Keplerian rotational motion have been observed around a number of Class 0 stars (Tobin et al., 2010, 2012), including L 1157 with a structure extending to 2×10^4 AU (Chiang et al., 2010). Tobin et al. (2012) suggest rotational motion would predict disks that are too large. What we may in fact be observing is a rotating, collapsing filamentary structure in the envelope, which mimics the same velocity field of a Keplerian disk. An example of such a structure would be a large flattened, rotating envelope undergoing fragmentation, as in Fig. 4.1.

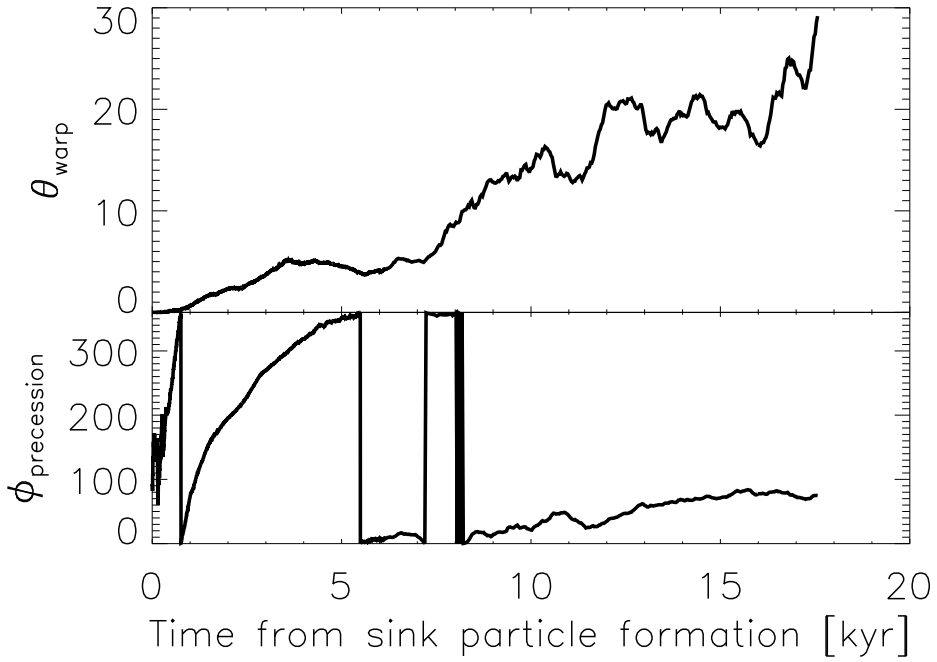

Figure 4.5 The warping angle $\theta_{\rm warp}$ and precession angles $\phi_{\rm warp}$ from the angular momentum vector of the protostellar disc.

4.4 Disc warp and precession

We observe the disc in our simulations to warp and precess. This is similar to the precession that is observed is some molecular outflows (Arce & Goodman, 2001a). We measure the angular momentum components of disc material relative to the centre of mass of the disc, $\boldsymbol{L} = (L_x, L_y, L_z)$. A disc, for the purposes of this calculation, is defined as gas which is sufficiently dense ($\rho > 10^{-15}$ g cm^{-3}) and infalling ($v_{\rm r} < 0$) and within 2000 AU of the centre. We can identify two important angles. First the warping angle $\cos\theta_{\rm warp} = L_z/L$ is the tilt of $\boldsymbol{L}$ with respect to the z–axis. Second, we identify the precession angle $\phi_{\rm prec}$ as the angle between the x–axis and $\boldsymbol{L}$ projected onto the xy–plane.

The angles are plotted in Figure 4.5. For the first 2.6×10^5 yr before

the sink particle was created the plane of rotation remains flat ($\boldsymbol{L}$ points along z–axis). However, afterwards the disc changes orientations. Over 15 kyr, the disc tilts by roughly 30° with respect to the z–axis, and has precessed a total of nearly 720° in the counter–clockwise direction. The warping precedes at a fairly constant rate, although small oscillations are observed. The precession occurs in the counter–clockwise direction, which is prograde (in the same direction as the rotation). For the first 1 kyr, the disc precesses through 1 period, although $\theta_{\rm warp} < 1°$. For the next 16 kyr, the disc precesses another 360°, with $\theta_{\rm warp} > 1°$. After 8 kyr, the precession slows down and even reverses on occasion reaching 90° once again. From start to finish, two full precession periods have passed.

We note that the angular momentum vector of the sink particle (as plotted in Figure 4.1 as a white line), remains consistent with its early accretion history (along the z–axis). Therefore, there is quite a significant tilt formed very early on between protostar and protostellar disc.

There are several proposed mechanisms for warping instabilities discussed in the literature. For galactic warps, the explanation is likely through an interaction with satellites, which enhance their tidal effects on the HI disc by distorting the surrounding dark matter halo (Levine et al., 2006). Other types of disc warps can be induced by radiatively driven winds (Schandl & Meyer, 1994), radiation pressure (Pringle, 1996), wind–driven Kelvin–Helmholtz instability (Quillen, 2001) as well as the stellar magnetic field (Lai et al., 2011).

Of particular relevance to magnetized discs with outflows, however, Lai (2003) showed that a warping instability occurs in rotating accretion discs threaded by a magnetic field. The author showed that a ring of material in the disc, when perturbed by a small angle, is unstable to a runaway warp

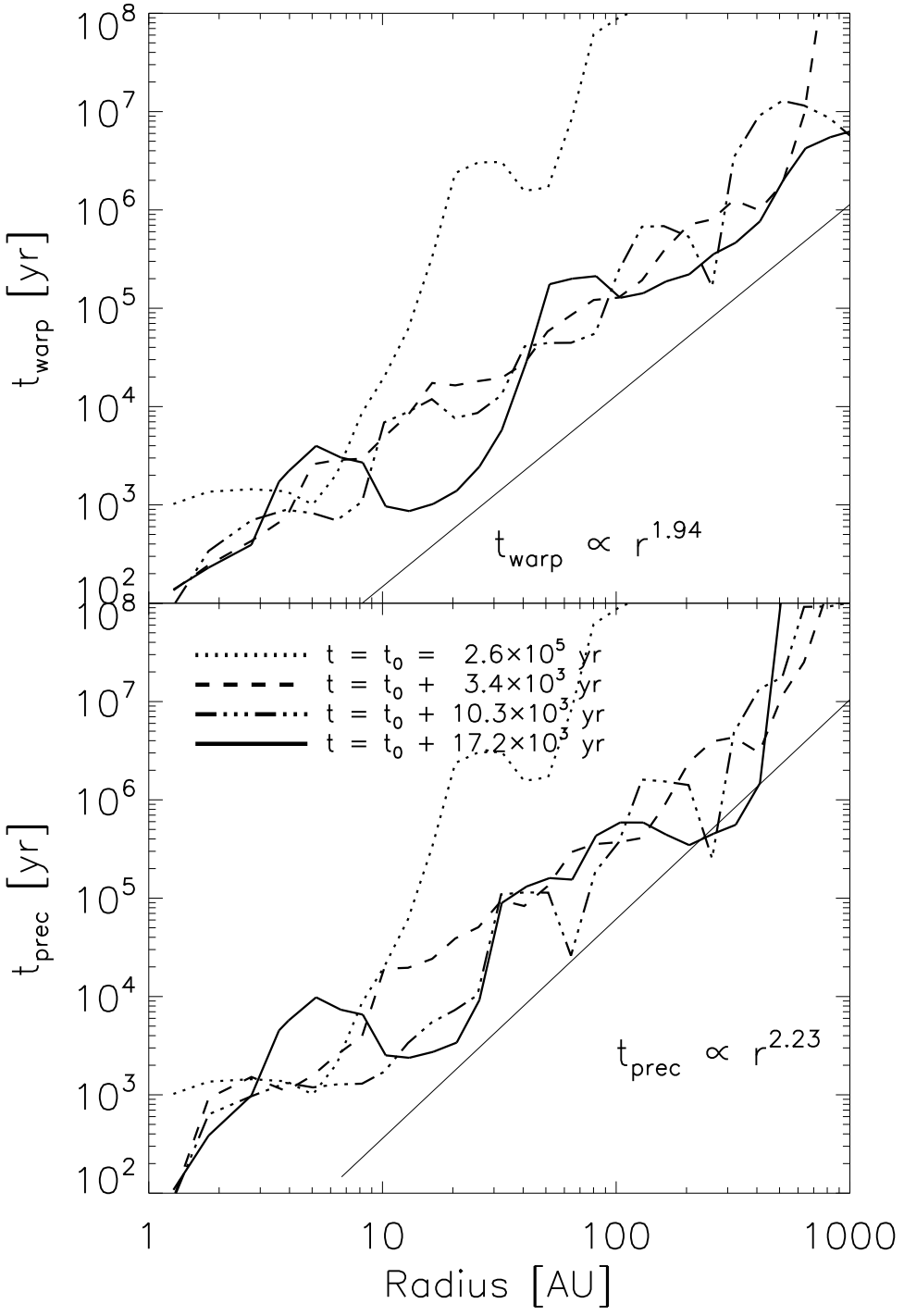

Figure 4.6 The warping (top) and precession time-scales (bottom) evaluated for radial fits from Figures 4.2 and 4.3 at different times.

and retrograde precession. The warping torque arises naturally when tilting the disc by a small angle and measuring the Lorentz force on the perturbed current loop. The tendency is for the disc to tilt perpendicular to the ambient magnetic field B_z. In both warp and precession, it is the viscous interaction of the ring of material with adjacent rings of material that allow the warping to stop and a steady state to develop. The warping and precession time–scales derived by Lai (2003) are

$$t_{\rm warp} = \frac{4\pi\Sigma v_\phi}{B_\phi B_z} \tag{4.2}$$

$$t_{\rm prec} = \frac{4\pi\Sigma v_\phi}{B_r B_z}, \tag{4.3}$$

where magnetic quantities are implied to be at the disc surface. Using Figures 4.2 and 4.3 along with a similar fit for $B_r \propto r^{1.92}$ we can estimate how these time–scales vary over radius assuming these values approximate well the conditions on the disc surface. We find that $t_{\rm warp} \approx 100(r/1\ {\rm AU})^{1.94}$ yr and $t_{\rm prec} \approx 50(r/1\ {\rm AU})^{2.23}$ yr. More specifically, we plot the time–scales in Figure 4.6 using the simulation data directly, and compile an evolutionary picture of the disc.

One can see from Figure 4.6 that the time–scales are generally less than 10^4 yr at 10 AU. Outside 10 AU, early warping time–scales are much higher than at later times. It is not until the early disc builds up that it is able to warp and precess. As described in Section 4.3, this settling is the quick evolution from a thick to a thin disc mediated by accretion onto the central particle. Also apparent from Figure 4.6 is that beyond 100 AU at late times, the time–scale for warping is comparable to the lifetime of discs. This is because, while v_ϕ and Σ remain fairly flat, B_z, B_r and B_ϕ decrease very quickly with radius

(see Table 4.2). It is this magnetic profile – frozen in from early times – that gives rise to a warped inner disc, but no warping at large radii.

We find that our disc undergoes warping at 10-100 AU. Using Figures 4.6 for values from 10-100 AU, we find a time–scale of approximately $(5-20)\times 10^4$ yr. This time–scale is a factor of a few larger than our simulation time 2×10^4 yr (taken after the sink formed). Noting that the warping time–scale is approximate so that these two time–scales are comparable.

It is likely that the mechanism proposed by Lai (2003) is at play in our simulation as it explains why inner regions of the disc would warp but not outer regions. However, we do not measure retrograde (clockwise) precession, outside of relatively short periods of times. In Figure 4.5, periods of strong prograde (counter–clockwise) precession dominate. Significant B_z reversals in the disc lead to a net reversal in precession torque described by Lai (2003). We measure gas and magnetic torques in Section 4.5 and show that this is indeed the case.

4.4.1 Perturbations to the disc

Is the disc warping a numerical artifact? To investigate this possibility, we have performed the simulation with different sink sizes (3.2 and 12.7 AU), with cooling or a polytropic equation of state, with 5 different Riemann solvers available in FLASH (Roe, HLLE, HLLD, Bouchut 3–wave, Bouchut 5–wave), by cleaning $\nabla\cdot\boldsymbol{B}$ with either projection and diffusive methods, and by mixing most combinations. The disc is resolved such that 1 cell is at most 1/32 of a local Jeans length. The disc warps in all MHD simulations, even with larger sinks.

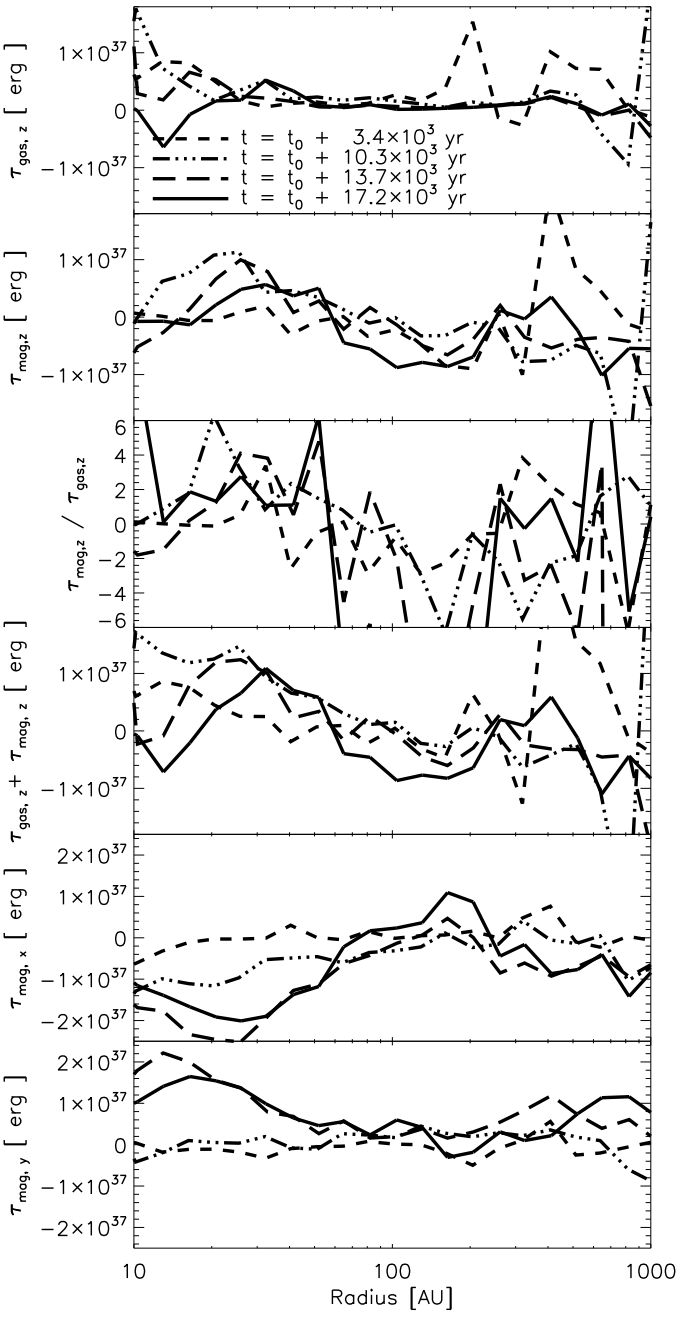

Figure 4.7 The gas and magnetic torques in the x, y, and z direction, over several time periods from 10 to 1000 AU. The ratio of the two torques is shown in the third panel. The sum of the two torques is shown in the fourth panel.

To start up the disc warping, some source of initial perturbations to the disc orientation is required. Our initial conditions have no turbulent motions to break symmetry on either side of the xy–plane (although we do have a 10% m=2 perturbation). The Bonnor–Ebert sphere creates Kelvin–Helmholtz turbulence as it rotates through the ambient, non–rotating medium, but this is far from the inner disc on the scale of the core. Turbulence is also generated as the jet pierces through the lower speed outflow material, although it is not evident that this is sufficient to perturb the disc surface.

The disc and larger pseudo-disc are gravitationally unstable. As seen in Figure 4.1, the inner 100 AU of the disc forms strong spiral waves while the outer regions fragment and form a possible clump. This turbulent density distribution is the most likely candidate for shaking our disc slightly off the xy plane in order for the warping instability to take over.

It is interesting that the simulations by Machida et al. (2011) and Machida & Matsumoto (2012) did not produce warped discs. We note that these authors implement Ohmic diffusion in the region where their sink particle resides to diffuse out excess magnetic flux. This can create an effective dead zone on the order of 60 AU in their simulations (Inutsuka et al., 2010), the region where warping would be expected to take place. However, from detailed calculations of dead zone sizes, it is surprising that dead zones could grow so large (Matsumura & Pudritz, 2003). For instance, in our simulations, the dead zone would be less than 1 AU as $\Sigma < 100$ g cm^{-2} at this distance.

A Parker instability on the disk surface results in the shedding of magnetic loops, as described by Johansen & Levin (2008). These bubbles create ripples along the disc surface which likely aid the instability in initializing. Our bubbles are relatively small and confined to the outflow region above the

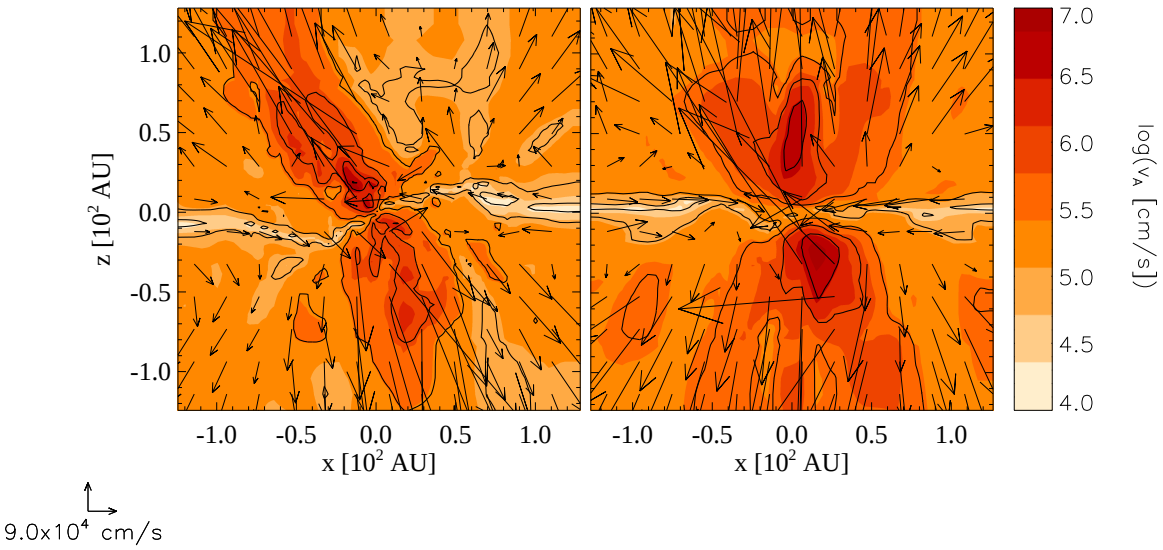

Figure 4.8 Comparison of Alfven velcoity at identical outflow heights (and similar times, around $t = t_0 + 3000$ yr) using different resolutions. Vectors are gas velocity. In the left panel, the simulation using 3.2 AU sink particles. In the right panel, the lower resolution simulation using 12 AU sink particles. Both simulations have identical cooling functions. The outflow has less structure in the low res simulations and the disc warp is not as developed.

disc.

Figure 4.8 shows the non-uniform flow of the outflow off the disc surface (e.g. the shedding of magnetic loops). It compares the dynamics of the simulation for different resolutions but similar times. In both simulations, the bubbles have similar characteristics. At higher resolutions, the bubbles have more sub–structure. Additionally, the onset of the warp is more prominent in the high resolution run than in the low resolution run. This resolution study therefore shows that the loops and bubbles are real and don't go away when higher resolution is used.

4.5 Magnetic Torques and Disc Formation

We compute values of torque in order to deduce why a disc forms, why it warps and why it precesses in a prograde direction. The torque per cell is computed and binned in cylindrical radius, averaged over the z-axis (inside the original core) and weighted by density (only inflowing gas is considered). The hydrodynamic and magnetic torques are

$$\boldsymbol{\tau}_{\rm mag} = \int \boldsymbol{r} \times ([\nabla \times \boldsymbol{B}] \times \boldsymbol{B}) \ dV \tag{4.4}$$

$$\boldsymbol{\tau}_{\rm gas} = -\int \boldsymbol{r} \times \nabla \cdot (\rho \boldsymbol{v}\boldsymbol{v}) \ dV, \tag{4.5}$$

where $(\boldsymbol{v}\boldsymbol{v})_{ij} = v_i v_j$ is tensor product of velocities, and $[\nabla \cdot \rho \boldsymbol{v}\boldsymbol{v}]_j = (\rho v_i v_j)_{,i}$. The original cloud has an angular momentum in the z-direction, so torques in this direction control the rotational evolution of the disc. The torques in the x and y direction relate to warping and precession.

In Figure 4.7 we plot the torques due to the magnetic field and the accreting gas over several time periods. For comparison, we also show their sum and ratio in the third and fourth panels respectively. Hydrodynamic torques (top panel) have small values across the disc when compared with magnetic torques. Our disc never develops a very strong spiral wave which gravitational torques down the disk. The third frame shows that $\tau_{{\rm mag},z} > \tau_{{\rm gas},z}$ typically everywhere in the flattened structure. The second frame shows that the magnetic torques, by contrast, are significant in the inner regions of the disc. Magnetic braking strongly torques down the gas outside of 65 AU (torque is negative), however inside of 65 AU the field torques up the disc on average (torque is positive).

The consequence of a positive magnetic braking torque is the formation of a large rotationally dominated disc early on (see Figure 4.2a-b). For a strong background B_z, we would expect a correspondingly strong and negative magnetic torque in the z direction. We show below reversals in B_z are present in the disc in Figure 4.9, and these are responsible for the reversal in magnetic braking.

Summarizing from Lai (2003), the warping and precession torques per unit area, averaged about a ring of material in the disc, is

$$< \tau_{\rm warp} > = -\frac{1}{4\pi}\zeta r B_z^2 \cos\theta_{\rm warp}(\hat{\boldsymbol{l}} - [\hat{\boldsymbol{l}} \cdot \hat{\boldsymbol{z}}]\hat{\boldsymbol{z}}), \tag{4.6}$$

$$< \tau_{\rm prec} > = -\frac{1}{2c} K_\phi B_z \hat{\boldsymbol{z}} \times \hat{\boldsymbol{l}}, \tag{4.7}$$

where $\theta_{\rm warp}$ inclination angle, $\hat{\boldsymbol{l}}$ is normalized direction of the ring's angular momentum, K_ϕ is the toroidal surface current, c is the speed of light, $B_\phi^\pm = \mp\zeta B_z$ and $B_\phi^\pm$ is the toroidal field above or below the disc plane. For disc winds, ζ is positive if the disc rotates faster than the outflow. Both torques are orthogonal in the xy-plane. The mean precession torque is in the direction orthogonal to the warp, causing a precession of the disc around the z-axis

$$\Omega_{\rm prec} = -\frac{K_\phi B_z}{2c\Sigma r \Omega_d}\hat{\boldsymbol{z}}, \tag{4.8}$$

where Ω_d is the rotation rate of the disc.

We have computed torques from the magnetic field on the disc in the x and y directions, shown in the bottom panels of Figure 4.7. These demonstrate that there is a strong signal of a warp and precession due to the magnetic field, as predicted by Lai (2003). Note the strengths of these torques outweigh the

values of torque in the z-direction. By late times, the disc is inclined up to 30° to the z-axis and has precessed 720°.

The precession we observe is prograde (see Figure 4.5). From Equation (4.8) we would expect a retrograde precession. However, if reversals of B_z are present in the disc (relative to the mean rotation), the sign of the precession flips.

In order to both reverse magnetic braking and precession direction we require large regions where $B_z < 0$ in the disc. In the theory of Lai (2003), the ambient B_z cannot change directions with respect to the current. In Figure 4.9 we find large regions in the disc where $B_z < 0$. In our simulation, while B_z reverses, B_ϕ and v_ϕ do not change directions.

The fact that the B_z component of the field has reversals is a consequence of the eruption of magnetic loops and bubbles on the disc surface, as illustrated in Figure 4.10. This is caused by a Parker instability as demonstrated in local simulations of idealised Keplerian discs threaded by a mean toroidal magnetic field (Johansen & Levin, 2008). These eruptions inflate pieces of the disc's toroidal as well as radial field components, generating B_z with reversals in the disc. The inner edge of the bubble will torque down the disc while the outer region will torque up the disc. As a consequence, angular momentum is transfered outwards and the disc can grow.

We explicitly show the gradual scrambling of the initially well ordered mean field (B_z component) to a more disordered state in Figure 4.9. The inhomogeneous character of the outflow is evident in the lower panels where v_A is shown. Regions of high v_A have low density and high magnetic field strength, helping us identify bubbles. The radial and/or toroidal disc field erupts out of the disc due to magnetic buoyancy, creating regions of disorganized B_z field

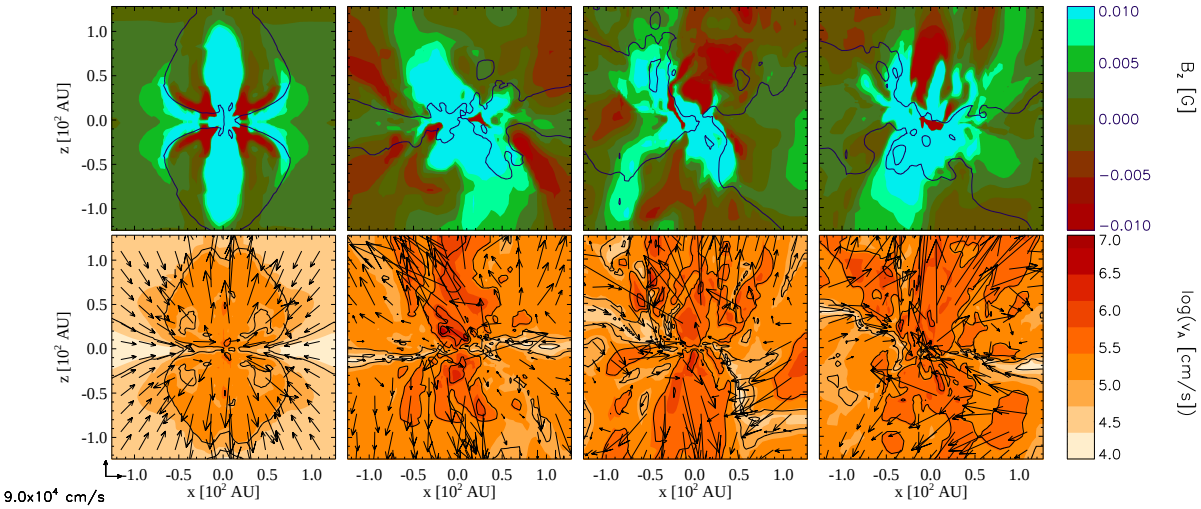

Figure 4.9 Time series from left to right of B_z reversals (top panels) and Alfven velocity (lower panels) for the principle simulation "MHD+cooling". Note that reversals of B_z correspond to reversals of magnetic braking torque. The images are taken for times $t_0 = 2.6 \times 10^5$ yr, $t_0 + 3.4 \times 10^3$ yr, $t_0 + 11.2 \times 10^3$ yr and $t_0 + 17.2 \times 10^3$ yr. In top panels $B_z > 0$ is blue and $B_z < 0$ is red and the contour separates regions of positive and negative v_r.

with reversals.

4.6 Discussion

4.6.1 Bubble dynamics: angular momentum flow in the disc and outflow

Ordered magnetic fields threading a collapsed structure exert a strong braking torque on discs that is so efficient it can lead to the prevention of disc formation, except in the hydrodynamic limit (e.g. Mellon & Li, 2008). The angular momentum is then carried out by the ordered flow into the outflow or envelope material. Turbulence, however, degrades the mean threading field of an accretion disc and diminishing the efficiency of magnetic braking (Seifried

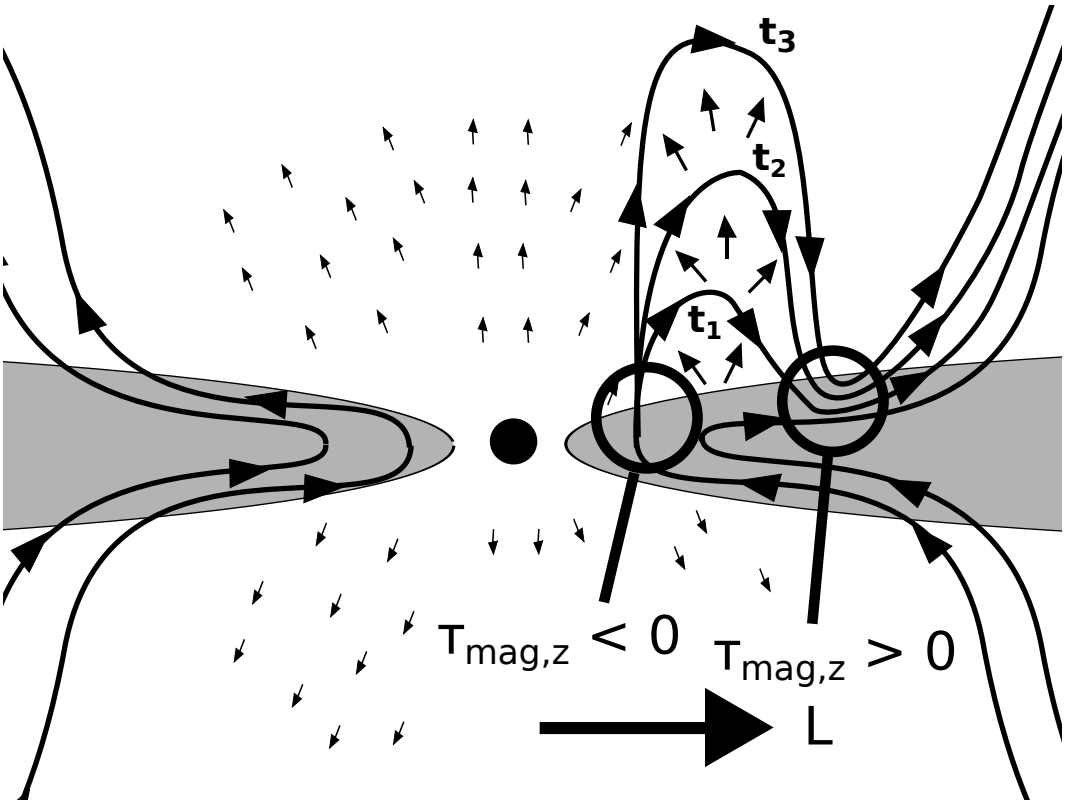

Figure 4.10 Schematic image of a magnetic eruption on the disc surface inducing a reversal of the vertical component of the magnetic field B_z. A time evolution of the eruption is labelled by advancing times t_1, t_2 and t_3. The inner region of the bubble spins down the disc $\tau_{\rm mag,z} < 0$ while the outer region of the bubble spins up the disc $\tau_{\rm mag,z} > 0$. There is a net transfer of angular momentum L outwards. Such reversals, if strong enough, can cause the magnetic braking and precession of the disc to reverse.

et al., 2012a).

More explicitly, protostellar disks can be unstable to a Parker instability. Buoyant magnetic bubbles are launched and act to directly scramble the mean field of the disc. The net loss of angular momentum is reduced by the collection of bubble eruptions across the disc surface.

Magnetic bubbles connect different regions of the disc. The inner part of the bubble is associated with negative torque so it spins down the disc. However, the outer part of the bubble with its reversed field spins up the ma-

terial. Angular momentum in the disc is therefore shifted outwards, somewhat analogously to what happens in viscous stresses. Thus, a portion of the angular momentum in the disc originally destined to be removed from the disc by the mean flow, is now transported radially through the disc to larger radii by the collection of buoyant loops. It is this process that aids in the formation and growth of a Keplerian disc early on.

4.6.2 Implications for planet formation

Warping of protostellar discs by their magnetic field help explain why molecular outflows and protostellar jets precess (Gueth et al., 1998; Arce & Goodman, 2001a). They could also help explain why the Solar System's principle orbital plane is tilted with respect to the Sun's rotation axis by 7.15° (Beck & Giles, 2005). Planets that form in warped discs would orbit at an inclined trajectory with respect to their star's axis of rotation.

Hot Jupiters are planets of masses comparable to Jupiter with orbits comparable to the stellar radii of their host stars (and for this reason, they have high temperatures). Hot Jupiters have been detected at highly inclined orbits to their parent stars. Using the HARPS spectrograph on 6 transiting hot Jupiters, Triaud et al. (2010) measure values of β, the sky projected value of obliquity $\phi_{\rm warp}$. The authors found that 3 planets had β greater than 90°, while the other three planets had obliquities consistent with 0° (however, we note that the error bars sometimes allow for significant spreads; these systems had β of -4^{+43}_{-34}, -12^{+10}_{-8} and -4^{+5}_{-5}). At the time of this publication, 26 known hot Jupiters have measured sky-projected obliquities. The authors argue that it is possible up to 85% of these planets to have misaligned ($\phi > 30°$) orbits.

Our result offers a way of allowing the formation of misaligned hot Jupiters through disc migration, but at moderate mis–alignments (e.g. 30°).

One successful method of producing a range of misaligned hot Jupiters is through a Kozai perturber orbiting around a slightly misaligned disc (Fabrycky & Tremaine, 2007). Kozai cycles occur in three body interactions where there is an inner binary (say a central star and a planet) inside the orbit of a third object much further out (e.g. a star orbiting a distance much greater than the separation of the inner binary). If the third object's orbit is slightly perturbed (e.g. inclined, but still circular), then it drives oscillations in the relative inclinations and eccentricities in the inner binary, called Kozai cycles (Kozai, 1962). Tidal friction between the star and Hot Jupiter will circularize the planet's orbit. We call the far binary star in this case the Kozai perturber. Our simulation produces a misaligned inner disc (30°) with a possible Kozai perturber at 300-400 AU.

A wide binary companion would likely limit the final mass accretion onto the central star through so–called fragmentation induced starvation (Peters et al., 2011b; Girichidis et al., 2012). It would also act as an excellent perturber of any planetesimals as discussed above, through which an excellent method of forming mis–aligned hot Jupiters exists (Fabrycky & Tremaine, 2007).

Figure 4.5 does not hint at a halt in the warping process. If we could simulate further, would the disc continue to warp? Would it produce a strong misalignment? The theoretical model of Lai (2003) predicts that without considering the viscosity in the disc, the warping instability would act to warp the disc along the direction of the background field (mis-aligned 180°). However the dynamical evolution as well as the details of the disc viscosity are difficult

to model theoretically. Could we produce smaller or larger misalignments? We leave this for future studies.

4.7 Conclusions

We have presented the results of the simulated collapse of a magnetised, rotating BE sphere reaching the early Class 0 phases through the use of sink particles. The principle model forms a 0.2 $M_{\odot}$ particle by the end of the simulation in addition to a rotationally dominated disc (not considering the support by the magnetic field) to about 100 AU, with a larger rotational structure extending out to 2000 AU. The motion inside 100 AU is dominated by rotation. The larger scale ($>$ 100 AU) flattened structure only lasts a fraction of a local rotation period before fragmenting. A fragment is formed 300-400 AU from the star. This disc is an important example of disc formation under ideal MHD conditions – previous studies found that cores with high magnetisations and highly ordered fields could not form (Mellon & Li, 2008; Hennebelle & Fromang, 2008; Zhao et al., 2011). The disc and the flattened rotating core launch a large outflow into the external medium clearing out a significant amount of mass from the envelope.

Our principal finding is that magnetised accretion discs in low mass systems generate turbulence due to the shedding of magnetic field loops from the disc surface via a Parker instability (Johansen & Levin, 2008). This degrades the mean magnetic field threading the disc, reducing and even reversing the magnetic braking torque. The result is that a sub-Keplerian accretion disc is assembled. This self-consistent process connects well with previous work (Seifried et al., 2012a) which demonstrated that turbulence can degrade mag-

netic torques in regions of massive star formation, leading to the formation of Keplerian accretion discs. In low mass cores, which have small line widths and are not dominated by large scale turbulence, it is important that the disc itself can generate the needed local stochastic shedding of buoyant magnetic loops, effectively creating a localized turbulent environment.

A feature predicted by Lai (2003), is the spontaneous warping of the protostellar disc relative to the initial rotation axis. The disc warps out to 30° relative to the z–axis without slowing and precesses in a prograde fashion. The time–scales for this match well with predictions by Lai (2003) with $t_{\rm warp} = 10^5$ yr at 100 AU. Our simulation runs for 2×10^4 yr after forming a sink particle. Strong magnetic torques in the x and y directions are measured and are responsible for the warp of the disc. The precession is prograde, in the direction opposite to that predicted if the field is arranged in a classical fashion (e.g. as described by Blandford & Payne, 1982). However, our disc material contains regions where $B_z < 0$. The precession of the disk reversed for the same reasons magnetic braking is reversed inside 65 AU.

We speculate that if our disc continues to misalign with the central star, we could form misaligned Hot Jupiters through planetary migration. Although, this mechanism is more likely to explain minor mis–alignment such as the 7.15° inclination of the solar system with respect to the Sun's rotation.

In summary, we have found that the solution to the magnetic braking catastrophe in low mass stars is that the turbulent conditions generated by magnetic buoyancy and loops produced by the collapsed structure result in field reversals in B_z. These downgrade the magnetic braking torque produced by the mean threading field on the disc. Keplerian discs can therefore form early on in regions of fairly strong magnetic field and rotation. This conclu-

sion requires further investigation for a grid of models with different initial magnetisations and rotational energies.

Acknowledgements

We thank Christoph Federrath concerning implementation of sink particles in FLASH. D.D. is supported by McMaster University and R.E.P by a Discovery grant from NSERC of Canada. D.S especially thanks the Heidelberg Graduate School of Fundamental Physics for funding a research visit at McMaster University, Hamilton. RB acknowledge funding of Emmy–Noether grant BA3706 by the DFG. RSK acknowledges support by contract research Internationale Spitzenforschung II of the Baden–Württemberg (grant P–LS–SPII/18), from the German Bundesministerium für Bildung und Forschung via the ASTRONET project STAR FORMAT (grant 05A09VHA), from the Deutsche Forschungsgemeinschaft (DFG) under grants KL1358/11-1 and KL1358/14-1, and via the SFB 881 – The Milky Way System. We are pleased to acknowledge the SHARCNET HPC Consortium for the use of its facilities at McMaster University. The FLASH code was developed partly by the DOE–supported Alliances centre for Astrophysical Thermonuclear Flashes (ASC) at the University of Chicago.

Chapter 5

The long–term evolution of magnetized pre–stellar cores II: precessing outflows and the efficiency of star formation.

5.1 Introduction

Understanding the origin of the initial mass function of stars is one of the most fundamental unsolved problems in star formation (Mac Low & Klessen, 2004; McKee & Ostriker, 2007). Reducing the problem to understanding the origin of the initial mass function of cores simplifies the problem if there exists a way to physically link the initial core mass to the final stellar mass.

It has been argued that the mass of low mass stars is limited by how much mass is cleared out by early gravito-magnetically driven outflows. There are many observations of protostellar outflows around young, embedded, class

0/I objects (e.g. Arce et al., 2007; Cyganowski et al., 2011). These outflows are 0.1-1 pc long, probably rotate (Zapata et al., 2010), are turbulent, and contain internal shocks and kinks (Gueth et al., 1998). These jets are often times episodic (Arce & Goodman, 2001b) and in some cases precess about the system rotation axis (Gueth et al., 1998; Arce & Goodman, 2001a).

It is expected that these early outflows are strong enough to clear out a significant fraction of mass from the protostellar envelope (Matzner & McKee, 2000) and limit the final mass of gas that makes its way onto the newly formed star. The core mass function is predicted to resemble the IMF as a consequence of supersonic turbulence (Myers, 2009; Padoan et al., 2001). Recent Herschel observations of the Aquila star–forming region reveal a Core Mass Function (CMF) which strongly resembles the Initial Mass Function of Protostars within a factor shifted to higher masses by 2.5-5 (André et al., 2010). The authors suggest that this would be understandable if individual cores had a low star formation efficiency of $\varepsilon_{\rm core} = M_{\rm star}/M_{\rm core} = 0.2 - 0.4$.

Measuring star formation efficiencies by this method has been questioned. This is because measuring the masses depends on a number of factors, such as the orientation of the cloud, effects of resolution and uncertain core fitting parameters (Smith et al., 2008). In a theoretical critique, Clark et al. (2007) note that for a group of cores with similar Jeans masses, the smaller mass cores evolve on shorter evolutionary timescales. At a given point in time, it is not guaranteed that the observed CMF has the same shape as the IMF. The fact that cores will also evolve by competitive accretion and fragmentation (Smith et al., 2009) suggests that outflows alone will not be the sole reason the CMF and IMF appear to have similar shapes.

Models of star formation efficiencies in the literature give a wide range

of predictions relating the initial core mass to final star mass (defined as $\varepsilon = M_{\rm star}/M_{\rm core}$. As an example, Matzner & McKee (2000) predict $\varepsilon = 0.25 - 0.75$, with the rest of the core mass being ejected by protostellar outflows, depending on the properties of the initial core such as the degree of flattening. Recent simulations by Machida & Matsumoto (2012) find that $\varepsilon_{\rm core} = 0.5 - 0.9$ of the initial cloud mass makes it onto the star (if we include the mass remaining in the protostellar disk), for a range of initial core masses (0.015-1.5 $M_{\odot}$). Price et al. (2012) find that their sink particle accretes $0.6 M_{\odot}$ after 1.2 free–fall times, giving $\varepsilon_{\rm core} = 0.6$. Numerical results suggest that star formation is more efficient than expected from the models and observations, and this requires elucidation.

The size, momentum, onset, collimation and timing of the outflow are important factors to consider in a model used to predict star formation efficiencies of cores.

Several theoretical models exist in the literature that describe the physical launching of magnetised outflows from rotating discs of gas. Using ideal magneto–hydrodynamic equations for a disc, and considering invariants along field lines Blandford & Payne (1982) derive a static disc–wind model describing the launching of gas co–rotating with the field. The gas is launched centrifugally from the disc provided the field satisfies certain conditions. One such criterion is that the field lines be inclined above the disc surface by no more than 60°. In contrast, the 'magnetic tower' model considers the growth of a transient magnetic bubble. This model describes, in a hydrostatic sense, the evolution and collimation of a magnetic tower driven by a rotating disc (Lynden-Bell, 2003; Sherwin & Lynden-Bell, 2007). The first model is often used to describe high speed jets launched from T–Tauri stars, while the 'magnetic tower' has

been used to describe an outflow pushed out by the toroidal magnetic field in numerical simulations of collapsing protostellar cores (Banerjee & Pudritz, 2007; Hennebelle & Fromang, 2008; Machida et al., 2009; Hennebelle & Ciardi, 2009).

By generalizing the approach of Blandford & Payne (1982) to outflows launched from a more general disc (e.g. not infinitely thin or Keplerian) and for outflow motions that are not only co–rotational, a more comprehensive disc–wind theory can be derived which describes the magnetised launching of gas under regimes which include both classical disc wind theory and magnetic configurations similar to the 'magnetic tower' (Pelletier & Pudritz, 1992; Seifried et al., 2012b).

In this study, we simulate an initial, low mass magnetized Bonnor-Ebert Sphere which is embedded in a much larger and more massive uniform medium. We show that our envelope first settles into a pseudo-disc before an outflow is launched which allows more mass to make it onto the star. Both the physical nature of the outflow along with the evolution are important factors to consider when predicting star formation efficiencies.

This chapter discusses first the physical properties of the outflow, such as its energy, momentum and velocity. We describe in detail the physical mechanism driving the outflow and compare these to observations. We then estimate the star formation efficiency of our protostellar core model. We discuss why our results differ from theoretical predictions.

5.2 Initial conditions and numerical methods

The model is identical to our previous studies of low–mass star formation (Banerjee et al., 2004; Duffin & Pudritz, 2009). In the first paper of the present series we focused on the formation of protostellar discs and the subsequent disc warping (Duffin et al., 2012b). Here we focus on the outflow, its physical properties and the resulting star formation efficiency.

In our model, we embed a 1.2 $M_\odot$ Bonnor–Ebert (BE) sphere (Bonnor, 1956; Ebert, 1955) in a low density environment, such that the density of this environment is 100 times less dense than the edge of the sphere. The box is roughly 0.81 pc in length, more than 10 times the size of the BE sphere. In total, there is a reservoir of $318 M_\odot$ in the box. This background has consequences for star formation efficiency, which are discussed later.

The BE sphere is at critical mass to which we also apply an additional 10% overdensity and a $m = 2$ perturbation such that $\rho(r) = \rho_{\rm BE}(1.1 + 0.1\cos(2\theta))$. We choose a magnetic field strength such that it has an initial mass to flux ratio relative to critical of $\mu/\mu_0 = 3.5$, ratio of rotational energy to gravitational energy $\beta_{\rm rot} = 0.3$ and temperature $T = 20$ K. These correspond to observations of magnetisations and rotational energies of real cores (Goodman et al., 1993; Crutcher, 1999).

We use a customized version of the FLASH 2.5 code with the newly developed Bouchut approximate Riemann solver for 3D magnetohydrodynamics (Bouchut et al., 2007, 2010). We use both 3.2 and 12.7 AU sink particles of Federrath et al. (2010a), corresponding to 2.5 times the smallest cell lengths. We use a cooling function which incorporates numerous factors such as radiative cooling by molecular line emission, gas–dust interaction and radiative

diffusion in the optically thick regime (Banerjee et al., 2006). For comparison with other papers, we also use a polytropic equation of state as described by Machida et al. (2007b). The different combinations of physical models are summarized in Table 4.1. The principle results presented here are from the model 'MHD+cooling'. We refer to our earlier paper, (Duffin et al., 2012b), for further details.

The disc surface sheds bubbles of magnetic flux from its surface due to a Parker instability (Duffin et al., 2012b), resulting in regions of relatively low density. The instability, coupled to a gravitational field which changes with height z above the disk midplane, can break symmetry above and below the xy–plane (Horiuchi et al., 1988). This results in very high Alfven velocities and corresponding small timesteps. We fix this by employing a density floor of 10^{-18} g cm^{-3} in the region 1000 AU from the centre of the box.

5.3 Outflow properties

In this section we address the principle questions concerning the protostellar outflow. What is driving the outflow and how? How much energy and momentum is being launched into the ambient medium? How much material is being launched off the disc surface? We demonstrate that the outflow has both a centrifugally driven and a B_ϕ dominated component. It is the central component which drives the warping of the disc and its precession, as presented in Duffin et al. (2012b).

Figure 5.1 shows a visualization in 3D of the structure of the disc, outflow and magnetic field lines. We plot density contours in purple and black to show the radial extent of the gas (about 2000 AU by the end of the

simulation). Black field lines thread the outskirts of the disc before rising in a highly wrapped fashion. Note how strongly the field is dragged inwards in the accretion disc. One begins to observe the precession of the jet in this image on scales of thousands of AU. The inner part of the disc ($r < 100AU$) is misaligned with the xy–plane by 30°, as is the inner region of the outflow misaligned with the z–axis (drawn in yellow for velocities $|v_z| > 1.5$ km s^{-1}). The effects of precession expand the bubble at higher distances from the disc midplane.

5.3.1 Physical properties

In previous studies of pre–class 0 collapse, outflows have been called magnetic towers (Banerjee & Pudritz, 2007; Hennebelle & Fromang, 2008; Machida et al., 2009), collimated, centrifugally launched jets (Blandford & Payne, 1982; Machida et al., 2006b) or in certain cases a mix of both jet and tower (Banerjee & Pudritz, 2006; Machida et al., 2007a). But it remains unclear what the physical difference between these two mechanisms is. As argued by Seifried et al. (2012b), both centrifugal driving as well as toroidal field dominated outflows are contained within a generalized version of disc–wind theory. However, physical conditions in an outflow vary greatly. A slow–moving, dense molecular outflow is different than a high speed molecular jet. In the following we will present our outflow results by first discussing their physical properties. We will then attempt to discern if our outflow is a jet, a tower, or something in between. Finally, we compare our results to observations of molecular outflows (e.g. Class 0/I type observations).

The numerical data show that we can decompose the outflow into two

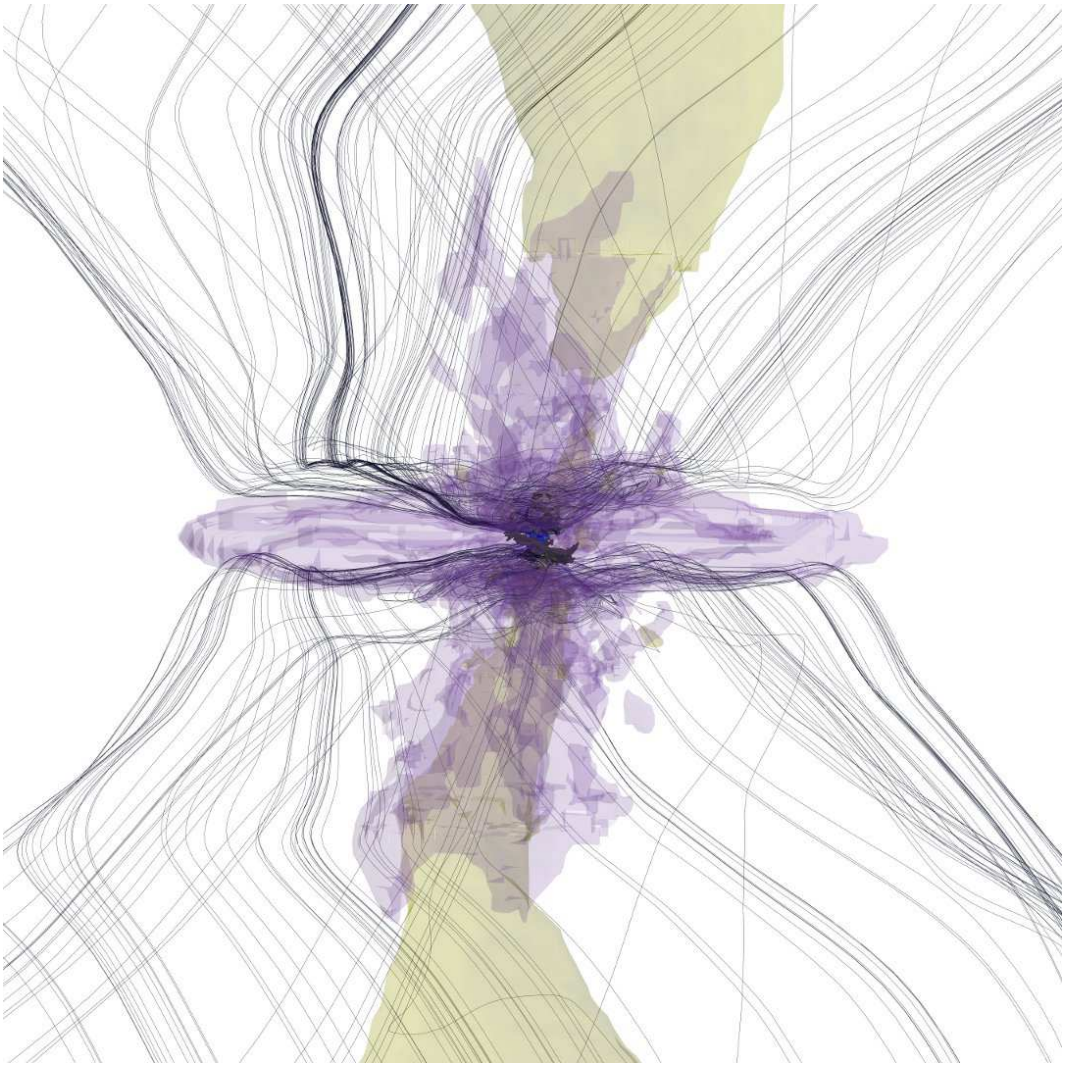

Figure 5.1 Three dimensional image of disc and outflow. Note that the purple contour has a radial extent of approximately 2000 AU. Purple contour corresponds to 3.3×10^{-17} g cm^{-3} ($n = 8.5 \times 10^{6}$ cm^{-3}) and black contours to 1.3×10^{-15} g cm^{-3} ($n = 3.4 \times 10^{8}$ cm^{-3}). Yellow contours correspond to outflowing velocities $v_z > 1.5$ km s^{-1}, and extends to a height of 10^4 AU. Black lines are magnetic field lines.

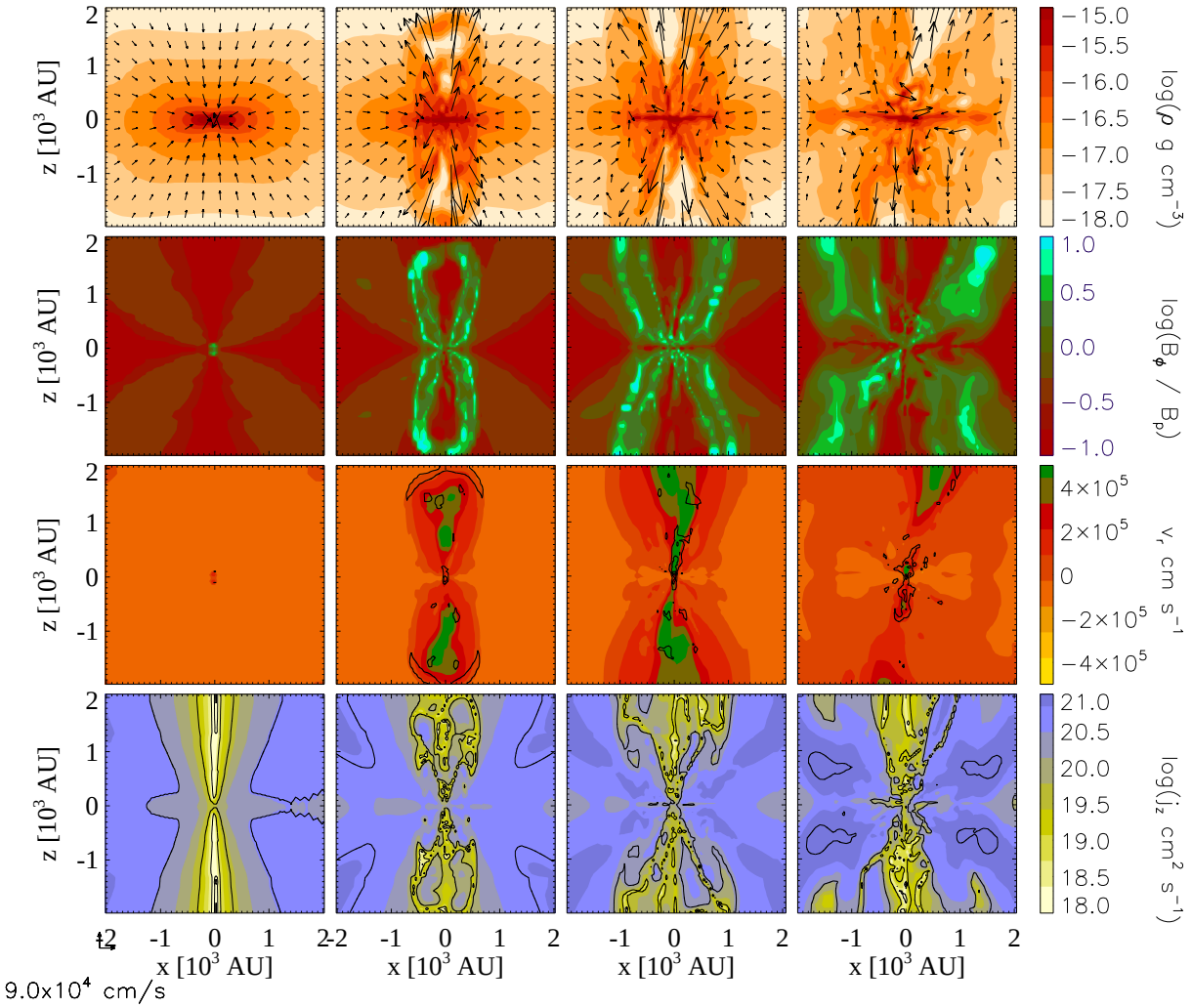

Figure 5.2 The physical properties of the disc and outflow system on a scale of thousands of AU (from left to right $t = t_0 + (0, 3.4, 10.3, 17.2) \times 10^3$ yr, where $t_0 = 2.6 \times 10^5$ yr). The top row shows the logarithm of density and velocity vectors similar to Figure 5.5. The second row shows the logarithm of the ratio B_ϕ/B_p. The third row show spherical radial velocity along with contours of logarithmic temperature. The fourth panel shows the logarithm of specific angular momentum in the z–direction, $j_z = (\boldsymbol{r} \times \boldsymbol{v})_z$, along with contours of the same quantity.

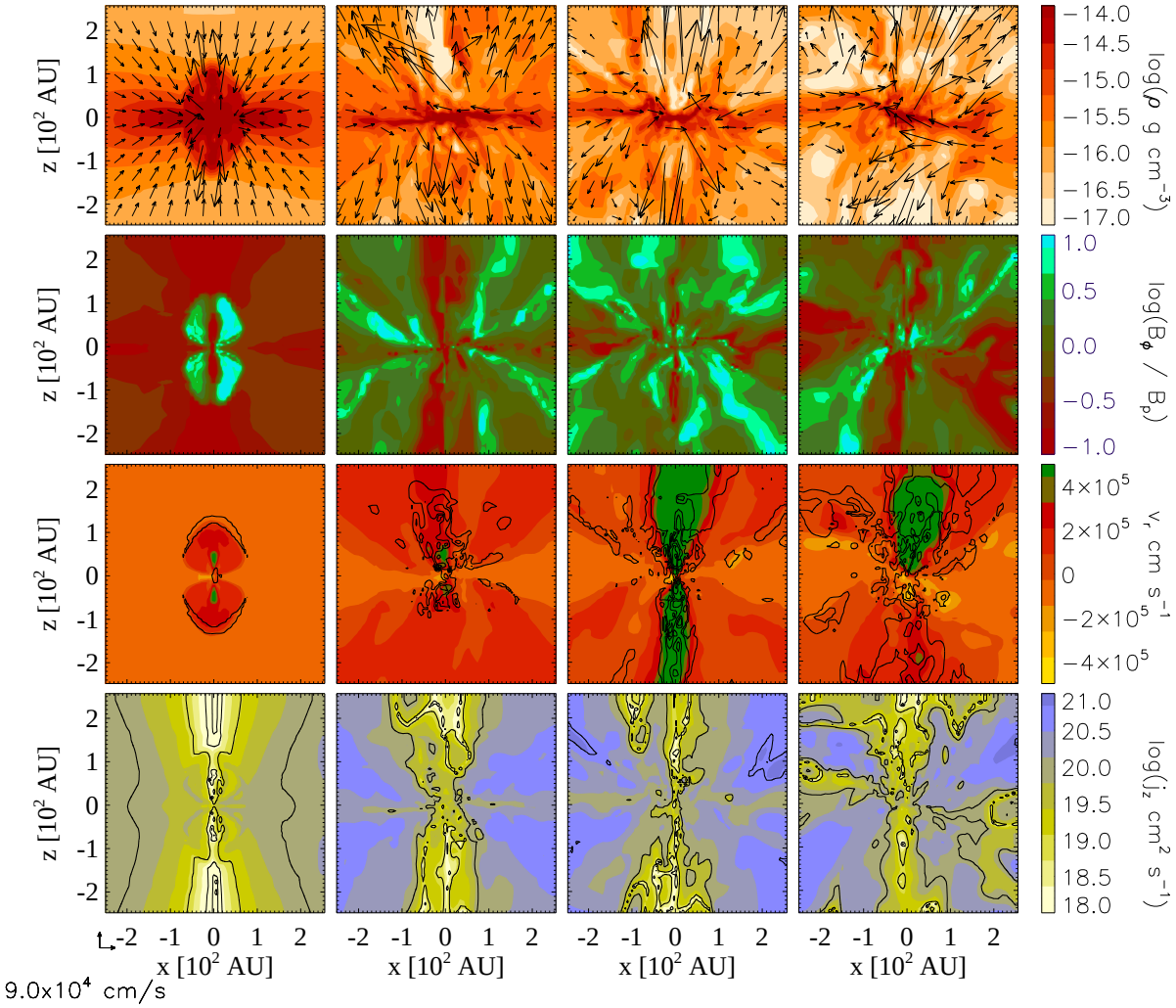

Figure 5.3 The physical properties of the disc and outflow system on a scale of hundreds of AU. See Figure 5.2 for details.

regions, a central component (inner region) and a shell encompassing it (outer region). Shown in Figure 5.2 and 5.3 is the time evolution of the outflow from left to right for different physical quantities on scales of 4000 AU and 400 AU respectively. We note that the outer region has higher densities and lower speeds ($\rho \sim 10^{-16.5}$ g cm^{-3} and $v_r < 1.5$ km s^{-1}) than the inner region ($\rho < 10^{-18}$ g cm^{-3} and $v_r > 4$ km s^{-1}). Furthermore, the magnetic field structure in the outer region is composed mostly of a toroidal component

($B_\phi/B_p > 10$) which suggests the main driving mechanism involves the toroidal field. The inner region's field is mostly poloidally dominated ($\boldsymbol{B}_p = \boldsymbol{B}_z + \boldsymbol{B}_r$), suggesting that the outflow is being flung out centrifugally along field lines.

An interesting point is that the outflow drives quite a bit of heating in the outflow and the inner disc. A bow shock of about 100 K is clearly visible in the contours of the third rows of Figures 5.2 and 5.3. Inside the outflow, internal shocks develop. The highest speeds of the jet are accompanied by heating up to a few 1000 K. What can, early on, be identified as a "first core" because of the temperature structure, is quickly confused as the outflow heats the surrounding gas. These features are sensitive to the cooling function we use and are not seen in runs with a polytropic equation. In the latter case, the gas temperature is tied to the gas density and hence it remains mostly isothermal, except in the inner regions of the disc.

Figures 5.2 and 5.3 also reveal that the specific angular momentum ($\boldsymbol{j} = \boldsymbol{r} \times \boldsymbol{v}$) is larger in the outer region ($j_z \sim 10^{21}$ cm^2 s^{-1}) than the inner region ($j_z < 10^{19}$ cm^2 s^{-1}). Note that our initial conditions of solid body rotation imply $j \propto r^2$, and this is imprinted somewhat in the first panel of the series of j_z. The outer region is larger in volume and at higher average densities than the inner region. The total angular momentum ($\boldsymbol{L} = m\boldsymbol{j}$) is contained mostly in the outer region. The angular momentum of the disc itself on the other hand looks to be fairly smooth ($j_z \approx 10^{20.5}$ cm^2 s^{-1}).

It is clear that different regions of the disc lose differing amounts of angular momentum. The relation of outflowing and inflowing mass rates is a measure of how efficient the outflow process is in driving mass accretion. Similarly, it is also a measure of how efficient the wind is at extracting mass or angular momentum from the disc. Disc wind theories predict a ratio of

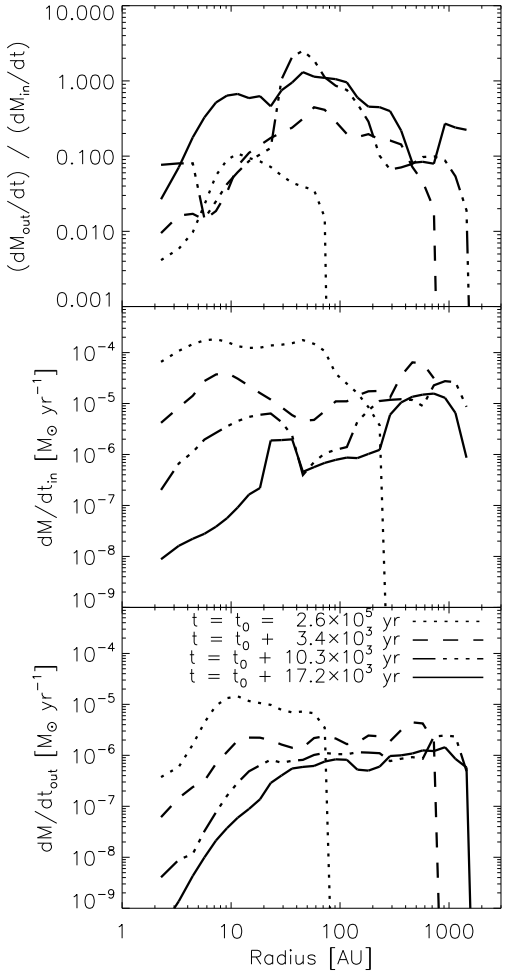

Figure 5.4 The outward mass flux $\dot{M}_{\rm out}$ compared to the inward mass flux $\dot{M}_{\rm in}$ at various times at surfaces near the launching point of the outflow.

outflowing mass flux from the disc surface to inflowing mass flux in the disc (Pudritz et al., 2007) of the order of 0.1. As an example, forbidden line studies of the late stages of jet evolution find values in the range (Ray et al., 2007)

$$\frac{\dot{M}_{\rm outflow}}{\dot{M}_{\rm disc}} \approx 0.05 - 0.1, \tag{5.1}$$

in agreement with theory.

We measure this ratio at various radii and at various times in the formation process to see if there is a fundamental difference between the two outflow regions. We define a disk surface in our simulation in the following way. First we define hollow cylinders at various radii. We extend the height by powers of 2 times the smallest cell size to ensure a cell can exist at the surface (unless we are too high and too close to the centre of the simulation). We also choose the height such that it is just above the zero velocity surface (the average speed in the hollow cylinder is greater than zero). In this sense, the outflowing flux is $\dot{M}_{\rm outflow} = \sum_{\rm cells} \rho v_z A_{\rm cell}$, where $A_{\rm cell}$ is the surface cell area, and is easy to measure for top and bottom surfaces of each hollow cylinder. The inward flux is measured by taking the volume averaged value of ρv_r and multiplying by the average area $\pi(r_{\rm in} + r_{\rm out})H$, where $r_{\rm in,\ out}$ is the inner and outer radius of the hollow cylinder, respectively and H is the height.

We plot the radially binned values of outward and inward mass flux from the disc in Figure 5.4. We find that near the centre of the simulation $\dot{M}_{\rm outflow}/\dot{M}_{\rm inflow} \sim 0.1$, where the inner region is more prominent. However, for the outer region dominated by the tower flow, we find a higher value $\dot{M}_{\rm out}/\dot{M}_{\rm in} \sim 1.0$.

There are two ways to see these differing mass flux ratios. Firstly, the outer region loses a lot more mass than the inner region per unit mass accreted inwards. Therefore, in the outer region, the disc wind mass flux is quite prominent. This makes sense, as the density in the outer region ($\rho \sim 10^{-16.5}$ g cm^{-3}) is much higher than the density in the inner region ($\rho < 10^{-18}$ g cm^{-3}). Secondly, the outer region is less efficient at extracting angular momentum than the inner region by a factor 10. If the outflow extracts angular momentum and drives accretion, the accretion rates would be higher per unit

mass in the inner region than the outer region.

We note that at the last time plotted, the transition of $\dot{M}_{\rm out}/\dot{M}_{\rm in}$ from 1 to 0.1 occurs at about 7 AU, which is close to the sink radius of 3.2 AU. At this distance, the transition is no longer clear. However, at early times, a transition is seen at about 20 AU.

5.3.2 Velocity structure

Figure 5.5 shows a more detailed evolution of the density and velocity field of the accreting and outflowing gas. The development of both regions of the outflow, along with the onset of the disc warping and clearing of the envelope are evident. Note that the fastest outflow speeds are very likely dependent on sink particle size; faster speeds are expected to be launched deeper within the potential well of the star and this is limited by the size of the sink particle. For about 2000 years after the sink particle forms, the outflow is fairly symmetric with respect to the xy–plane but gradually becomes mis–aligned and tilted, along with the disc which drives it (Duffin et al., 2012b). Some of the central outflow is missed in the later stages of Figure 5.5 because it is tilted away from the density slice. On larger scales, the disc continues to grow in radial size and the outflow extends out in a nearly self–similar way, maintaining a similar shape or aspect ratio (as in Figures 5.2 and 5.3). The internal structure is highly turbulent, non–symmetric with many kinks, internal shocks and containing a significant amount of mass.

In Figure 5.6, we plot the sonic ($\mathcal{M} = v_r/c_s = 1$), Alfvenic ($\mathcal{M}_{\rm A} = v_r/v_{\rm A} = 1$) and approximations of fast and slow magneto-sonic surfaces ($\mathcal{M}_{c_{\rm fast,\ slow}} \approx v_r/\sqrt{|v_{\rm A}^2 \pm c_s^2|} = 1$ in the wind). The majority of the material in the outflow

is moving not just supersonically, but super–Alfvenically. This suggests that most of the material in the outflow bubble will escape the core. For guidance, the bubble is drawn for $v_r = 0$, the transition from outflow to inflow velocity. Note that v_r is the spherical radial velocity.

5.3.3 Driving Mechanism

The protostellar outflow is ultimately driven by the gravity of the protostellar system, but requires the magnetic field in order to tap this reservoir and to convert it into ordered outflow (Pudritz et al., 2007). Although small ($z <$ 50 AU) outflows have been produced in numerical simulations using simply radiation pressure and hydrodynamics (Bate, 2010), it is not clear whether these outflows can be driven to the scales of observed outflows (pc scales), or have the rotational properties observed in outflows around T–Tauri stars (Coffey et al., 2007).

Previous protostellar winds have been modelled in detail through hydrostatic, self–similar disc–wind theories (Blandford & Payne, 1982; Pelletier & Pudritz, 1992) and for self–similar models (Krasnopolsky & Königl, 2002) which describe a centrifugally driven wind (e.g. 'flinging' of gas by the magnetic field). This wind theory in turn has been used to describe the high–speed jets present in early (Class 0/I/II) protostellar systems (Pudritz & Norman, 1986). Separately, Lynden-Bell (2003) developed a hydrostatic model to describe the driving of a highly collimated outflow 'bubble' and the work done by the continual winding and twisting of the magnetic field in the disc. In this model, a magnetic tower is created which if continually driven, drives material at the 'pressure head' outwards in face of a generalized external pressure.

It is a common misconception that the magnetic tower describes an outflow which is purely driven by a wrapping of the magnetic field and that disc wind theories are dominated by a flinging of material. Indeed, B_ϕ/B_p can be high as 10 in disc wind models. And while the twisting of the field by the disc is key to magnetic tower model, non–toroidal components of the field become important when considering the expansion of the 'magnetic bubble' (Sherwin & Lynden-Bell, 2007). Rather, these are two extremes of to disc wind theory where the field is primarily pushing material up like a spring, or flinging it out centrifugally. We demonstrate that both configurations exist in the outflow bubble in our simulation.

We have recently worked out a more generalized criterion of disc wind theory – assuming that the gas is not necessarily co–rotating with the field and that the disc and field can have more generic features than previously considered. This model shows that disc–wind theories can have acceleration mechanisms that are driven by centrifugal forces as well as toroidal fields. Both magnetic tower and disc–wind theories are therefore understood as a consequence of the same disc–wind model (Seifried et al., 2012b).

The model results as a solution to the ideal magneto–hydrostatic equations considering several invariants along the poloidal magnetic field lines (Pelletier & Pudritz, 1992). This generalization reveals that two regimes in the outflow exist, 1) a component that is co–rotational with the gas where the centrifugal ('flinging') force dominates and 2) a component where the field is not co–rotational with the gas and the toroidal component of the field plays a stronger role. In our principal simulation we show that both regimes are

present. We use the generalized criterion developed in (Seifried et al., 2012b):

$$\partial_{\rm pol}\left(\frac{1}{2}v_\phi^2+\Phi-\frac{v_\phi}{v_{\rm p}}\frac{B_\phi B_{\rm p}}{4\pi\rho}+\frac{B_\phi^2}{4\pi\rho}\right)<0, \tag{5.2}$$

where $\partial_{\rm pol}$, is the derivative along the poloidal field line $\boldsymbol{B}_{\rm p}=\boldsymbol{B}_z+\boldsymbol{B}_r$, Φ is the gravitational potential, and $v_{\rm p}$ is the poloidal velocity ($v_p=|\boldsymbol{v}_z+\boldsymbol{v}_r|$). Here we estimate the gravitational potential by using the mass of the sink particle, so we are underestimating this factor. However we should still be able to track regions which are strongly driven by the field as described by the disc wind theory.

We apply this criterion to data at early times ($t=t_0+1300$ yr), as the outflow is more symmetric. We average data azimuthally to smooth out the 3D nature of the outflow. Our results are shown in Figure 5.7 on the left. Much of the outflow is being accelerated by the magnetic field. This helps us understand why our outflow is knotty in structure and contains many internal shocks and turbulent motions.

A more specific criterion for centrifugal acceleration was also derived in Seifried et al. (2012b), but for the case where the gas is predominantly co–rotating with the magnetic field and the effect of B_ϕ can be omitted. In this case, the criterion is:

$$\frac{r}{z}\frac{1}{GM}\left(\frac{v_\phi^2}{r^2}\left(r^2+z^2\right)^{3/2}-GM\right)/\left(\frac{B_z}{B_r}\right)>1, \tag{5.3}$$

where (r,z) are points in the simulation in cylindrical coordinates and M is the enclosed mass (which we again approximate here by the mass of the sink particle). This theory can be applied to discs which are neither infinitesimally

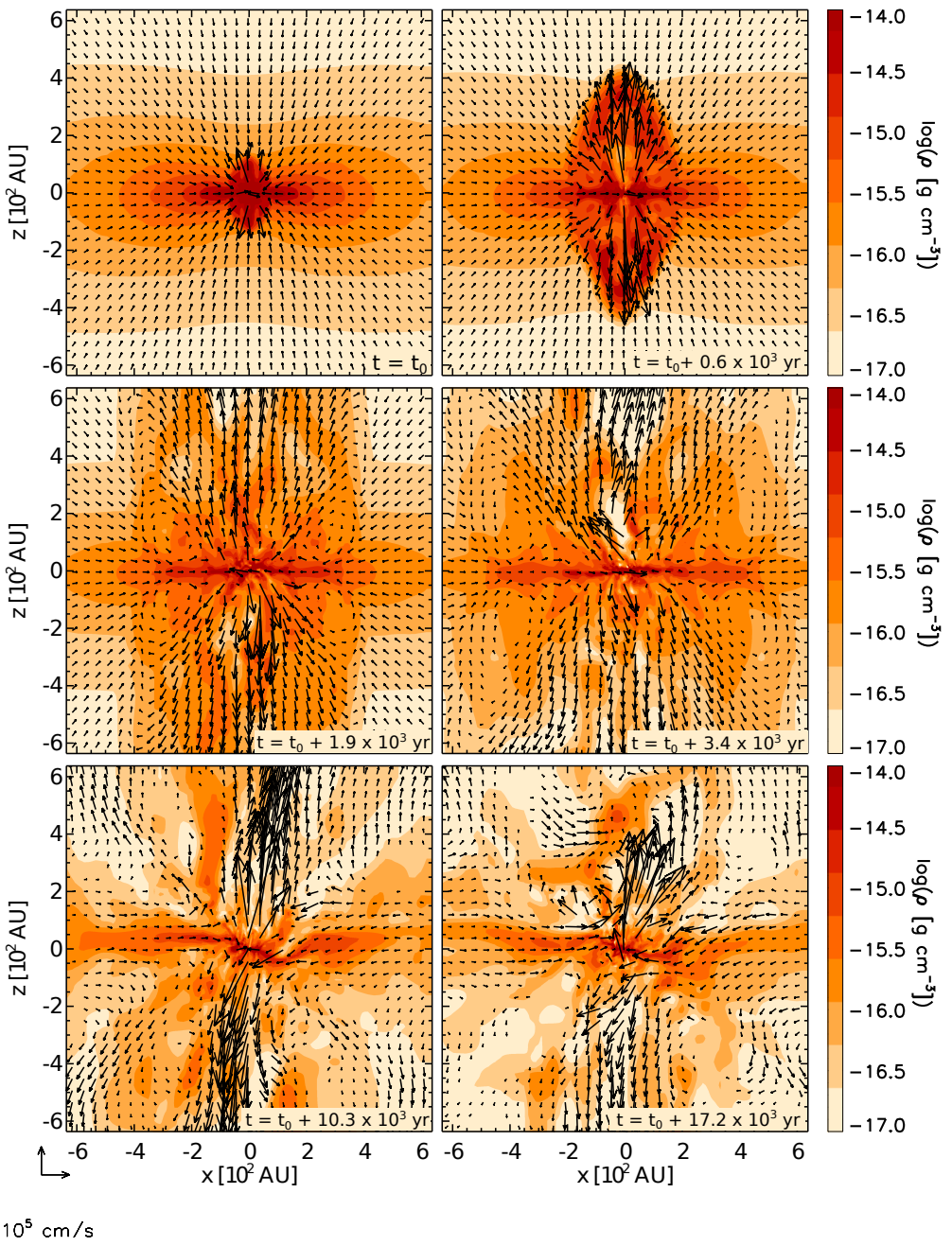

Figure 5.5 Time evolution of the outflow. Cross–sectional density slices of the disc at various times in the evolution of the outflow (advancing from left to right, top to bottom $t = t_0 + (0, 0.6, 1.9, 3.4, 10.3, 17.2) \times 10^3$ yr, where $t_0 = 2.6 \times 10^5$ yr), showing velocity vectors. The low velocity bubble grows symmetrically until the onset of a high–speed inner component. The disc tilts relative to the slice and only a portion of the jet structure is visible.

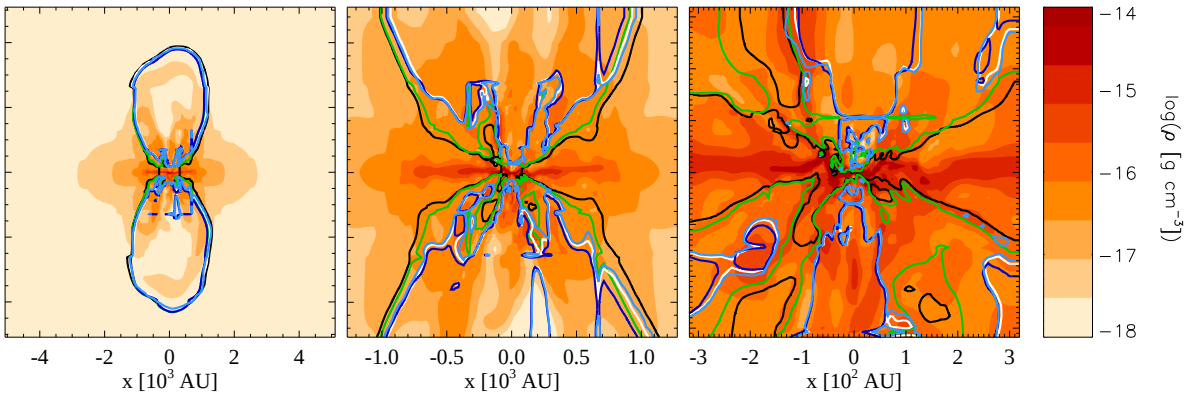

Figure 5.6 Contours of outward velocity v_r such that $v_r = 0$ (black), $\mathcal{M} = v_r/c_s = 1$, $\mathcal{M}_{\rm A} = v_r/v_{\rm A} = 1$ (white), $\mathcal{M}_{c_{\rm fast}} \approx v_r/(v_{\rm A} + c_s) = 1$ (dark blue), and $\mathcal{M}_{c_{\rm slow}} \approx v_r/(v_{\rm A} - c_s) = 1$ (light blue). Colours are density given at a mid–state of the simulation such that $t = t_0 + 10.3 \times 10^3$ yr at different zoom factors. This is as a time $t = t_0 + 10.3 \times 10^3$ yr.

thin nor purely Keplerian. We apply this criterion to our results in Figure 5.7 on the right. Now only the central regions of the outflow agree with the criterion.

Putting the two panels of Figure 5.7 together, we complete the physical picture of the protostellar outflow in our simulation. The *inner region* is dominated by centrifugal driving. It is precessing at an angle 30° to z-axis, has high speeds ($v_r > 1.5$ km s^{-1}), high temperatures (T up to 3000 K) and low densities ($\rho < 10^{-18}$ g cm^{-3}). It is dominated by the poloidal magnetic field ($B_\phi/B_p < 0.1$) and contains less specific angular momentum ($j_z < 10^{19}$ cm^2 s^{-1}) than the outer region. Furthermore, in comparison to the outer region, it has a smaller mass flux and is more efficient at driving mass accretion through the disc per unit mass driven outwards ($\dot{M}_{\rm out}/\dot{M}_{\rm in} \sim 0.1$). We suggest this region corresponds to molecular jets observed around younger to older protostars (Class 0/I/II).

The *outer region* is dominated by toroidal driving. It has low speeds

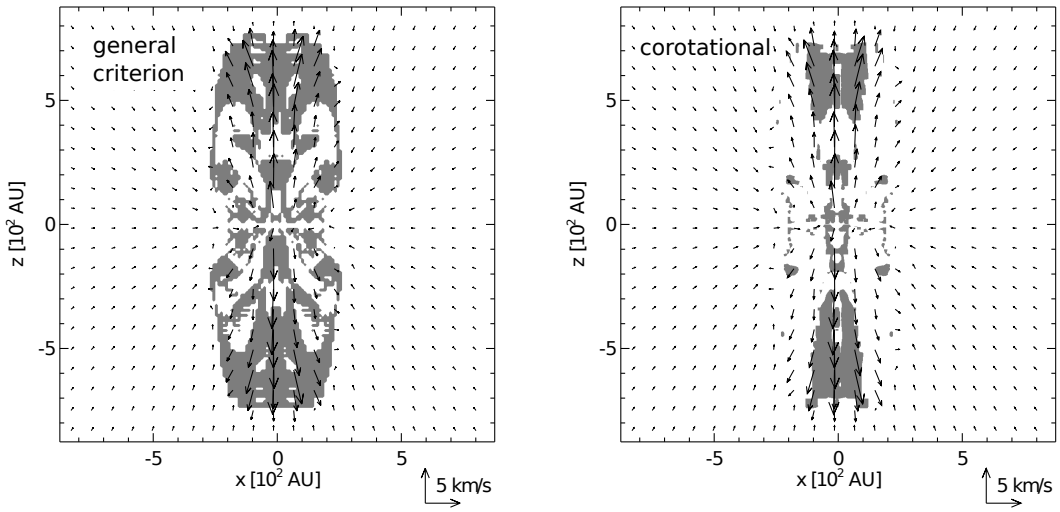

Figure 5.7 The disc–wind driving criterion is satisfied in dark regions for early times ($t = t_0 + 1300$ yr). Numerical data is averaged azimuthally. The left panel shows the general criterion as in Equation 5.2. The right panel shows the criterion assuming the gas co–rotates with the field as in Equation 5.3, which highlights centrifugally driven gas. The difference in the two images marks the region where the toroidal field is the dominant driver of the outflow.

($v_r < 1.5$ km s^{-1}), low temperatures ($T = 20$ K, except in bow shocks), and high densities ($\rho \sim 10^{-16.5}$ g cm^{-3}). It is dominated by the toroidal magnetic field ($B_\phi/B_p > 10$) and contains more specific angular momentum ($j_z \sim 10^{21}$ cm^2 s^{-1}) than the inner region. Furthermore, in comparison to the inner region, it has a significant mass flux off the disc surface and is less efficient at driving mass accretion through the disc ($\dot{M}_{\rm out}/\dot{M}_{\rm in} \sim 1$). We suggest this region corresponds to molecular outflows observed near Class 0 objects.

5.3.4 Energetics and Momentum

We take all material in the outflow bubble and plot over time its mass, energy, momentum and volume, as shown in Figure 5.8. The bubble grows in the z–direction, but also in the x and y–directions. The volume of the bubble grows

as $V_{\rm outflow} \propto t^{2-3}$ while other quantities grow much more linearly. Therefore, although energy and momentum inside the bubble grow, they become more dispersed, so that momentum and kinetic energy density decreases.

One also notices that around 12 kyr, the slope of the kinetic energy versus time becomes shallower. Thermal losses from molecular cooling start to become significant as the outflow leaves the confines of the BE sphere. The head of the outflow bubble is very hot (around 100 K) as the gas is compressed, however molecular cooling is very efficient at this density, so there is a continual loss of energy in the bubble. Similarly, the high speed jet has temperatures in excess of 1000 K, and cools rapidly.

5.3.5 Comparing to observations

When comparing to observations, the values of kinetic energy ($\approx 2.5 \times 10^{43}$ erg) and momentum ($\approx 0.7 M_\odot$ km s^{-1}) we obtain seem to be in the right range, despite the fact that we are not resolving the fastest motions launched within 3.2 AU of our sink particle. Arce & Sargent (2005) made 3mm continuum interferometer observations of the RNO43 outflow within 2×10^4 AU of its source, the class 0 protostar IRAS 05295+1247. Correcting for an inclination of 15°, they measure the kinetic energy (1.5×10^{43} erg) and momentum ($0.8 M_\odot$ km s^{-1}) in gas traced by C^{18}O emission inside 2×10^4 AU, where the envelope is approximated as 2.3 $M_\odot$. In a more diverse sample, the same authors analyze molecular outflows within 10^4 AU of their source for several low–mass class 0, I and II envelopes (Arce & Sargent, 2006). In particular, two different class 0 sources, IRAS 3282+ and HH 114mms are measured to have momentum of $0.091/\sin\theta$ and $0.044/\sin\theta$ $M_\odot$ km s^{-1} and kinetic energies

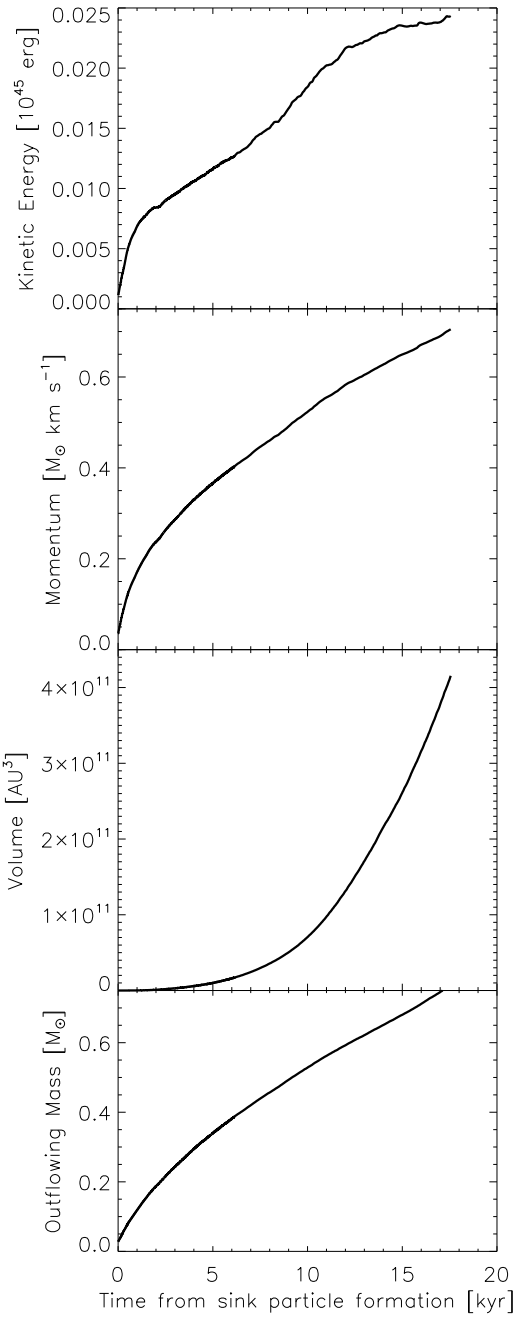

Figure 5.8 The change over time of the kinetic energy, momentum, volume and mass of outflowing gas in the principle simulation.

of $0.484 \times 10^{43} \sin^2\theta$ and $0.195 \times 10^{43} / \sin^2\theta$ erg respectively, where θ is the inclination angle of the outflow. These observations compare very favourably to our simulations because our outflowing region is approximately 10^4 AU in size, while our source is a Class 0. Our envelope mass is also similar to the masses in these observations. It is encouraging that our results have produced general properties that agree with observed values.

5.4 Sink Particle Evolution

The sink particle is not a star, but simply gas mass and momentum that has been removed from the simulation and put into a particle which interacts only gravitationally with the gas. We cannot solve the collapse problem down to a stellar radii, so indeed further fragmentation and even outflows can occur on scales inside the sink particle that we do not account for. Outflowing gas that would otherwise be driven from inside the sink particle will be faster as it must overcome a deeper gravitational potential. The particle mass is an upper limit to the mass of any star that may form in a collapse. We compare the sink particle mass and angular momentum with that of its envelope, disc and outflow as a way of understanding the star formation process in simple terms.

We define a flattened cylinder with a radius and height equal to the radius of the original over–dense BE–sphere, $r_{\rm BE} \approx 1.5 \times 10^4$ AU. This 'core' is larger than the BE sphere, and therefore more massive (starting at $1.6 M_\odot$). We do this because the BE–sphere flattens over time. This is a simple way of tracking the evolution of mass and angular momentum inside the core.

We define the pseudo–disc by identifying the furthest cell with infall

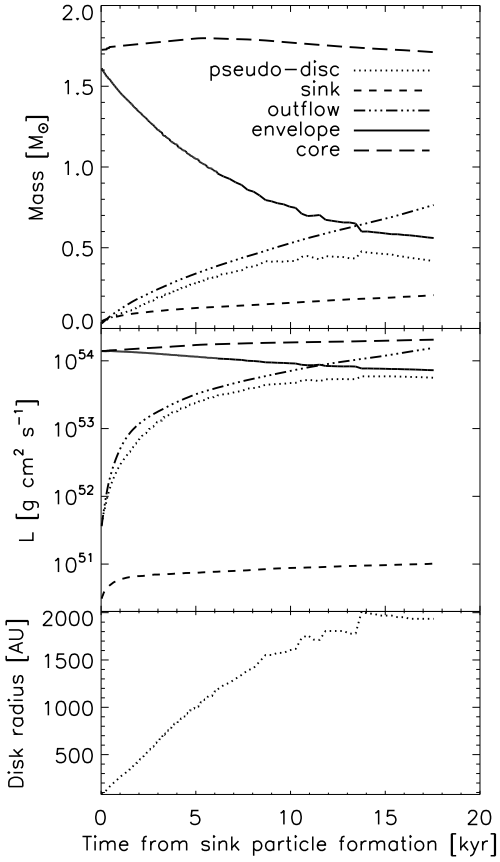

Figure 5.9 Top panel: the time evolution of pseudo-disc, sink particle, envelope, outflowing gas and core masses. Middle panel: similar, but for angular momentum $L = m|\boldsymbol{v} \times \boldsymbol{r}|$. Bottom panel: the evolution of the pseudo-disc radius $r_{\rm pseudo-disc}$. The outflowing gas is all gas in the simulation that is outflowing (even outside the core). The pseudo-disc mass is all mass inside a flattened cylinder of radius and height $r_{\rm pseudo-disc}$ that is infalling. The envelope mass is all gas within a cylinder with radius and height $r_{\rm BE}$ that is not in the other components. The core mass is the total mass inside a flattened cylinder of radius and height $r_{\rm BE}$, encompassing the original core.

motion such that $v_\phi/v_r > 5$[1], and use this to define a cylindrical disc radius and height, $r_{\rm pseudo-disc}$. We define all gas with outflowing motions in the simulation as 'outflow' mass (e.g. including entrained envelope material, far from the core). Much of the material in the outflow is entrained gas outside of the original BE sphere. Star mass is considered to be anything accreted by the sink particle. Anything in the 'core' that is not outflowing, in the pseudo disc (or disc) or in the sink particle, is considered as 'envelope' gas.

We plot these values in Figure 5.9. We find that the pseudo–disc continually grows in size, extending to 2000 AU. Over time, the envelope is either accreted onto the pseudo–disc or pushed out by the outflow. Near the end of the simulation, the envelope has a mass of $0.5M_\odot$, less massive than the outflowing gas ($0.8M_\odot$) and nearly as massive as the pseudo–disc ($0.4M_\odot$). While the disc mass wanes, the outflow mass continues to grow. We note also that the growth of the sink particle mass is much slower than that of the disc or outflow. At the end of our simulation, we have an early Class 0 object because our envelope mass is similar to our pseudo–disc, while our pesudo–disc is more massive than our sink particle. The Bonnor-Ebert sphere is embedded in a low-density environment 100 times less dense and continues to accrete from this surrounding medium.

The angular momentum is presented in the middle panel of Figure 5.9. By the end of our simulation, more angular momentum is contained in the outflow ($1.1 \times 10^5 L_\odot$) than either the disc ($4 \times 10^4 L_\odot$) or envelope ($6 \times 10^4 L_\odot$). However, the angular momentum in the sink particle is at a much smaller value than the other components. The angular momentum of

[1]a factor 5 rather than 1 helps us exclude inflowing material on the edge of the outflow bubble that is highly rotating

the Sun is $L_{\odot} \approx 1.1 \times 10^{49}$ g cm^2 s^{-1}, and the angular momentum of the sink is $L_{\rm sink} = 10^{51}$ g cm^2 s^{-1} $= 91 L_{\odot}$. The star unlikely will attain this much angular momentum as we are missing processes of angular momentum extraction inside of 3.2 AU such as magnetic braking of a protostellar disc or the outflow operating on these small scales.

5.4.1 Larger sink particle sizes

Initially we ran simulations with larger sink particles (12.7 AU rather than 3.2 AU) to ascertain the effect of resolution on gross features such as disc warping, jet precession and disc/outflow size. We plot the mass evolution of the sink particle(s), pseudo–disc, envelope and outflow masses for a range of simulations in Figure 5.10.

The 12.7 AU sink particle runs shown in Figure 5.10 evolve for several 10s of kyr further in time than the 3.2 AU particle runs. It is clear that a larger sink gains a larger initial mass and grows at a faster rate than the smaller sink particle. Both runs show that the envelope mass flattens out to 0.2 $M_{\odot}$, while the sink continues to accrete. The run with the polytropic prescription is run for 80 kyr and shows that the pseudo-disc mass grows and then shrinks to a mass of about 0.3 $M_{\odot}$. The particle continues to grow, reaching 0.75 $M_{\odot}$ (they only reach 0.5 $M_{\odot}$ in the run with cooling, evolved for 40 kyr), showing no sign of stopping. Intriguingly, the outflow reaches a maximum mass and turns over around 60 kyr. This is due to the outflow dissipating outside the envelope.

In 'Hydro+Cooling' simulation, the initial disc fragments into 3 particles. Formed through fragmentation of the disc, these particles do not accrete

much after they form. The disc continues to grow without producing new particles. In the polytropic prescription, the hydro run very quickly builds up a 0.4 $M_\odot$ sink particle in 20 kyr at the centre of a disc. This is twice as much mass as the particle in the MHD run in the same time. We note again that the cooling prescription used in the simulation changes the result of the simulation, chiefly for reasons of disc stability.

We compare the MHD and hydro runs with cooling in Figure 5.10. There is a difference in the evolution of the disc mass. At 8 kyr, the hydro with cooling simulation reaches a disc mass of 0.5 $M_\odot$. In the MHD with cooling run the disc is 0.4 $M_\odot$ at 8 kyr. The outflow does not seem to be limiting the gas mass accreting onto the disc. This is because gas first settles into a disc before launching the outflow.

5.5 Discussion: Star formation efficiencies

Ultimately, we are interested in understanding how the star is assembled from the core. Our initial core has near–critical magnetic field strength and rotational energy. In general, one would expect cores to have a variety of initial conditions leading to various outflow sizes and strengths, with correspondingly different amounts of instability and fragmentation in their discs. Outflows and fragmentation both limit mass accretion onto the principal star. In our simulations, the magnetic field suppresses fragmentation relative to the purely hydrodynamic case. Here we ask the question, how do outflows limit the assembly of the star?

Understanding star formation efficiencies may help explain the apparent one–to–one relation between the CMF and the IMF (Motte et al., 1998;

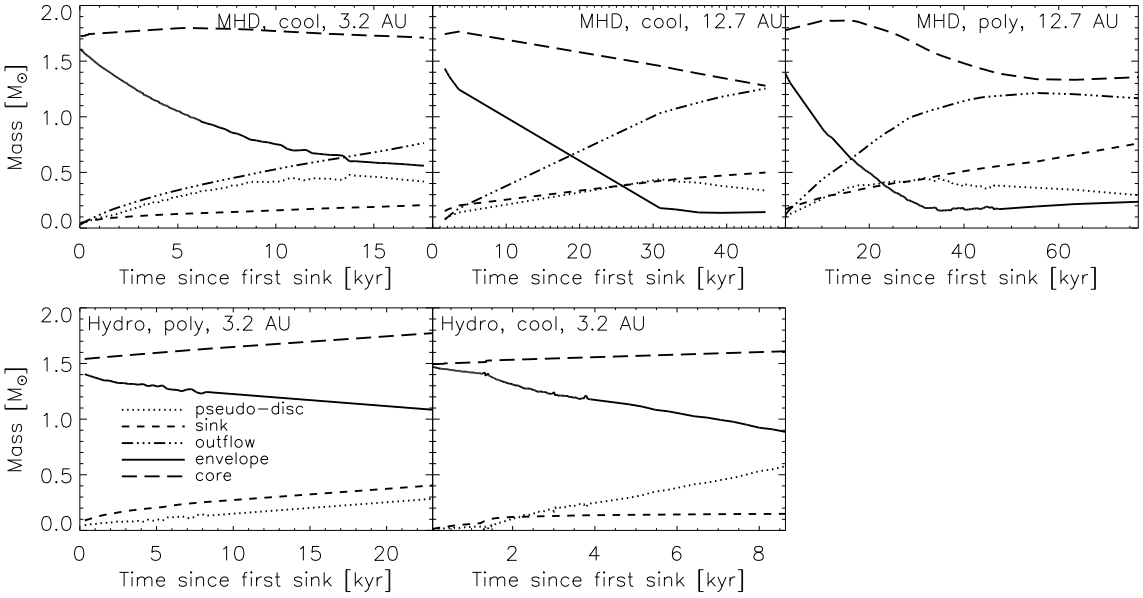

Figure 5.10 The same as Figure 5.9, but for more models with or without a magnetic field, with different sink particle sizes (3.2 or 12.7 AU) and cooling functions (polytropic prescription or cooling function). Note the definitions of envelope, disc and outflow material in the text. In the run labelled "Hydro, cool, 3.2 AU", we have plotted the sum of all sink particle masses (there are three).

Johnstone et al., 2001; André et al., 2010). The observed CMF and IMF appear to have similar distributions, with the CMF shifted to higher mass by a factor of 2.5–5, giving star formation efficiencies of $\varepsilon_{\rm core} = 0.2 - 0.4$.

Recent results of high mass cores (100 $M_\odot$) with varying initial magnetic field strengths and rotational energies result in different disc structures (stable or unstable) as well as outflow shapes and strengths (Seifried et al., 2011, 2012b). Despite this, mass accretion rates lie within a factor of a few $(0.35 - 0.95)$ of the non–rotating, non–magnetised case. In these studies, it is difficult to comment on overall 'star formation efficiencies' considering that total sink particle masses only reach a maximum of few solar masses, or a few percent of the initial core mass. Nevertheless, because the accretion rates

are all similar to each other, the conclusion is that outflows do a poor job at limiting mass of the forming star or stars.

Similarly, we do not observe the so–called 'end–state' of accretion in our principal simulation. However, by the end of our simulation the mass of the envelope is similar to the mass of our pseudo–disc (see Figure 5.9). We have simulated the formation of a Class 0 object. In our lower resolution runs, the sink particle has accreted 63 percent the mass of the original core material (0.75 $M_{\odot}$ compared to the 1.2 $M_{\odot}$ BE sphere), with no signs of stopping. In this sense, our simulations offer a unique window into the star formation efficiency of an individual core.

The model of Matzner & McKee (2000) predicts star formation efficiencies of $\varepsilon_{\rm core} = M_{\rm star}/M_{\rm core} = 0.25 - 0.75$ for various degrees of core flattening. For our core, we know the degree of flattening so we can narrow down this predicted range to $\varepsilon_{\rm core} = 0.29 - 0.39$ by incorporating our numerical results into their model (see Appendix 5.7).

The model predicts the outflow will push out material from the core based on a projected momentum distribution. Mass from the disc wind itself is considered to be negligible when compared with entrained material (thus, predicted efficiencies are upper limits). It requires information about outflow mass and momentum in order to predict an opening angle for a radial outflow. It also requires information about the initial core mass.

Summarizing our results on efficiences, we find that the model has several important shortcomings, documented below

- The core is a static object in mass, however real cores are not. Our BE sphere because it is embedded in a low density environment, accretes

mass over the timescales of the simulation. Real cores exist in a dynamic gaseous environment which will accrete mass from their surroundings over time (Smith et al., 2009; Myers, 2009). For example, the mass within our core changes from 1.7 $M_\odot$ to 1.4 $M_\odot$ over the course of 8×10^4 yr (model 'MHD, poly, 12.7 AU', Fig. 5.10) despite having an outflow ejecting gas outside the core with total outflowing mass equal to $1.2 M_\odot$.

- We find that it is the exact time at which the outflow is launched that is a key control variable - and this can make all the difference in predicting how efficient the process will be. We find that the envelope condenses first into a pseudo–disc before the highly collimated outflow is launched from the disk surface. This increases the star formation efficiency significantly by limiting the amount of envelope material that can be cleared away.

- The structure of the simulated outflow is highly collimated and launched from the pseudo–disc surface. In the model of Matzner & McKee (2000), the outflow is radial, being launched from a central point, based on the X-wind model (Shu et al., 1988). An updated model could be constructed that incorporate the structure of the earliest outflows from numerical simulations to better estimate the amount of material pushed out of the core.

The approach of this theory is still useful – the relation between initial core mass and star mass can be used to understand the relation between CMF and the IMF of stars in clusters. However our understanding of the early evolution of cores has changed with the advent of simulations, which can now self–consistently simulate the launching of massive outflows, the clearing of

the protostellar envelope and the formation of a protostellar disc. We now have a better understanding of the dynamic nature of the core, along with the structure, collimation and mass–loading of the outflow, in addition to the size, stability and rotational properties of the protostellar disc.

A parameter study of evolving cores with differing physical conditions would allow us to better understand the variation of outflow sizes and collimations.

5.6 Conclusions

We have presented results of the simulated collapse of a magnetised, rotating BE sphere attaining the early Class 0 phase. This was achieved by using small (3.2 AU) sink particles. The fiducial model forms a 0.2 $M_{\odot}$ star by the end of the simulation. A nearly Keplerian disc forms (not considering the support by the magnetic field) to about 100 AU, with a larger rotation structure extending out to 2000 AU. The disc and the flattened rotating core launch a large outflow into the external medium clearing out a significant amount of mass from the envelope.

The outflow has two components. One is a low velocity, high density component launched primarily by the toroidal magnetic field as described in the theory of magneto–centrifugal winds. This component has a high outflowing mass flux, such that $\dot{M}_{\rm out}/\dot{M}_{\rm in} \sim 1$. This component drives a 100 K bow shock into the ambient environment and would be observed as a molecular outflow. Embedded in this outflow is a faster, less dense component, launched through centrifugal driving from the poloidal magnetic field in the inner region of the disk. This outflow is tilted and precesses due to magnetic warping of the

disk to 30° relative to the z–axis (Duffin et al., 2012b). It has a smaller mass loading such that $\dot{M}_{\rm out}/\dot{M}_{\rm in} \sim 0.1$, comparable to observations of protostellar jets (Ray et al., 2007). This component of the outflow would be observed as a protostellar jet ejected from a young Class 0/I protostar, embedded in the lower speed molecular outflow.

Lastly, we find a high star formation efficiency of $\varepsilon_{\rm core} = 0.63$ (in model 'MHD poly, 12.7 AU'), in agreement with recent numerical simulations which find $\varepsilon_{\rm core} = 0.5 - 0.9$ (Machida & Matsumoto, 2012; Price et al., 2012). This is in contrast to theoretical predictions by Matzner & McKee (2000) which predict $\varepsilon_{\rm core} = 0.29 - 0.39$ when applied to our simulation. We explain that the outflow models used by Matzner & McKee (2000) underestimate the importance of i) the dynamic nature of the core and ii) the physical nature and structure of the early outflow. In our calculations, we have discovered that the time of onset of the flow during disc formation is a key new element in understanding the efficiency of jets in clearing material.

Simulated star formation efficiencies are also higher than what is expected from observations of the CMF, which predict $\varepsilon_{\rm core} = 0.2 - 0.4$ (André et al., 2010). We suggest that limitations due process of identifying cores and measuring their masses makes estimates of the overall position of the CMF relative to the IMF highly uncertain (Smith et al., 2008).

A parameter study of such models may be able to tell us more about the relation of the initial core mass to the final mass in stars and whether a one–to–one relation indeed exists.

Acknowledgements

We thank Christoph Federrath concerning implementation of sink particles in FLASH. We also thank Chris McKee, James Wadsley and Christine Wilson for constructive discussions. D.D. is supported by McMaster University and R.E.P by a Discovery grant from NSERC of Canada. D.S especially thanks the Heidelberg Graduate School of Fundamental Physics for funding a research visit. RB acknowledge funding of Emmy–Noether grant BA3706 by the DFG. RSK acknowledges support by contract research Internationale Spitzenforschung II of the Baden–Württemberg (grant P–LS–SPII/18), from the German Bundesministerium für Bildung und Forschung via the ASTRONET project STAR FORMAT (grant 05A09VHA), from the Deutsche Forschungsgemeinschaft (DFG) under grants KL1358/11-1 and KL1358/14-1, and via the SFB 881 – The Milky Way System. We are pleased to acknowledge the SHARCNET HPC Consortium for the use of its facilities at McMaster University. The FLASH code was developed partly by the DOE–supported Alliances centre for Astrophysical Thermonuclear Flashes (ASC) at the University of Chicago.

5.7 APPENDIX: Star formation efficiency calculations

For the purposes of the discussion, we briefly summarize the theory of Matzner & McKee (2000) and how we use our simulation data to predict star formation efficiencies from their model.

The authors define a core efficiency as the amount of mass in a core

that makes it into stars

$$\varepsilon_{\rm core} = \frac{M_{\rm star}}{M_{\rm star} + M_{\rm ejected}} \approx \frac{M_{\rm star}}{M_{\rm core}}, \tag{5.4}$$

where the mass in stars $M_{\rm star}$ and the mass in ejected material $M_{\rm ejected}$ is all that is left after the star formation process (e.g. the disc and envelope have dissipated and planetary masses are negligible). The authors define an *efficiency parameter* X such that

$$X = 0.132 \left(\frac{c_g}{1}\right) \left(\frac{v_{\rm esc}}{1 \text{ km s}^{-1}}\right) \left(\frac{\ln(2/\theta_0)}{\ln(200)}\right) \left(\frac{40 \text{ km s}^{-1}}{f_w v_w}\right), \tag{5.5}$$

where $c_g \geq 1$ is a parameter describing self–gravity of the outflow, $f_w = M_{\rm outflow}/M_{\rm star}$ is the mass in the outflow and $\theta_0 = 0.57°$ is the angle of the fine component of the jet which caries the majority of the momentum. The authors suggest to measure $f_w v_w$ as the ratio of the wind momentum p_w to the final star mass $M_{\rm star}$. However, we find that this doesn't properly represent values of v_w. We measure v_w as the average speed of the furthest point of the outflow from the star. For an isotropic core model (uniform density), the prediction is that

$$\varepsilon_{\rm iso} = \frac{2X}{1 + \sqrt{1 + 4(1 + f_w)^2 X^2}}. \tag{5.6}$$

Furthermore, the theory also predicts efficiencies for flattened, singular isothermal toroids of Li & Shu (1996). The value of X and ε become

$$X_{\rm SIT} = 0.32(1 + H_0) \left(\frac{\ln(2/\theta_0)}{\ln(200)}\right) \left(\frac{40 \text{ km s}^{-1}}{f_w v_w}\right), \tag{5.7}$$

$$\varepsilon_{\rm SIT} = \frac{2(1 + H_0)^{3/2} X}{1 + \sqrt{1 + 4(1 + H_0)^3 (1 + f_w)^2 X^2}}, \tag{5.8}$$

We substitute $v_{\rm esc} = 0.3$ km s^{-1} (for a core of 10^4 AU and mass around $1M_\odot$), $c_g = 1$, $v_w = 1.6$ km s^{-1} $f_w = 1.53$. These values are taken from the end state of the 'MHD, poly 12.7 AU' model, shown on the right panel of Figure 5.10). For this model, $M_{\rm star} = 0.76M_\odot$, $p_w = 0.47M_\odot$ km s^{-1}, $M_{\rm outflow} = 1.16M_\odot$. We find aspect ratios of our core $\chi = 2 - 2.32$ (length over width), taken near the onset of outflows using density contours $\rho = 1.73 \times 10^{-18} - 8.5 \times 10^{-19}$ g cm^{-3}. From Table 1 in Li & Shu (1996), these correspond roughly to $H_0 = 0.375 - 0.5$. Plugging the numbers in, we find

$$\varepsilon_{\rm iso} = 0.29 \tag{5.9}$$

$$\varepsilon_{\rm SIT} = 0.39. \tag{5.10}$$

The outflow is modelled as a double cone centred on the star. The opening angle of the cone is predicted to be $\cos\theta = \varepsilon(1 + f_w)$, where θ is the angle from the z-axis the edge of the outflow. The model predicts opening angles

$$\theta_{\rm iso} = 42.3^\circ \tag{5.11}$$

$$\theta_{\rm SIT} = 9.47^\circ. \tag{5.12}$$

If we take our simulation at the time the sink particle is created and carve out a double cone with the above opening angles, we find that the masses contained are

$$M_{\rm cavity,iso} = 0.34M_\odot \tag{5.13}$$

$$M_{\rm cavity,SIT} = 0.05M_\odot \tag{5.14}$$

respectively, whereas the measured mass in our outflow is $1.16 M_{\odot}$. The model therefore predicts that a significant portion of the mass of the outflow is contributed from the disc wind itself, which contradicts one of its primary assumptions.

Chapter 6

Discussion and Summary

6.1 Future Directions

The models we described have a narrow range of parameters, focusing on a principle model with high magnetic flux and rotation. Seifried et al. (2011) performed a parameter study over rotational and magnetic energies for high–mass ($100 M_{\odot}$), Jeans unstable cores. They found a variety of disk and pseudo-disk structures and no disk warping. However, these latter simulations did not run for a long time and ended when sink particles accreted about a few percent the total cloud mass. The theoretical models show that it takes some time for warps to be produced (§4.4). There is an opportunity to study disk formation, warping, the launching of outflows and the entrainment of the envelope over a parameter space of initial conditions such as this, but in the context of low–mass star formation. Of particular interest are the questions: When do disks warp? When does the launching of magnetised bubbles via a Parker instability promote disk formation? What are the various structures and collimations of the outflows that can form? What range of star formation efficiencies occur

and how do they depend on the initial conditions?

In the following we speculate on possible future directions for simulations. We support our discussion with some progress we've already made in these directions.

6.1.1 Non-ideal MHD

6.1.1.1 Ambipolar diffusion

We demonstrated in Chapter 3 that ambipolar diffusion (AD) is important in the earliest stages of the collapse as it reduces the effects of magnetic tension. The outflow is launched with much drift heating, enough that we speculate on the shock heating of chondrules. We note that in longer term simulations, the effect of drift heating can run–away to unrealistic temperatures. Drift heating due to ambipolar diffusion is

$$\frac{\partial E}{\partial t} = 4\pi\beta_{\rm AD}||\boldsymbol{J}\times\boldsymbol{B}|| = 4\pi\beta_{\rm AD}\boldsymbol{f}_{\rm m}, \tag{6.1}$$

where $\boldsymbol{f}_{\rm m}$ is the magnetic force density and $\beta_{\rm AD}\rightarrow 0$ as ionization increases. As ionization increases, AD is no longer valid and there is little or no drift heating. The entire outflow bubble will be under strong magnetic forcing, so drift heating should be strong. In the outflow formed in Chapter 3, temperatures of $T > 1000K$ were formed in small regions, hot enough to ionize the gas. If we were to simulate the later evolution with AD, we would need to adjust ionization in regions of high temperatures.

It is unclear how AD will affect the disk formation and outflow. Will disks grow faster with the inclusion of AD in 3D, contrary to simulations of

Mellon & Li (2009)? How would the long–term stability of the disk be affected? Will the Parker Instability operate under non–ideal conditions? Will the disk–warping mechanism operate? What would be the structure of the outflow and the change in the collimation?

We have earlier implemented an explicit scheme for AD in FLASH2.5 (Duffin & Pudritz, 2008) and recently ported the code to FLASH4. We have already run experiments with sink particles and AD, however the timestep quickly becomes too small as $\Delta t_{\rm AD} \propto \eta_{\rm AD}^{-1} \Delta x^2$. Resolution should not have halted our run, rather the outflow created hot regions of low density, high B and correspondingly high $v_{\rm A}$ and high $\eta_{\rm AD}$. There are a couple possible ways to solve this. One would be to turn off AD in high ($T > 10^3$ K) regions where the gas as discussed above.

The second is to implement a semi–implicit method called Super–Time–Stepping (STS, Alexiades et al., 1996), a fix for any explicit diffusive scheme. This has been recently been implemented in the ATHENA code (Choi et al., 2008) and had been previously used in one other customized non-ideal MHD code (O'Sullivan & Downes, 2006, 2007).

This STS procedure starts by desiring stability over some given super-step, which allows one to derive

$$t_{\rm STS} = t_{\rm AD} \frac{N}{2\sqrt{\nu}} \left[\frac{(1+\sqrt{\nu})^{2N} - (1-\sqrt{\nu})^{2N}}{(1+\sqrt{\nu})^{2N} + (1-\sqrt{\nu})^{2N}} \right], \tag{6.2}$$

where many details can be found in Alexiades et al. (1996). The factor N is the number of sub–steps, which we will describe shortly. The factor $\nu \in (0, 1)$ acts as a fudge factor for a given simulation. The sub–steps are uniquely defined

such that

$$t_j = t_{\rm AD}\left[(\nu-1)\cos\left(\frac{2j-1}{N}\frac{\pi}{2}\right)+\nu+1\right]^{-1}. \tag{6.3}$$

The effective factor increase in timestep can be measured as

$$\frac{t_{\rm STS}}{Nt_{\rm AD}} = \frac{1}{Nt_{\rm AD}}\sum_{j=1}^{N} t_j. \tag{6.4}$$

This is shown in Figure 6.1 and tells us to maximize N and minimize ν, limited by round off error. We plan to implement this in FLASH2.5 in order answer the questions discussed above

6.1.1.2 Ohmic diffusion

Ohmic diffusion (OD) becomes as important as AD for densities $n > 10^{12.5}$ cm^{-3} (Tassis & Mouschovias, 2007a,b,c). We note that for our 3.2 AU sink particles in Chapters 4-5, gas is accreted into sinks if $n > 9.53 \times 10^{11}$ cm^{-3}. Simulations by Dapp & Basu (2010) suggest that disks form in regions dominated by Ohmic diffusion. Inutsuka et al. (2010) simulated protostellar collapse with sink particles and OD finding decoupled regions of 60 AU. This is much larger than theoretical expectations based on ionization rates which suggest dead zones of at most 10 AU (Matsumura & Pudritz, 2003). Similar small sizes are found by detailed multi-fluid calculations (Tassis & Mouschovias, 2007b). This large decoupled region led to the formation of protostellar disks. Excessive amounts of magnetic diffusion are one way to solve the magnetic braking catastrophe (Zhao et al., 2011).

Ohmic diffusion would still prove interesting to implement, especially in isolated collapse where more computational resources could resolve inside

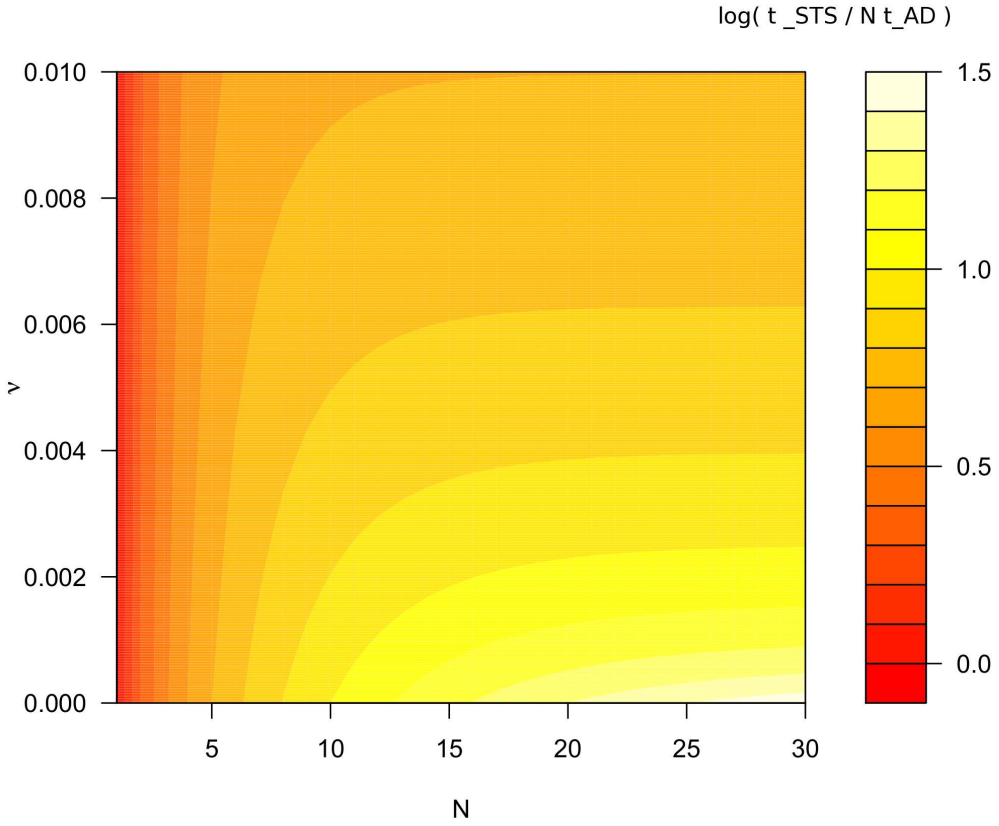

Figure 6.1 Log factor improvement in explicit AD timestep with addition of STS. Comparing an entire superstep to N normal AD timesteps without STS. A superstep consists of N sub–steps of varying sizes.

3.2 AU. However, the future of low–mass star formation lies in simulations with more realistic initial conditions. Stars form in clusters and computational resources would likely be better spent on this.

6.1.2 Star formation in turbulent molecular clouds

Stars form in clusters (Kroupa, 2001) which themselves form in supersonic, turbulent molecular clouds of many Jeans masses, and total mass $10^2 - 10^6 M_\odot$.

The turnover in the IMF is around $0.5M_{\odot}$, so we'd expect clusters to form with $10^2 - 10^6$ stars at most, unless total star formation efficiencies are quite low, as the star formation rate in the Galaxy suggests (see Chapters 1-2).

Recent simulations suggest that protostellar outflows inject turbulent energy back into molecular clouds, prolonging star formation to match observed star formation rates in the Galaxy (Wang et al., 2010; Krumholz et al., 2012, using the ENZO and ORION codes respectively). However, these simulations use simple approximations to protostellar outflows, ejecting mass, momentum and energy from sink particles (the ORION code does not yet consider the magnetic field in these simulations, despite the fact that magnetic energy is on par with turbulent and kinetic energy in molecular clouds). The simulations themselves are not resolved enough to generate outflows self–consistently as we have in Chapter 5. If we use our data, we can demonstrate the overestimation made in these simple models, presented in Table 6.1. Both models consider low mass fluxes from the disc surface (e.g. that $\dot{M}_{\rm w}/\dot{M}_{\rm acc} = 0.1, 0.27$ respectively). We show in Chapter 5 that most of the early outflow is dominated by the tower flow and has a large mass loading such that $\dot{M}_{\rm w}/\dot{M}_{\rm a} \approx 1$.

To properly model the effects of outflows, we propose a simulation of a turbulent box with MHD, resolving down sinks to the 3.2-12 AU scale as we have done in the case of isolated collapse. Will the results of previous simulations, albeit using different outflow models, stand-up? A simulation along these lines has been performed with RAMSES with the use of a barotropic equation of state to stop the gas from accreting to high densities (Hennebelle et al., 2011). The smallest grid cells (2-8 AU) are comparable to our sink particle sizes above (our finest resolution was 1 AU). However, the baratropic approach limits resolution of the inner region of the collapse as gas piles up.

Table 6.1 Comparison of the self-consistent launching of protostellar outflows from the MHD simulations of Duffin et al. (2012a) to simplified protostellar outflow models used in large cluster formation simulations Wang et al. (2010); Krumholz et al. (2012). See also (Cunningham et al., 2011) for details of the implementation of sink particles in ORION. Both assume for low mass loading and high velocities. While these may be correct for very fine jets produced close to the star, the outflow on large scales is characterised by the lower speed component with high mass.

M_* [$M_\odot$]	Duffin et al. (2012a) [$P_{\rm out}$, $M_{\rm out}$]	Wang et al. (2010) [$P_{\rm out}$, $M_{\rm out}$]	Krumholz et al. (2012) [$P_{\rm out}$, $M_{\rm out}$]
0.1	[0.1, 0.1]	[0.5,0.01]	[—,0.03]
0.2	[0.2, 0.3]	[1.2,0.02]	[—,0.06]
0.3	[0.8, 0.9]	[2.1,0.03]	[—,0.09]

Sinks may offer higher resolution near the high–speed component of the flow.

6.2 Summary

In this thesis we have discussed significant theoretical discoveries through numerical experiments which reveal how disks are formed, how they evolve and the nature of protostellar outflows that are launched from their surfaces. Most importantly, these discoveries have helped us better understand how a star is made.

In Chapter 3 we described evidence for the beginning of a protostellar disk in the very early phases of protostar formation. Drift heating may be an important contribution to the outflow in the later phases that we discuss below. In this Chapter, we also found that the fragmentation crisis could be partially resolved through the effects of ambipolar diffusion, although our simulations were limited to high rotation models.

With the implementation of sink particles (Federrath et al., 2010a), we were able to extend the collapse in the ideal MHD and HD cases. In Chapter

4, we showed the disk formation process continued and created a disk roughly 100 AU in radius in face of high initial mass–to–flux. A major result of this thesis is in finding a solution to the magnetic braking catastrophe. Without turbulence, magnetic braking prevents the formation of disks (Mellon & Li, 2008) until the protostellar envelope has cleared. Indeed we form a pseudo–disk in our simulations with a radius of 2000 AU that has rotational motion and launches a disk wind. The formation of a disk is promoted by the eruption of magnetic loops and bubbles into the disk corona as a consequence of the Parker instability (Johansen & Levin, 2008). The shedding of field loops scrambles the mean threading field and decreases the efficiencies of magnetic braking.

The inner disk warps to 30° with respect to the z–axis due to the magnetic field. This may explain the 7°.15 mis–alignment of the Solar System with respect to the Sun (Beck & Giles, 2005), or minor precession of jets and outflows like the 7° tilt of L 1157 (Gueth et al., 1998). It may also help explain major mis–alignments like that of Hot Jupiters (Triaud et al., 2010).

Another principal result of this thesis is that protostellar outflows are not efficient enough to explain the observed offset of the CMF relative to the IMF, as described in Chapter 5. Star formation efficiencies from our simulation and others are high $50 - 75\%$ (Duffin et al., 2012a; Machida & Matsumoto, 2012; Price et al., 2012) rather than 30% from theory (Matzner & McKee, 2000) and 20-40% from observations (André et al., 2010). We suggest the theory underestimates efficiencies due to the dynamic nature of the core and an outdated physical structure and evolutionary model of the outflow. The observations may underestimate core masses on average simply because of the fine tuning of core finding algorithms and observation constraints such as orientation and resolution of the molecular cloud (Smith et al., 2008).

Our outflow has components launched both by magneto–centrifugal forces and toroidal magnetic field pressure, requiring a new treatment of the MHD disc–wind equations to properly describe the acceleration of the gas. There is currently no theoretical model of such an outflow, however different components can be described by both 'magnetic tower' (Lynden-Bell, 2003) and magneto-centrifugal winds (Pelletier & Pudritz, 1992). However a theoretical framework exists on how such an outflow operates in numerical simulations (Seifried et al., 2012b).

We are excited by the prospects for further studies of the evolution of protostellar outflows in dynamic, turbulent environments and their possible impact on the star formation rate in molecular clouds. The picture of modern star formation is beginning to become clear, while new frontiers lie on the horizon. For example, understanding the interplay between the formation of molecular clouds and the generation of self–consistent initial conditions to the star formation problem can be addressed, for example through colliding flows mediated by magnetic fields and ambipolar diffusion (Vázquez-Semadeni et al., 2011). The next decade will see the focus shift to the first stars and the importance of magnetic fields, protostellar disks and outflows on a whole new scale fundamental to the nature of the Universe.

Bibliography

Alexiades V., Amiez G., Gremaud P., 1996, Comm. Num. Meth. Eng., 12, 31

Allen A., Li Z.-Y., Shu F. H., 2003, ApJ, 599, 363

Alves J. F., Lada C. J., Lada E. A., 2001, Nat, 409, 159

André P., Men'shchikov A., Bontemps S., Könyves V., Motte F., Schneider N., Didelon P., Minier V., Saraceno P., Ward-Thompson D., di Francesco J., White G., Molinari S., Testi L., Abergel A., Griffin M., Henning T., Royer P., Merín B., Vavrek R., Attard M., Arzoumanian D., Wilson C. D., Ade P., Aussel H., Baluteau J.-P., Benedettini M., Bernard J.-P., Blommaert J. A. D. L., Cambrésy L., Cox P., di Giorgio A., Hargrave P., Hennemann M., Huang M., Kirk J., Krause O., Launhardt R., Leeks S., Le Pennec J., Li J. Z., Martin P. G., Maury A., Olofsson G., Omont A., Peretto N., Pezzuto S., Prusti T., Roussel H., Russeil D., Sauvage M., Sibthorpe B., Sicilia-Aguilar A., Spinoglio L., Waelkens C., Woodcraft A., Zavagno A., 2010, A&A, 518, L102

Arce H. G., Goodman A. A., 2001a, ApJ, 554, 132

—, 2001b, ApJ, 551, L171

Arce H. G., Sargent A. I., 2005, ApJ, 624, 232

—, 2006, ApJ, 646, 1070

Arce H. G., Shepherd D., Gueth F., Lee C.-F., Bachiller R., Rosen A., Beuther H., 2007, in Protostars and Planets V, Reipurth B., Jewitt D., Keil K., eds., pp. 245–260

Arzoumanian D., André P., Didelon P., Könyves V., Schneider N., Men'shchikov A., Sousbie T., Zavagno A., Bontemps S., di Francesco J.,

Griffin M., Hennemann M., Hill T., Kirk J., Martin P., Minier V., Molinari S., Motte F., Peretto N., Pezzuto S., Spinoglio L., Ward-Thompson D., White G., Wilson C. D., 2011, A&A, 529, L6

Ballesteros-Paredes J., Klessen R. S., Vázquez-Semadeni E., 2003, ApJ, 592, 188

Ballesteros-Paredes J., Vázquez-Semadeni E., Gazol A., Hartmann L. W., Heitsch F., Colín P., 2011, MNRAS, 416, 1436

Bally J., Reipurth B., Davis C. J., 2007, Protostars and Planets V, 215

Banerjee R., Pudritz R. E., 2006, ApJ, 641, 949

—, 2007, ApJ, 660, 479

Banerjee R., Pudritz R. E., Anderson D. W., 2006, MNRAS, 373, 1091

Banerjee R., Pudritz R. E., Holmes L., 2004, MNRAS, 355, 248

Basu S., Mouschovias T. C., 1994, ApJ, 432, 720

Bate M. R., 2010, MNRAS, 404, L79

—, 2012, MNRAS, 419, 3115

Bate M. R., Bonnell I. A., Price N. M., 1995, MNRAS, 277, 362

Beck J. G., Giles P., 2005, ApJ, 621, L153

Berger M. J., Collela P., 1989, J. Chem. Phys., 82, 64

Blandford R. D., Payne D. G., 1982, MNRAS, 199, 883

Boily C. M., Lynden-Bell D., 1996, Ap&SS, 243, 29

Bonnor W. B., 1956, MNRAS, 116, 351

Boss A. P., Bodenheimer P., 1979, ApJ, 234, 289

Bouchut F., Klingenberg C., Waagan K., 2007, J. Chem. Phys., 108, 7

—, 2010, J. Chem. Phys., 115, 647

Brackbill J. U., Barnes D. C., 1980, J. Chem. Phys., 35, 426

Brandenburg A., Zweibel E. G., 1994, ApJl, 427, L91

Bürzle F., Clark P. C., Stasyszyn F., Dolag K., Klessen R. S., 2011, MNRAS, 417, L61

Chabrier G., 2005, in Astrophysics and Space Science Library, Vol. 327, The Initial Mass Function 50 Years Later, Corbelli E., Palla F., Zinnecker H., eds., p. 41

Chen X., Launhardt R., Henning T., 2007, ApJ, 669, 1058

Chiang H.-F., Looney L. W., Tobin J. J., Hartmann L., 2010, ApJ, 709, 470

Choi E., Kim J., Wiita P. J., 2008, ArXiv e-prints

Clark P. C., Klessen R. S., Bonnell I. A., 2007, MNRAS, 379, 57

Coffey D., Bacciotti F., Ray T. P., Eislöffel J., Woitas J., 2007, ApJ, 663, 350

Commerçon B., Hennebelle P., Audit E., Chabrier G., Teyssier R., 2010, A&A, 510, L3

Commerçon B., Hennebelle P., Henning T., 2011, ApJ, 742, L9

Crida A., 2009, ApJ, 698, 606

Crutcher R. M., 1999, ApJ, 520, 706

Crutcher R. M., Wandelt B., Heiles C., Falgarone E., Troland T. H., 2010, ApJ, 725, 466

Cunningham A. J., Klein R. I., Krumholz M. R., McKee C. F., 2011, ApJ, 740, 107

Cyganowski C. J., Brogan C. L., Hunter T. R., Churchwell E., Zhang Q., 2011, ApJ, 729, 124

Dapp W. B., Basu S., 2009, MNRAS, 395, 1092

—, 2010, A&A, 521, L56

Desch S. J., Ciesla F. J., Hood L. L., Nakamoto T., 2005, in Astronomical Society of the Pacific Conference Series, Vol. 341, Chondrites and the Protoplanetary Disk, Krot A. N., Scott E. R. D., Reipurth B., eds., pp. 849–+

Desch S. J., Mouschovias T. C., 2001, ApJ, 550, 314

Duffin D., Pudritz R. E., Seifried D., Banerjee R., S. K. R., 2012a, in prep.

—, 2012b, submitted to MNRAS.

Duffin D. F., Pudritz R. E., 2008, MNRAS, 391, 1659

—, 2009, ApJ, 706, L46

Duquennoy A., Mayor M., 1991, A&A, 248, 485

Ebert R., 1955, Zeitschrift fur Astrophysik, 37, 217

Enoch M. L., Corder S., Duchêne G., Bock D. C., Bolatto A. D., Culverhouse T. L., Kwon W., Lamb J. W., Leitch E. M., Marrone D. P., Muchovej S. J., Pérez L. M., Scott S. L., Teuben P. J., Wright M. C. H., Zauderer B. A., 2011, ApJS, 195, 21

Fabrycky D., Tremaine S., 2007, ApJ, 669, 1298

Federrath C., Banerjee R., Clark P. C., Klessen R. S., 2010a, ApJ, 713, 269

Federrath C., Roman-Duval J., Klessen R. S., Schmidt W., Mac Low M.-M., 2010b, A&A, 512, A81

Ferreira J., 1997, A&A, 319, 340

Ferreira J., Pelletier G., 1995, A&A, 295, 807

Fiedler R. A., Mouschovias T. C., 1993, ApJ, 415, 680

Fiege J. D., Pudritz R. E., 2000, ApJ, 534, 291

Foster P. N., Chevalier R. A., 1993, ApJ, 416, 303

Fryxell B., Olson K., Ricker P., Timmes F. X., Zingale M., Lamb D. Q., MacNeice P., Rosner R., Truran J. W., Tufo H., 2000, ApJs, 131, 273

Galli D., Lizano S., Shu F. H., Allen A., 2006, ApJ, 647, 374

Gammie C. F., 2001, ApJ, 553, 174

Girichidis P., Federrath C., Banerjee R., Klessen R. S., 2012, MNRAS, 420, 613

Gomez de Castro A., Pudritz R. E., 1992, ApJ, 395, 501

Goodman A. A., Benson P. J., Fuller G. A., Myers P. C., 1993, ApJ, 406, 528

Gueth F., Guilloteau S., Bachiller R., 1998, A&A, 333, 287

Hartigan P., Frank A., Foster J. M., Wilde B. H., Douglas M., Rosen P. A., Coker R. F., Blue B. E., Hansen J. F., 2011, ApJ, 736, 29

Hartmann L., Calvet N., 1995, AJ, 109, 1846

Hayashi C., 1981, Progress of Theoretical Physics Supplement, 70, 35

Hennebelle P., Ciardi A., 2009, A&A, 506, L29

Hennebelle P., Commerçon B., Joos M., Klessen R. S., Krumholz M., Tan J. C., Teyssier R., 2011, A&A, 528, A72

Hennebelle P., Fromang S., 2008, A&A, 477, 9

Hennebelle P., Teyssier R., 2008, A&A, 477, 25

Horiuchi T., Matsumoto R., Hanawa T., Shibata K., 1988, PASJ, 40, 147

Hosking J. G., Whitworth A. P., 2004, MNRAS, 347, 1001

Hotzel S., Harju J., Juvela M., 2002, A&A, 395, L5

Inutsuka S.-i., Machida M. N., Matsumoto T., 2010, ApJ, 718, L58

Jappsen A.-K., Klessen R. S., Larson R. B., Li Y., Mac Low M.-M., 2005, Mem. Soc. Astron. Italiana, 76, 199

Johansen A., Levin Y., 2008, A&A, 490, 501

Johnstone D., Fich M., Mitchell G. F., Moriarty-Schieven G., 2001, ApJ, 559, 307

Jørgensen J. K., van Dishoeck E. F., Visser R., Bourke T. L., Wilner D. J., Lommen D., Hogerheijde M. R., Myers P. C., 2009, A&A, 507, 861

Joung M. R., Mac Low M.-M., Bryan G. L., 2009, ApJ, 704, 137

Kainulainen J., Beuther H., Henning T., Plume R., 2009, A&A, 508, L35

Kevlahan N., Pudritz R. E., 2009, ApJ, 702, 39

Kim W.-T., Ostriker E. C., 2001, ApJ, 559, 70

Kim W.-T., Ostriker E. C., Stone J. M., 2002, ApJ, 581, 1080

Kirk J. M., Crutcher R. M., Ward-Thompson D., 2009, ApJ, 701, 1044

Kozai Y., 1962, AJ, 67, 591

Krasnopolsky R., Königl A., 2002, ApJ, 580, 987

Kroupa P., 2001, MNRAS, 322, 231

—, 2002, Science, 295, 82

Krumholz M. R., Klein R. I., McKee C. F., 2007, ApJ, 656, 959

—, 2012, ApJ, 754, 71

Krumholz M. R., McKee C. F., Klein R. I., 2004, ApJ, 611, 399

Kudoh T., Basu S., Ogata Y., Yabe T., 2007, MNRAS, 380, 499

Lada C. J., Bergin E. A., Alves J. F., Huard T. L., 2003, ApJ, 586, 286

Lai D., 2003, ApJ, 591, L119

Lai D., Foucart F., Lin D. N. C., 2011, MNRAS, 412, 2790

Larson R. B., 1969, MNRAS, 145, 271

—, 1981, MNRAS, 194, 809

—, 2010, Reports on Progress in Physics, 73, 014901

Levine E. S., Blitz L., Heiles C., Weinberg M., 2006, ArXiv Astrophysics e-prints

Li P. S., McKee C. F., Klein R. I., 2012, ApJ, 744, 73

Li Z.-Y., Krasnopolsky R., Shang H., 2011, ApJ, 738, 180

Li Z.-Y., Shu F. H., 1996, ApJ, 472, 211

Lynden-Bell D., 2003, MNRAS, 341, 1360

Mac Low M.-M., Klessen R. S., 2004, Reviews of Modern Physics, 76, 125

Machida M. N., Inutsuka S.-i., Matsumoto T., 2007a, ArXiv e-prints, 705

—, 2007b, ApJ, 670, 1198

—, 2009, ApJ, 699, L157

Machida M. N., Inutsuka S.-I., Matsumoto T., 2011, PASJ, 63, 555

Machida M. N., Matsumoto T., 2012, MNRAS, 421, 588

Machida M. N., Matsumoto T., Hanawa T., Tomisaka K., 2006a, ApJ, 645, 1227

Machida M. N., Omukai K., Matsumoto T., Inutsuka S.-i., 2006b, ApJ, 647, L1

Marder B., 1987, J. Chem. Phys., 68, 48

Matsumura S., Pudritz R. E., 2003, ApJ, 598, 645

Matsumura S., Pudritz R. E., Thommes E. W., 2009, ApJ, 691, 1764

Matt S., Pudritz R. E., 2005, ApJ, 632, L135

Matzner C. D., McKee C. F., 2000, ApJ, 545, 364

McDaniel E. W., Mason E. A., 1973, The mobility and diffusion of ions in gases. New York Wiley, 1973. 372 p.

McKee C. F., 1999, in NATO ASIC Proc. 540: The Origin of Stars and Planetary Systems, Lada C. J., Kylafis N. D., eds., p. 29

McKee C. F., Ostriker E. C., 2007, ARA&A, 45, 565

McKinney J. C., Tchekhovskoy A., Blandford R. D., 2012, MNRAS, 423, 3083

Mellon R. R., Li Z.-Y., 2008, ApJ, 681, 1356

—, 2009, ApJ, 698, 922

Men'shchikov A., André P., Didelon P., Könyves V., Schneider N., Motte F., Bontemps S., Arzoumanian D., Attard M., Abergel A., Baluteau J.-P., Bernard J.-P., Cambrésy L., Cox P., di Francesco J., di Giorgio A. M., Griffin M., Hargrave P., Huang M., Kirk J., Li J. Z., Martin P., Minier V., Miville-Deschênes M.-A., Molinari S., Olofsson G., Pezzuto S., Roussel H., Russeil D., Saraceno P., Sauvage M., Sibthorpe B., Spinoglio L., Testi L., Ward-Thompson D., White G., Wilson C. D., Woodcraft A., Zavagno A., 2010, A&A, 518, L103

Mestel L., Spitzer Jr. L., 1956, MNRAS, 116, 503

Motte F., Andre P., Neri R., 1998, A&A, 336, 150

Mouschovias T. C., Paleologou E. V., 1980, ApJ, 237, 877

—, 1986, ApJ, 308, 781

Murray N., 2011, ApJ, 729, 133

Myers P. C., 2009, ApJ, 706, 1341

Nakamura F., Li Z.-Y., 2008, ApJ, 687, 354

Nakano T., Nakamura T., 1978, PASJ, 30, 671

Offner S. S. R., Klein R. I., McKee C. F., Krumholz M. R., 2009, ApJ, 703, 131

Ostriker J., 1964, ApJ, 140, 1529

O'Sullivan S., Downes T. P., 2006, MNRAS, 366, 1329

—, 2007, MNRAS, 376, 1648

Padoan P., Juvela M., Goodman A. A., Nordlund Å., 2001, ApJ, 553, 227

Padoan P., Nordlund Å., 2011, ApJ, 730, 40

Padoan P., Nordlund A., Jones B. J. T., 1997, MNRAS, 288, 145

Parker E. N., 1966, ApJ, 145, 811

Pelletier G., Pudritz R. E., 1992, ApJ, 394, 117

Penston M. V., 1969, MNRAS, 145, 457

Peters T., Banerjee R., Klessen R. S., Mac Low M.-M., 2011a, ApJ, 729, 72

Peters T., Klessen R. S., Mac Low M.-M., Banerjee R., 2011b, ArXiv e-prints

Pineda J. E., Goodman A. A., Arce H. G., Caselli P., Foster J. B., Myers P. C., Rosolowsky E. W., 2010, ApJ, 712, L116

Pineda J. E., Goodman A. A., Arce H. G., Caselli P., Longmore S., Corder S., 2011, ApJ, 739, L2

Price D., Bate M., 2008, ArXiv e-prints, 801

Price D. J., Bate M. R., 2007, MNRAS, 377, 77

—, 2009, ArXiv e-prints

Price D. J., Tricco T. S., Bate M. R., 2012, MNRAS, 423, L45

Pringle J. E., 1996, MNRAS, 281, 357

Pudritz R. E., Norman C. A., 1986, ApJ, 301, 571

Pudritz R. E., Ouyed R., Fendt C., Brandenburg A., 2007, in Protostars and Planets V, Reipurth B., Jewitt D., Keil K., eds., pp. 277–294

Quillen A. C., 2001, ApJ, 563, 313

Ray T., Dougados C., Bacciotti F., Eislöffel J., Chrysostomou A., 2007, in Protostars and Planets V, Reipurth B., Jewitt D., Keil K., eds., pp. 231–244

Rogers P. D., Wadsley J., 2011, MNRAS, 414, 913

Salpeter E. E., 1955, ApJ, 121, 161

Schandl S., Meyer F., 1994, A&A, 289, 149

Schober J., Schleicher D., Federrath C., Glover S., Klessen R. S., Banerjee R., 2012, ApJ, 754, 99

Seifried D., Banerjee R., Klessen R. S., Duffin D., Pudritz R. E., 2011, MNRAS, 417, 1054

Seifried D., Banerjee R., Pudritz R. E., Klessen R. S., 2012a, MNRAS, 423, L40

Seifried D., Pudritz R. E., Banerjee R., Duffin D., Klessen R. S., 2012b, MNRAS, 422, 347

Sherwin B. D., Lynden-Bell D., 2007, MNRAS, 378, 409

Shetty R., Ostriker E. C., 2006, ApJ, 647, 997

Shu F. H., 1977, ApJ, 214, 488

Shu F. H., Lizano S., Ruden S. P., Najita J., 1988, ApJ, 328, L19

Smith R. J., Clark P. C., Bonnell I. A., 2008, MNRAS, 391, 1091

—, 2009, MNRAS, 396, 830

Smith R. J., Glover S. C. O., Bonnell I. A., Clark P. C., Klessen R. S., 2011, MNRAS, 411, 1354

Solomon P. M., Rivolo A. R., Barrett J., Yahil A., 1987, ApJ, 319, 730

Tasker E. J., Tan J. C., 2009, ApJ, 700, 358

Tassis K., Mouschovias T. C., 2007a, ApJ, 660, 370

—, 2007b, ApJ, 660, 388

—, 2007c, ApJ, 660, 402

Teixeira P. S., Lada C. J., Alves J. F., 2005, ApJ, 629, 276

Tilley D. A., Balsara D. S., 2008, MNRAS, 902

Tilley D. A., Pudritz R. E., 2007, MNRAS, 382, 73

Tobin J. J., Hartmann L., Bergin E., Chiang H.-F., Looney L. W., Chandler C. J., Maret S., Heitsch F., 2012, ApJ, 748, 16

Tobin J. J., Hartmann L., Looney L. W., Chiang H.-F., 2010, ApJ, 712, 1010

Tomisaka K., Ikeuchi S., Nakamura T., 1988, ApJ, 335, 239

Triaud A. H. M. J., Collier Cameron A., Queloz D., Anderson D. R., Gillon M., Hebb L., Hellier C., Loeillet B., Maxted P. F. L., Mayor M., Pepe F., Pollacco D., Ségransan D., Smalley B., Udry S., West R. G., Wheatley P. J., 2010, A&A, 524, A25

Troland T. H., Crutcher R. M., 2008, ApJ, 680, 457

Truelove J. K., Klein R. I., McKee C. F., Holliman II J. H., Howell L. H., Greenough J. A., 1997, ApJl, 489, L179+

Umebayashi T., Nakano T., 1981, PASJ, 33, 617

Vázquez-Semadeni E., Banerjee R., Gómez G. C., Hennebelle P., Duffin D., Klessen R. S., 2011, MNRAS, 414, 2511

Wang P., Li Z.-Y., Abel T., Nakamura F., 2010, ApJ, 709, 27

Wardle M., 1991, MNRAS, 251, 119

Whelan E. T., Ray T. P., Bacciotti F., Natta A., Testi L., Randich S., 2005, Nature, 435, 652

Wooden D., Desch S., Harker D., Gail H.-P., Keller L., 2007, in Protostars and Planets V, Reipurth B., Jewitt D., Keil K., eds., pp. 815–833

Zapata L. A., Schmid-Burgk J., Muders D., Schilke P., Menten K., Guesten R., 2010, A&A, 510, A2

Zhao B., Li Z.-Y., Nakamura F., Krasnopolsky R., Shang H., 2011, ApJ, 742, 10

Zuckerman B., Evans II N. J., 1974, ApJ, 192, L149